Investigating Injury Pathology of Blast-induced Polytrauma and Assessing the Therapeutic Role of Hemostatic Nanoparticles after Blast Exposure

William Brad Hubbard

Dissertation submitted to the to the faculty of the Virginia Polytechnic Institute and State University in partial fulfillment of the requirements for the degree of

Doctor of Philosophy

In

Biomedical Engineering

Pamela J. VandeVord, Chair

J. Jason Hoth

Andrew R. Kemper

Erin B. Lavik

Yong Woo Lee

August 11. 2016

Blacksburg, Virginia

Keywords: blast, injury, polytrauma, hemorrhage, neuropathology, hemostatic nanoparticles

Investigating Biological Mechanisms of Blast-induced Polytrauma and Assessing the Therapeutic Role of Hemostatic Nanoparticles after Blast Exposure

William Brad Hubbard

ABSTRACT

Explosions cause the majority of injuries in the current conflicts, accounting for 79% of combat related injuries (Ramasamy et al. 2008). Blast overpressure from explosions can cause barotrauma to the lungs and the brain. Blast-induced mild traumatic brain injury has been labeled the 'signature wound' of current military conflicts in Iraq and Afghanistan (Snell and Halter 2010). In addition to elevated number of blast-induced traumatic brain injuries due to increased military conflicts overseas and the usage of improvised explosive devices, the incidence of blast-induced polytrauma has risen due to the prevalence of terrorist events around the world (Arnold et al. 2004, Rodoplu et al. 2004). Blast-induced polytrauma is a major concern as lung injury can cause immediate mortality and brain injury causes long-lasting neurocognitive impairment. There is a critical lack of understanding the pathology of blast-induced polytrauma since the needs are multifaceted and therefore few options for treatment. Thus, the research presented in this dissertation required the development of a military-relevant blast polytrauma model to examine injury pathology and subsequently study the effects of hemostatic nanoparticle therapy after blast-induced polytrauma. The pre-clinical model was characterized and static overpressure thresholds were determined for lethality risk. It was confirmed to have many of the classic hallmarks of primary blast lung injury (PBLI), as well as blast-induced neurotrauma (BINT) (Clemedson 1950). Global hemorrhaging was found in the lungs and well as reduced oxygen saturation. Markers of astrogliosis and blood-brain barrier disruption were examined in the amygdala after blast. The novel nanoparticle configuration (hemostatic dexamethasone-loaded nanoparticles (hDNP) functionalized with a peptide that binds with activated platelets) was investigated and hypothesized to increase survival, reduce cellular injury and reduce anxiety-like disorders after blast polytrauma. After investigating hDNP, it was found that the hDNP treatment benefited survival percentage after injury as well as reduced percent hemorrhage in the lungs and

improved physiology. Elevated anxiety parameters found in the controls were lower as compared to the hDNP group. Glial fibrillary acidic protein (GFAP) and cleaved caspase-3 were significantly elevated in the controls compared to the hDNP group in the amygdala. SMI-71 was also significantly elevated with the hDNP and hemostatic nanoparticle (hNP) treatments, similar to sham. In addition to the nanoparticles offering immediate life-saving qualities, administration of hemostatic nanoparticles improved amygdala pathology attributed to secondary mechanisms of blast injury, including blood-brain barrier disruption. This model of polytrauma can serve as a foundation for detailed pathological studies as well as testing therapeutics for injury modalities.

References (Abstract)

Arnold, J. L., P. Halpern, M. C. Tsai and H. Smithline (2004). "Mass casualty terrorist bombings: a comparison of outcomes by bombing type." Ann Emerg Med 43(2): 263-273.

Clemedson, C. J., Granstom, S.A. (1950). "Studies on the genesis of "rib markings" in lung blast injury." Acta Physiol Scand. 21: 131-144.

Ramasamy, A., S. E. Harrisson, J. C. Clasper and M. P. Stewart (2008). "Injuries from roadside improvised explosive devices." J Trauma 65(4): 910-914.

Rodoplu, U., Arnold, J. L., Tokyay, R., Ersoy, G., Cetiner, S., Yucel, T. (2004) “Mass-casualty terrorist bombings in Istanbul, Turkey, November 2003: reports of the events and the prehospital emergency response.” Prehosp Disaster Med 19(2):133-145.

Snell, F. I. and M. J. Halter (2010). "A signature wound of war: mild traumatic brain injury." *J Psychosoc Nurs Ment Health Serv* 48(2): 22-28.

Acknowledgments

I would first like to thank my advisor and mentor, Dr. Pamela VandeVord. Her background and knowledge of blast injuries was paramount to this research and well as guidance in establishing the new injury model. Without her expertise and collaborative approach, this research would not exist. Her patience and continual ideas helped develop all aspects of this dissertation. In addition to all of the research guidance, her encouragement to achieve my personal goals during graduate school was invaluable.

In addition, I would like to thank my committee members, Dr. Hoth, Dr. Kemper, Dr. Lavik and Dr. Lee, for input into this dissertation. Your expertise in each different area aided in the progress of every detail of this project. I would like to especially thank Dr. Lavik, Dr. Lashof-Sullivan, and their colleagues at Case Western Reserve University for the hemostatic nanoparticle collaboration. This collaboration was essential to this dissertation and all of this research would not have been possible without your help and guidance.

I would like to thank all of Dr. VandeVord's lab team throughout the years. Without the team effort that went into each round of animal testing, the research would not be at the level it is now. I would like to thank previous undergraduate students, especially Ryan Brady, Bryce Dunn, Carly Norris, and Joseph Eck, that spent many hours with behavioral tracking and histology. To fellow graduate students and research technicians in the lab, thank you for innovative ideas and contributions to publications.

Finally, I would like to thank my friends and family. Your encouragement and love during my time at VT was so helpful and I can't thank you enough. The deepest level of gratitude goes to my wife, Alex. Without your uplifting attitude on tough days and encouragement, I could not have achieved all of my feats in the lab.

Table of Contents

List of Figures

List of Tables

List of Equations

List of Abbreviations

ABmc	Accessory basal magnocellular subdivision
ABpc	Accessory basal parvicellular subdivision
ABS	Advanced blast simulator
AD	Alzheimer's disease
ANOVA	Analysis of variance
ARNT	Aryl hydrocarbon receptor nuclear translocator
ATLS	Advanced trauma life support
AUC	Area under the curve
BBB	Blood-brain barrier
BINT	Blast-induced neurotrauma
BOP	Blast overpressure
Bpc	Basal nucleus magnocellular subdivision
BPT	Blast-induced polytrauma
BSA	Bovine serum albumin
C-6	Coumarin
CD68	Cluster of Differentiation 68
CDC	Centers for Disease Control and Prevention
CDEs	Common data elements
cDNP	Control dexamethasone-loaded nanoparticles
cNP	Control nanoparticles

DAPI	4’,6-diamidino-2-phenylindole
DLS	Dynamic light scattering
DMSO	Dimethyl sulfoxide
EBA	Endothelial barrier antigen
e.c.	External capsule
EWE	End-wave eliminator
FITC	Fluorescein isothiocyanate
FJC	Fluorojade-C
GC	Glucocorticosteroid
GFAP	Glial fibrillary acidic protein
GRGDS	Glycine-arginine-glycine-aspartic acid-serine
hDNP	Hemostatic dexamethasone-loaded nanoparticles
H&E	Hematoxylin and eosin
HIF-1α	Hypoxia inducible factor-1α
hNPs	Hemostatic nanoparticles
IBA-1	Ionized calcium-binding adaptor molecule 1
ICAM-1	Intercellular adhesion molecule-1
IED	Improvised explosive device
IgG	Immunoglobulin G
IL-6	Interleukin-6
IO	Injury only

kPa	Kilopascals
Ladl	Lateral amygdala medial subdivision
Lam	Lateral amygdala medial subdivision
Lavl	Lateral amygdala ventrolateral subdivision
LR	Lactated ringer's
Mcd	Medial amygdala dorsal subdivision
Mcv	Medial amygdala ventral subdivision
MDD	Major depressive disorder
MEG	Magnetoencephalography
MMP	Matrix metalloproteinase
Mr	Medial amygdala rostral subdivision
NMR	Nuclear magnetic resonance
NOR	Novel object recognition
O.C.T.	Optimal cutting temperature
PAA	Poly(acrylic acid)
PAO2	Partial pressure of oxygen
PBLI	Primary blast lung injury
PBS	Phosphate buffered saline
PEG	Poly(ethylene glycol)
PHD	Prolyl hydroxylase domain
Pir	Piriform cortex

PLGA	Poly(lactic-co-glycolic acid)
psi	Pounds per square inch
PTSD	Post-traumatic stress disorder
RBCs	Red blood cells
SEM	Standard error of the mean
SOP	Static overpressure
s.t.	Stria terminalis
ST	Shock tubes
TBI	Traumatic brain injury
TNF-α	Tumor necrosis factor-α
TNT	Trinitrotoluene
TUNEL	Terminal deoxynucleotidyl transferase dUTP nick end labeling
µls	Microliters
µm	Micrometers
VEGF	Vascular endothelial growth factor
VHL	von Hippel-Lindau

Chapter 1: Background

Portions of this chapter are from "Cellular Mechanisms and Behavioral Outcomes in Blast-induced Neurotrauma: Comparing Experimental Set-ups" 2016, *Methods in Molecular Biology* "In Press" (Hubbard 2016)

1.1 Blast Wave Characteristics

In classic free-field blast, the fireball creates near-field and mid-field regimes; these have complex, non-uniform transient wave dynamics (VandeVord 2016). Beyond these regions, equilibrated flow is achieved and an idealized form of a shock wave is generated in far-field relative to the free-field explosive origin. The idealized wave is generally referred to as the Friedlander wave and is defined by the Friedlander equation (Friedlander 1955). The time course and waveform applies to all dynamic conditions in far-field areas from blast detonation, though peak overpressure and duration vary based on type and amount of charge.

Equation 1. Friedlander Equation

$P(t) = P_s e^{-\frac{t}{t_p}}(1 - \frac{t}{t_p})$, where Ps = peak overpressure and tp = positive phase duration. Representation of this equation is illustrated in Figure 1.

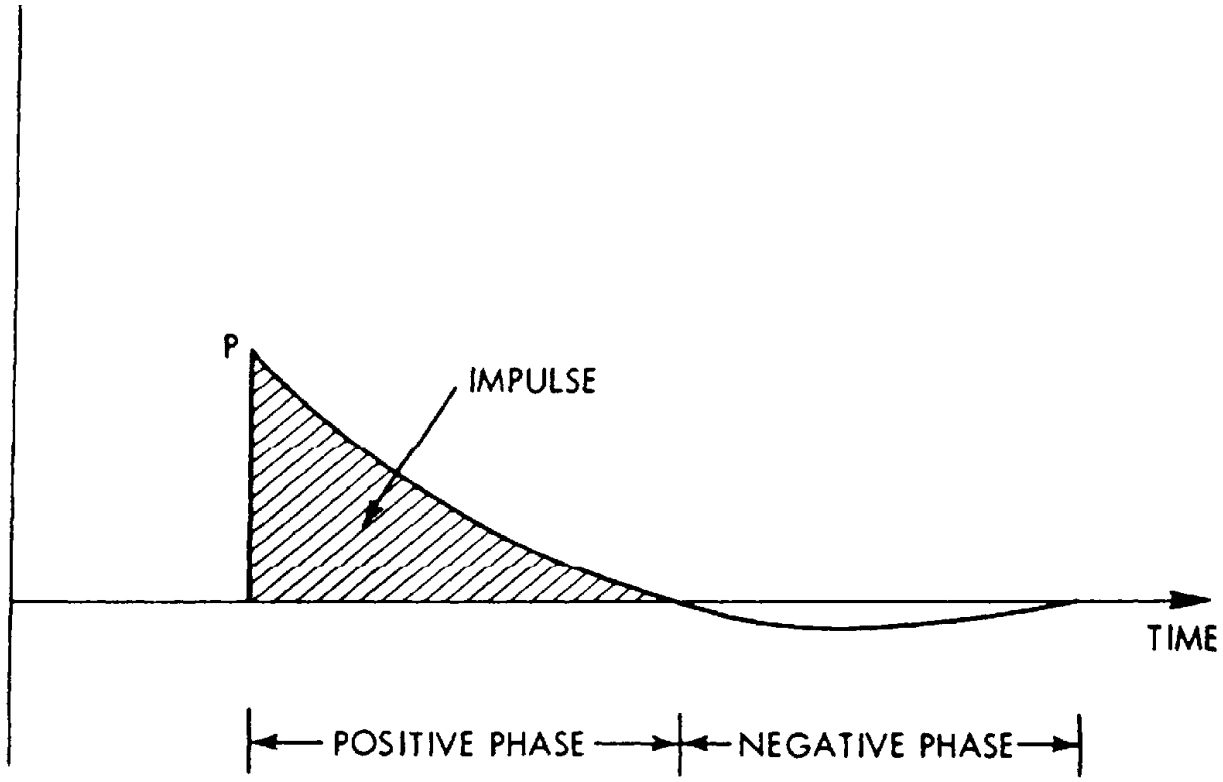

Figure 1. General Characteristics of a Friedlander Waveform; Overpressure vs. Time Source: Walter Reed Army Institute of Research *Public Domain

Blast waves generally consist of an initial shock front, which is a rapid jump in overpressure, followed by a positive overpressure phase that descends into a brief negative overpressure, or underpressure, phase. The negative phase is due to a "suctioning" effect from a partial vacuum that is created after blast as a result of the initial overexpansion of detonation. The positive impulse is the integral of overpressure and time until pressure reaches ambient and is seen by the shaded area in Figure 1. In Equation 1, peak overpressure refers to the peak of the initial shock front and positive phase duration refers to the time between the shock front and when the pressure returns to ambient pressure. Rise time, on the order of one microsecond, is the time it takes for the shock front to reach peak pressure from ambient pressure. A simplified blast wave (Figure 1) is typically what is used in controlled lab environments, but actual blast waves seen in theatre, an area where military events are progressing during warfare, can have multiple peaks and can be quite complex. A blast wave occurs on the scale of milliseconds (ms) and its rapid passage can cause deleterious effects on specimen or structures exposed to it. The blast wind can cause global movement of objects or persons back towards the blast origin due to a

vacuuming event. Another marker of blast is the secondary shock. This is developed from a negative phase due to the initial overexpansion of the detonation source, which creates a lower magnitude shock in the same direction as the incident blast wave.

1.2 Blast Overpressure Measurements

There are several different pressure terms that can describe a blast wave. An introduction into these terms is presented in order to fully assess blast exposure methods. Overpressure is the measurement of pressure relative to ambient level of pressure. Static, or side-on, pressure is the crushing force of the blast and is due to the thermodynamic state of the gas. For an ideal gas, static pressure is:

Equation 2. Static Pressure

$P_s = \rho RT$, where ρ is the density, R is the gas constant, and T is the temperature.

Static pressure is measured by a point where the measurement does not obstruct blast flow, or perpendicular to the flow, and is not exposed to any kinetic energy from the blast wave. Dynamic overpressure measurement is made up of the specific kinetic energy from the blast flow. Dynamic pressure is defined as:

Equation 3. Dynamic Pressure

$P_d = \frac{1}{2}\rho v^2$, where ρ is the local flow density and v is the velocity.

Dynamic pressure is responsible for displacement of exposed objects and cannot be measured by a sensor directly, rather is calculated by:

Equation 4. Relationship between Pressure Types

$P_d = P_t - P_s$, where P_t is the total pressure.

Total, or face-on, overpressure is simply the summation of static and dynamic overpressure (Figure 2) and can be measured using a Pitot-static sensor probe. Reflected pressure is the pressure experienced on a surface exposed to the shock front and is always higher than the total pressure. Mach stem (Figure 2) occurs when the reflected pressure and incident pressure come together to create one pressure wave that is around twice the pressure amplitude. Loading

conditions of a blast wave incorporate all type of pressure, including static and dynamic. Peak reflected pressure has been determined to simply encompass blast loading, defined by:

Equation 5. Peak Reflected Pressure

$P_{refl} = 2P_s + 2.4P_d$ (Iremonger 1997)

Unless otherwise specified, all blast overpressure measurements in this dissertation refer to static overpressure.

Table 1. Various types of pressure definitions. Adapted from (VandeVord 2016)

Pressure Measurement	Definition
Pressure	Describes fluid behavior; the force exerted per unit area or energy per unit volume.
Overpressure	Measurement of a change in pressure relative to ambient pressure.
Static Pressure	Pressure due to the thermodynamic state of a gas; known as the crushing force of a blast.
Dynamic Pressure	Specific kinetic energy of gas flow; referred to as the “blast wind”.
Total or Stagnation Pressure	Combination of static and dynamic pressure; measured by Pitot-static probe.
Reflected Pressure	Peak pressure exerted on a surface exposed to shock front; is dependent on incident shock strength and its angle to the surface.

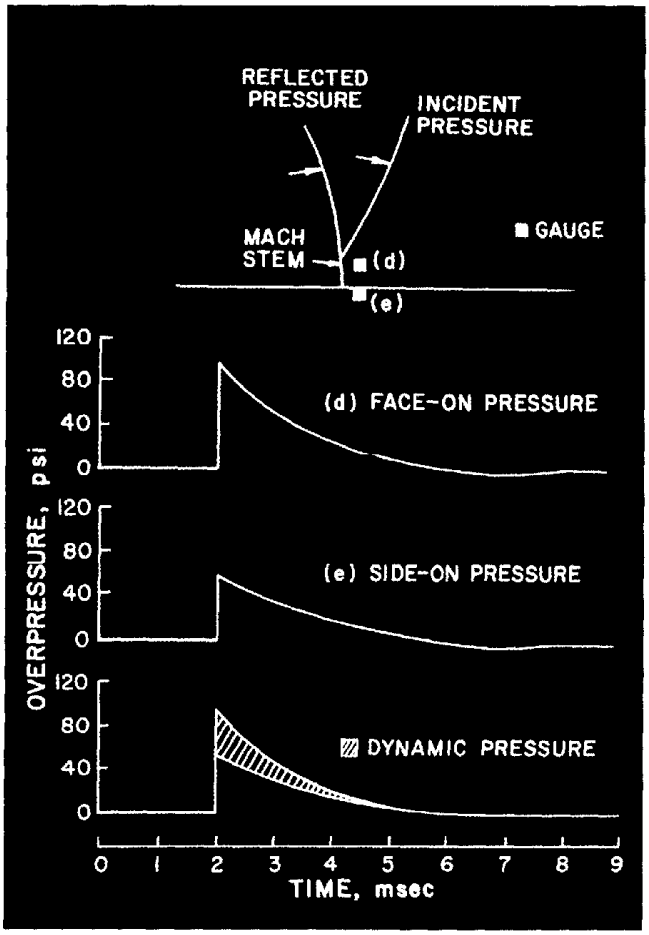

Figure 2. Graph of Face-on and Side-On Pressure (Stuhmiller in Conventional Warfare: Ballistic, Blast, and Burn Injuries). *Public Domain

1.3 Military Concern for Blast Injury

The first reports of injury by "wind of (cannon) ball" referred to injuries of air-filled organs during wartime (Blane 1785, Forbes 1812). Other reports of blast injury precede World War I with a number of cases cited in Clemedson, et al. (Clemedson 1949). Into the 1940s and 1950s, clinical reports of blast injury concerning burns, injury, and patient management were published (Barr et al. 1946, Musselman and Berry 1951, Sullivan 1951). Blast injury to the air-filled organs, especially the lungs, was a major source of initial concern due to mortality (1941). Prevalence and concern for blast lung injury has lessened due to better protective equipment though still remains an issue in in-vehicle environments (Singleton et al. 2013).

One report from World War I stated that soldiers sustained shock with no external wounds visible (Hooker 1924). Another described "shell shock" (headache, amnesia, depression) in soldiers as a result of high explosives in trench warfare during World War I (Mott 1916). The term "shell shock" was thought to be due to blast exposure despite some controversy surrounding its distinction (Jones et al. 2007). While brain injury from penetrating wounds and blunt impact was reported during and after World War II, primary blast-induced brain injury received much more attention and was labeled the "signature wound" of the conflicts in Iraq and Afghanistan (Snell and Halter 2010).

With the increased use of improvised explosive devices (IEDs) in warfare, blast loading is a major concern due to debilitating effects on exposed persons. IED is a generalized term that can refer to many different explosives, ranging from Molotov cocktails to pipe bombs, and are used in military conflicts as well as acts of terrorism (Wightman and Gladish 2001, CDC 2006). Injuries from blasts typically occur at interfaces of differing tissue densities and mechanisms can include spalling, implosion, and shearing forces (Wightman and Gladish 2001).

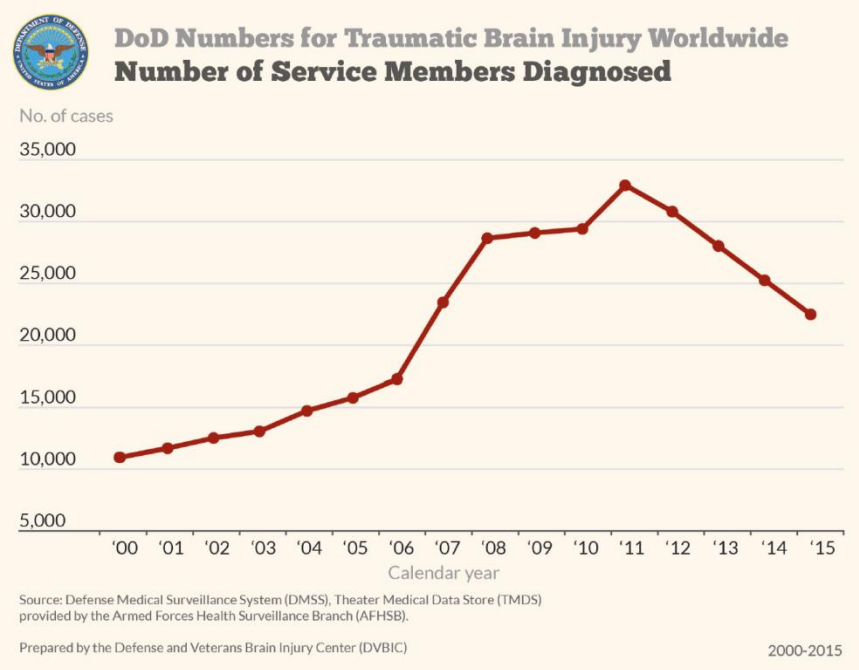

Figure 3. Number of Diagnosed TBIs in Military Service Members from 2000-2015. Source: Defense and Veteran Brain Injury Center. *Public Domain

Blast injuries have increased in the past decade due to increased involvement in overseas conflicts according to Centers for Disease Control and Prevention (CDC 2006). The number of service members diagnosed with traumatic brain injury (TBI) has increased from the early 2000's until 2011 due to the significant military involvement overseas as well as improved diagnostics for TBI (Figure 3). In recent years, these levels have dropped though remain above 20,000 per year. A rise in terrorism worldwide also fuels the TBI crisis as well as polytrauma (Figure 4; from RAND-MIPT Terrorism Incident Database). With the combination of IED usage and unprotected civilians, blast injuries and deaths have increased over the years. Reports from terrorist activity in the Middle East and Europe in the late twentieth century highlight the growing issues and prevalence of primary blast lung injury (PBLI) (Hirsch and Bazini 1969, Hadden et al. 1978, Brismar and Bergenwald 1982, Cooper et al. 1983, Frykberg and Tepas 1988, Katz et al. 1989, Pizov et al. 1999). Even without warfare, blast injuries will be a concern due to the fact that many occupations use explosives during work operations (mining operations, construction/demolition, and law enforcement).

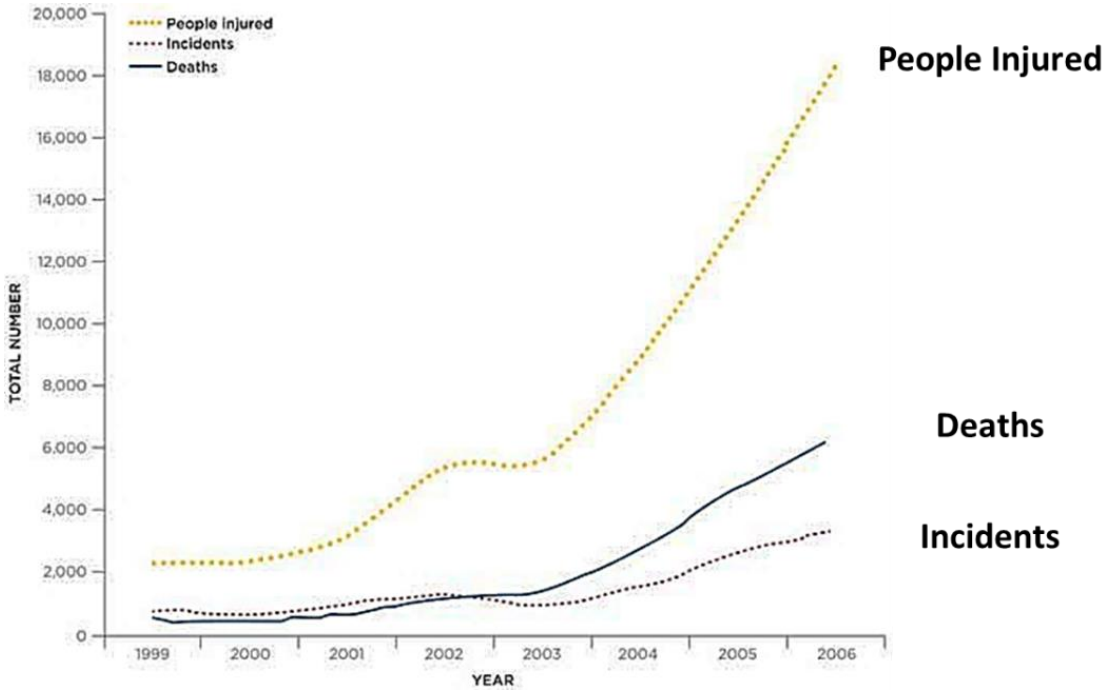

Figure 4. Worldwide Trends in Terrorist Explosive Events (Wolf et al. 2009). Wolf, S. J., V. S. Bebarta, C. J. Bonnett, P. T. Pons and S. V. Cantrill (2009). "Blast injuries." Lancet 374(9687): 405-415. *Fair use

1.4 Types of Blast Injuries

There are various types of injuries that can result from blast exposure (Figure 5). These are delineated by the mechanism of injury.

1) ***Primary blast injury*** is attributed to the static blast overpressure itself. Barotrauma, injury caused by pressure changes, after blast exposure is most commonly found in air-filled organs or at air-fluid interfaces. Injuries to several different organs can occur, including tympanic membrane of the ear, lungs, and the brain (Mackenzie and Tunnicliffe 2011, Yeh and Schecter 2012). While the tympanic membrane has the lowest blast threshold for primary injury, primary blast lung injury is the most life-threatening due to hemorrhage and edema (Coppel 1976). The mechanism by which primary blast exposure injures the brain is not fully understood but reports suggest multiple mechanisms can play a role (Moss et al. 2009, Bolander et al. 2011, Leonardi et al. 2011, Simard et al. 2014, Xu et al. 2016).

2) ***Secondary blast injury*** is due to debris (shrapnel) that strikes the body while carried by the dynamic forces of the initial blast front or the blast. Projectiles, such as metal casing, nails, or glass, are often incorporated into device design (Covey 2002). In addition, missiles, including rocks and dirt, can be accelerated by the blast (Gawande 2004, Rosenfeld 2006). This injury occurs at the site of projectile impact and can be defined as blunt or penetrating trauma (Ramasamy et al. 2008).

3) ***Tertiary blast injury*** occurs when the blast wind propels an exposed person into a solid object. Typically, this is considered a blunt impact of the body against a rigid structure. Concussion can be sustained which can exacerbate brain injury and make it difficult to distinguish from primary and tertiary blast-induced brain injury.

4) ***Quaternary blast injury*** encompasses any other source of injury that occurs as a result of the blast, including chemical exposure and thermal burns. Chemical warfare dates back to World War I and opened the door to this complex public health threat (Fitzgerald 2008). Acute inhalation injury is common after chemical or fire exposure and contributes to acute respiratory failure (Rabinowitz and Siegel 2002). Burns can result in irreversible tissue loss as well as impair system inflammatory and immune responses (Bourdeaux 2008). Lung injury due to chemical exposure and burns overlaid with primary blast lung injury results in devastating consequences.

This type of injury also includes crush injury which is a major cause of death in structural collapses (Arnold et al. 2004).

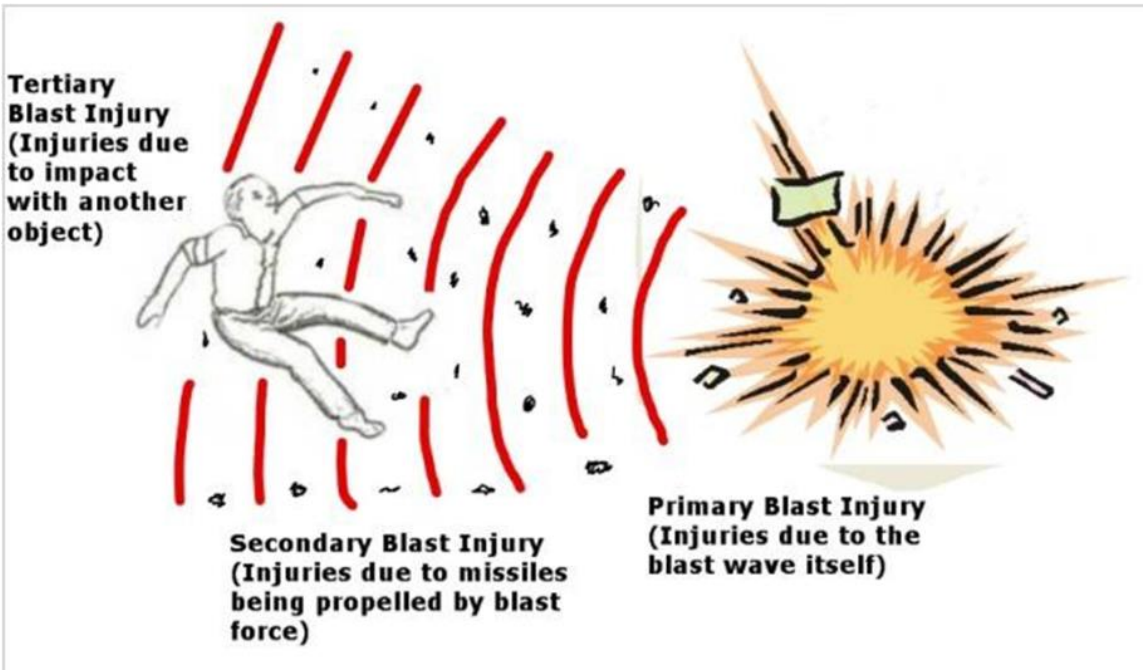

Figure 5. Types of Blast Injury (Stewart 2006). Stewart, C. (2006). "Blast Injuries: Preparing for the Inevitable." Emergency Medicine Practice 8(4). *Fair use

The research presented in this dissertation focuses on the effects of primary blast-induced polytrauma. The model used eliminates any secondary, tertiary, or quaternary effects from the blast (Appendix A).

1.5 Experimental Models of Primary Blast Injury

Pre-clinical research of blast injury has evolved in recent years however methods from producing experimental blast vary. Several experimental approaches are reported within the blast neurotrauma literature. Various methods may contribute to varied findings surrounding time course, recovery and extent of primary and secondary injury mechanisms in blast-induced neurotrauma (BINT). For those interested in studying the effects of blast overpressure (BOP) on the brain, isolation of the primary blast wave is crucial. However, some studies have examined the effect of composite injuries involving multiple injury modes (Svetlov, 2012 #42). Others

have studied the combined effects of primary and quaternary blast injuries in what is referred to as a burn-blast model (Chai et al. 2013). Knowing the exact blast parameters used to cause injury is crucial for comparison between data gathered from each of the research models.

1.5.1 Open Field Explosive Testing

Open field detonations (Figure 6A-B) use an explosive to induce BINT. An explosion is a phenomenon that results in a sudden release of energy and creates a blast wave which propagates outward from the explosion. Trinitrotoluene (TNT) is commonly used in varying amounts depending on the magnitude of the detonation required for animal testing. One advantage of conducting open field testing is that there is no flow hindrance of the blast wave, which allows for testing of either larger animal models or multiple small animal models (Axelsson et al. 2000, Pun et al. 2011, Rubovitch et al. 2011). On the other hand, administering anesthesia and controlling for bacterial exposure to survival animals is more difficult in the harsh outside environment.

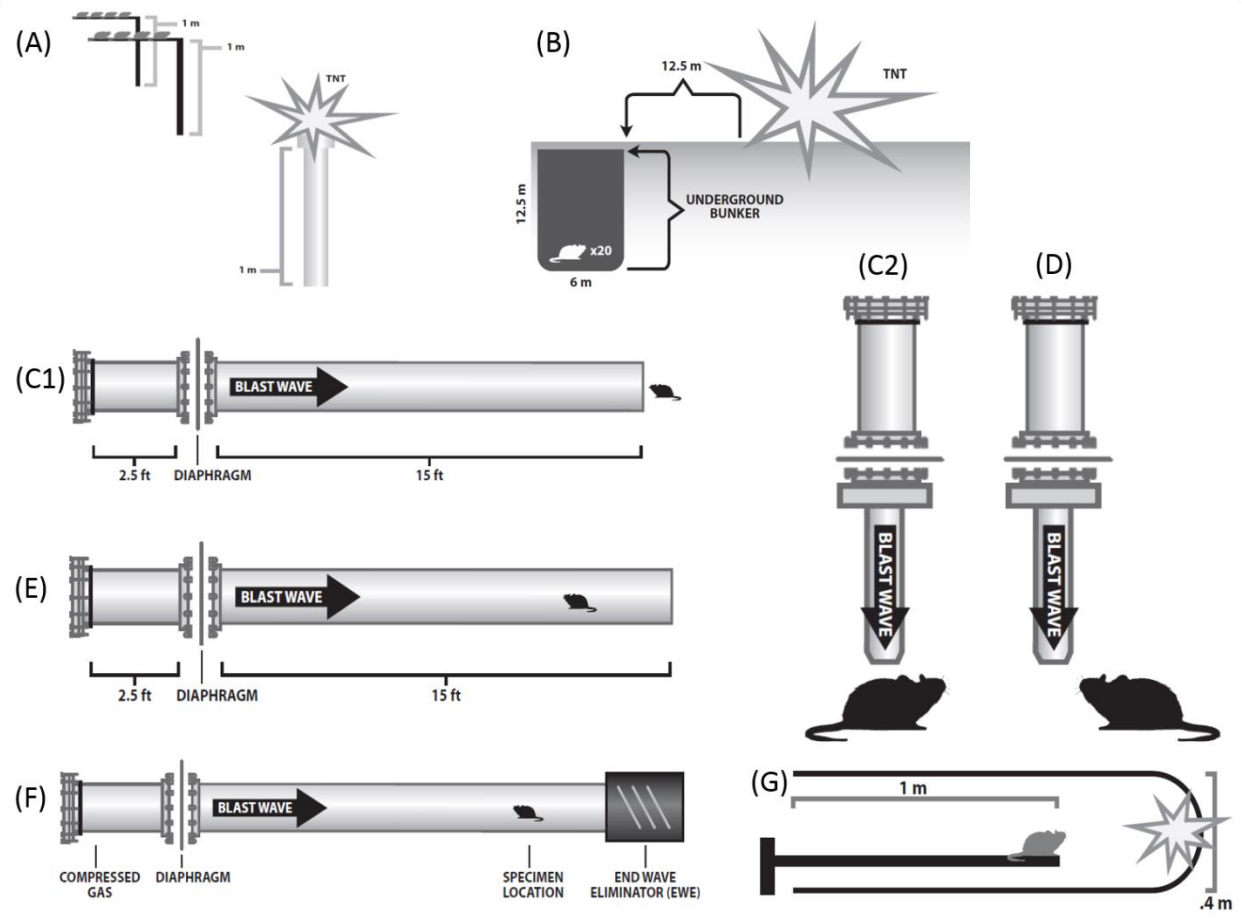

Figure 6. Diagram of open field, shock gun, and blast simulator set-ups.

While detonations are arguably the most successful in recreating battlefield explosions, a limitation is that repetition of the same testing conditions is nearly impossible given variability between explosive devices and reflections of the blast wave. This makes reproducing results and testing set parameters of blast overpressure and duration a formidable task. Though this may mimic IED warfare in theatre, consistent exposure is crucial for obtaining statistical significance within research data. Static overpressure profiles do not resemble the ideal Friedlander waveform and positive durations have been measured up to 18 ms (Pun et al. 2011). Obtaining the clearance to perform open field blast studies in an approved facility is difficult. Yet, some researchers have used explosives in conjunction with blast tubes to replicate battlefield explosions in an experimental environment, eliminating the need for open space (Saljo et al. 2000). Another drawback is that secondary injuries, such as those sustained from debris, often occur with explosives set-ups, thus pre-cautions (e.g. animal shielding) are required in order to limit studies to primary injuries. While it is difficult to isolate primary blast wave, animal protection such as containment within a cage has been utilized for open field blasts (Kaur et al. 1995, Rubovitch et al. 2011).

1.5.2 Shock Guns

Since live detonation testing is not optimal for research laboratories, several devices have been constructed to recreate shock waves. The shock gun method consists of a narrow tube (usually vertical) that contains a driver and driven tube separated by a diaphragm. Burst of the diaphragm creates a shock wave that is transmitted to a specimen positioned outside of the tube. In this set-up, positioning of the animal is crucial in terms of achieving exposure to static overpressure without exposure to the dynamic winds. The effects of positioning the animal perpendicular to the shock wave have been studied, and it was found that this orientation causes head accelerations atypical of blast TBI (Gullotti et al. 2014). Placing the animal directly under the tube causes very high dynamic overpressure exposure that is not representative of open field blast exposure. The fast expansion of the wave leaving the narrow tube causes rapid dissipation of energy and can therefore make it difficult to produce an accurate free-field blast wave. The combination of the emerging shock wave and venting gas causes the formation of a vortex and high flow velocity region called end-jet. As such, researchers using this device have modified

their methodology (Figure 6D) so that the animal is offset from the end-jet and not exposed to reflections (Svetlov et al. 2010, Yeoh et al. 2013). One advantage of using this method is that it is possible to use on a laboratory bench top due to the smaller size of the device. However, appropriate measurements need to be collected to verify that the conditions resemble an appropriate blast environment.

1.5.3 Blast Simulators

Historically, conventional shock tubes (ST) have been used to mimic blast conditions within the laboratory setting. This method allows for manipulation of the shock wave within a controlled environment with high repeatability. Most recently, modifications to the ST have led to the design of the Advanced Blast Simulator (ABS), which was designed to intrinsically replicate all the key features of blast wave flow conditions, including the negative phase and secondary shock as described previously by VandeVord et al. (VandeVord et al. 2012). The ST is composed of two separate chambers: the driver, where the pressure is created by means of an air compressor system or other gas, and the driven, where the shock wave propagates through the test section (Celander et al. 1955). Because the wave is produced by compressed gas bursting a membrane instead of an actual chemical explosion, the term shock wave is used instead of blast wave. It is important to understand how the shock wave develops within the tube and how end-of-tube rarefaction leads to an imbalance of high dynamic pressures yet reduced static pressure conditions, amounting to extremely adverse effects. Thus, experiments staged with a specimen near the end of the tube, where the static pressure decreases and dynamic pressure increases, should be avoided. In order to create a more accurate blast environment for animal testing, the ABS was designed (VandeVord et al. 2012). There are three chambers in the ABS device (Figure 6F): a driver, driven, and end-wave eliminator (EWE). The EWE consists of a dump tank that can contain the expanding gases from entering the lab-space and at the same time creates some overpressure reflection that counteracts the rarefaction wave. Baffling is incorporated into the EWE to break up the venting shock front and eliminate the waves from traveling back up the device, in contrary to the ST which has an open end causing a reflection of the wave and exposing the animal to multiple extraneous shocks that do not exist in real blast conditions. A disadvantage of using either the ST or ABS designs is that shock flow constraints require less than twenty percent restriction of specimen in the device in order to recreate the most accurate blast flow conditions. Large animal studies would require a much larger chamber (approximately

16 square foot cross section) or the addition of an expansion section for optimal flow specifications, which ultimately leads to laboratory space concerns.

1.5.4 Optimization of Blast Method

There are several variables that can be adjusted in shock/blast wave simulation in order to change injury modes and modify the application of the blast model. All of these variables can be tailored to create a specific injury due to settings surrounding blast exposure. These variables include, but are not limited to:

1. Blast Physics

The static and dynamic overpressure sensed by the test animal can be adjusted at the driving source of the experimental set-up or by the distance the animal is from the driving source of the blast. For open field testing with explosives, the amount of explosive used can be adjusted to increase or decrease the overpressure of the wave. In shock tube, shock gun, or blast simulator set-ups (Figure 6), a greater internal driver overpressure upon membrane burst will produce a higher blast overpressure in the test area for the specimen. For passive membrane ruptures, this is typically accomplished by increasing the thickness of the membrane or choosing a material that can sustain higher driver overpressure. In blast set-ups that utilize active membrane rupture techniques, the driver overpressure can be adjusted by the user. In all set-ups, changing animal distance from blast wave generation will affect the overpressure exposed to the animal.

2. Animal Position

The position of the test animal with respect to the tube can change the static blast overpressure profile as while as dynamic overpressure portions of the blast wave. If the shock tube has an open end, a rarefaction is created when the shock wave reaches the end of the tube. This creates increased out-flow velocity and recompression shock comes back toward the animal (VandeVord 2016). To effectively simulate explosive blast, animals should not be placed near the end of tube in these conditions. On the other hand, animals need to be placed far enough from the shock wave generation so the wave can properly form by the time it reaches the test location. The animal body should be fully enclosed in the tube as openings surrounding the animal would cause wave reflections on the specimen.

3. Animal Orientation

The orientation of the animal can determine what part of the animal's body is impacted first by the shock front. This can also determine overpressure gradients experienced within the body (head to toe; left to right), which can vary mechanism of primary blast exposure. If the model is for whole body exposure, orientation can determine extent and mechanism of the sustained lung injury.

4. Animal Harness

The harness or sling the animal is held in can actually contribute significantly to the type of injury or blast experienced. A sling with some ability to move with the dynamic blast wind will allow the animal to primarily be injured by static overpressure. An animal that is held in a rigid holder can potentially sustain blunt trauma if the blast wind propels the animal against the rigid surface. Also, if the harness constricts the body and leaves the head exposure, acceleration injury can be sustained (head motion relative to the thorax/body) (Garman et al. 2011).

5. Additional Factors

Relating to animal position, end wave eliminators can effectively eliminate any reflection of the blast wave back to the animal. This can ensure that the animal only experiences one "free-field" exposure to the blast wave, resembling a Friedlander blast curve. The animal can wear protective equipment to mitigate injury to organs underlying the shielding (Xu et al. 2016). As static overpressure causes a "crushing" force around the specimen, protective equipment occasionally does not prevent all underlying organ injury.

Overall, there are many inconsistencies between researchers in the methodology of inducing bTBI due to the high number of variables that can affect primary blast injury. These inconsistencies manifest in altered pathology due to the modes of injury and the injury severity. Some methods do not accurately recreate the free-field blast wave or use incorrect animal positioning, which can introduce secondary and tertiary forms of injury and are unrepresentative of BINT. This has become such a significant concern that the NIH/NINDS has recently developed a list of common data elements (CDEs) for pre-clinical TBI research to promote the

use of standard reporting and facilitate comparisons across studies (Hicks et al. 2010). The need for standardization in small animal research is crucial to advancing the field.

Chapter 2: Developing a Model of Blast Polytrauma

2.1 Introduction

2.1.1 Statement of Problem

While the military has taken protective measures to mitigate injury to the thorax and lungs during a blast exposure, PBLI is still evident in mounted/in vehicle cases during military conflicts (Singleton et al. 2013). Moreover, civilians, who are unprotected from blast exposure, can be severely harmed by terrorist attacks that use improvised explosive devices. Since the lungs are the most susceptible organ due to their air-filled nature, PBLI is one of the most serious injuries seen in civilian blast cases. Although PBLI has recently developed as a primary issue in traumatic injuries from IED exposure, the incidence is rising (Figure 4) so the need to understand pathology of primary blast to the lungs is needed now more than ever.

2.1.2 Significance

Determining lethality threshold for rodent studies is crucial to guide experimental designs centered on therapies for survival after PBLI or mechanistic understanding of blast-induced polytrauma (BPT) itself. Lethality risk trends based on static blast overpressure for rodent models may help in standardizing animal studies and contribute to scaling to the human level. Lethality thresholds for minor, moderate, and lethal primary blast to the lungs will give an indication of blast overpressure ranges to guide pre-clinical rodent studies. Patterns and severity of internal hemorrhaging could give indication of mechanisms relevant to blast exposure in terrorist bombings. Severity of lung injury could also play a role in secondary mechanism progression in BPT studies.

2.2 Literature Review

2.2.1 Lung Anatomy

The lungs are situated in the thoracic cavity and the right and left lung are separated by the mediastinum. The apex lies right above the first rib and base is concave and sits on the diaphragm. Each lung has a hilum where the root of the lung is located, which provides entrance

for the pulmonary arteries and veins as well as the bronchus. The pleural cavity is located between the visceral pleura, covering the surface of each lung, and the parietal pleura, which is attached to the inner surface of the thoracic cavity. Intrapleural pressure refers to the pressure in the pleural cavity and when the diaphragm contracts and the rib cage expands, intrapleural pressure is negative to facilitate inhalation. Blast injury can cause pneumothorax, which is usually described as a collapsed lung as it uncouples from the chest wall due to abnormal air accumulation in the pleural space (Phillips 1986).

The respiratory tract starts with the trachea and branches into bronchi (primary, secondary, and tertiary). Further branching continues to the bronchioles and lobules, which are the functional unit of the lung. The lobules house the respiratory bronchioles which branch into alveolar ducts and alveolar sacs. Oxygenation of the blood occurs at the alveoli-capillary interface. The lungs receive dual blood supply through systemic and pulmonary circulation.

General lung function and anatomy is similar between human and rodent lungs, though size and structure are vastly different. Even though rodents and humans have the same amount of lobes (five), human lungs have three on the right and two on the left, while rodent lungs has four lobes on the right and one lobe on the left (Figure 7). This discrepancy in lobe positioning could play a role in the macroscopic injury mechanism during blast exposure to the lungs.

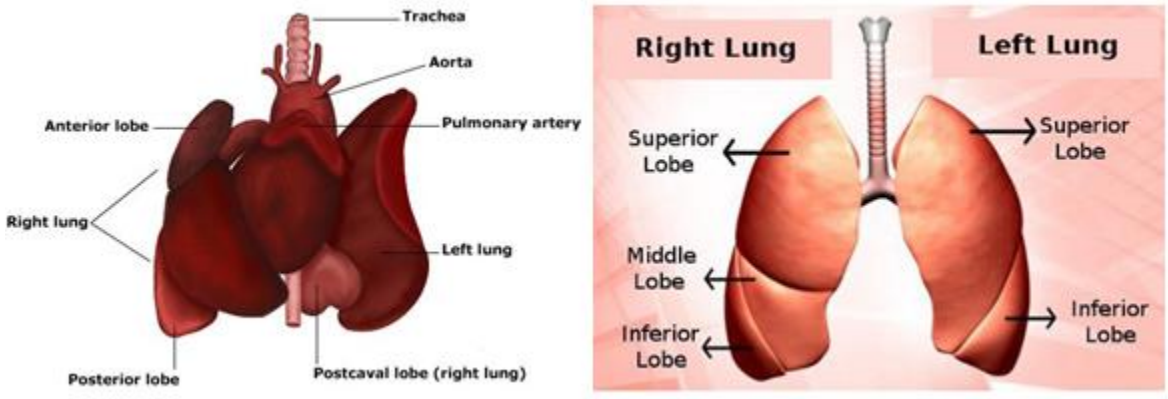

Figure 7. Rat, left, and Human, right, Lung Diagrams (Ruiz Junior et al. 2005). Ruiz Junior, R. L., L. R. de Carvalho and A. J. Cataneo (2005). "Compensatory lung growth: protein, DNA and RNA lung contents in undernourished trilobectomized rats." Acta Cir Bras 20(3): 219-224. *Fair use

Table 2 demonstrates size and structure differences between rodent and human lung (Tenney and Remmers 1963, Valerius 1996, Irvin and Bates 2003).

Table 2. Structural and Size Lung Differences between Rodent and Human

	Rodent	Human
Total Lung Capacity	10 mL	6,000 mL
Parenchymal fraction of the total lung	24%	12%
Size of alveoli	70 µm	200 µm
Blood-gas barrier thickness	0.38 µm	0.62 µm
Airway generations	Around 17	17-21

2.2.2 Transmission of Blast Overpressure to Lungs

The lungs are especially vulnerable to primary blast overpressure due to their air-filled nature. As seen in Figure 8, the air in alveoli is easily compressible and decompressible (implosion effects). The rapid exposure, usually less than twenty milliseconds, causes shear forces at the density interface (inertial effects). Blast overpressure causes injury to the lungs through several mechanisms (Mackenzie and Tunnicliffe 2011):

1. ***Spalling*** arises from high-low density mismatch and causes acceleration of high density material followed by expansion of low density phase. In terms of blast loading, spalling refers to fragmentation of material after the blast exposure. In the human body, this mechanism occurs at the rib cage/lung tissue interface as well as the alveolar/capillary interface due to density mismatch.

2. ***Implosion*** consists of rapid compression and decompression of gas-filled tissues. Implosion plays an important role in the process of cavitation, or rapid formation and implosion of bubbles caused by pressure changes. ***Cavitation*** has been shown to cause tissue injury (Nakagawa et al. 2011). Implosion itself can occur in any air-filled organ but all airways can be affected in the lungs (Forbes 1812).

3. ***Inertia*** refers to shearing of tissues of differing density levels, which are divergently accelerated by the shock wave. Energy is released at transition sites and focal mechanical

damage can result (Gean 2014). The result of high frequency waves on abrupt density interfaces, such as those in the lungs, is debilitating and causes micro-tearing of density barriers.

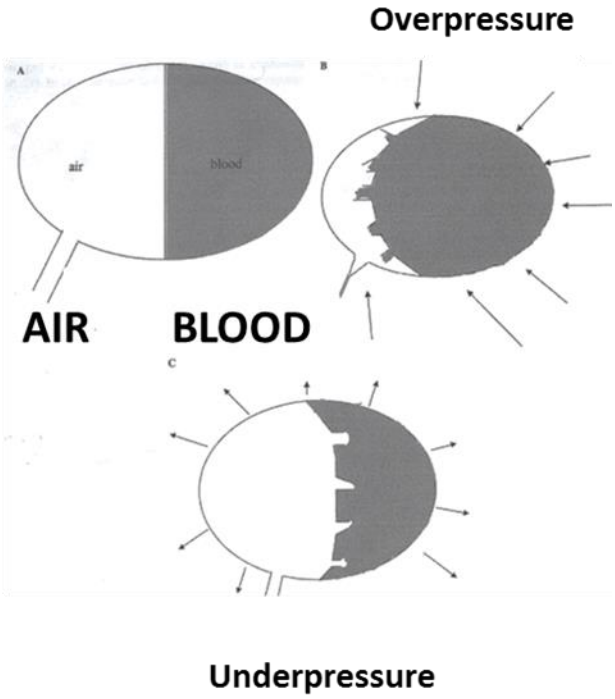

Figure 8. Vascular Mechanics at Capillary-Alveolar Interface in Lungs (Kuehn et al. 2011). Kuehn, R., P. F. Simard, I. Driscoll, K. Keledjian, S. Ivanova, C. Tosun, A. Williams, G. Bochicchio, V. Gerzanich and J. M. Simard (2011). "Rodent model of direct cranial blast injury." J Neurotrauma 28(10): 2155-2169. *Fair use

Pulmonary hemorrhaging occurs after BOP exposure to the thorax and is often due to the underpressure phase when the gas expands and compresses the blood vessels (Fung et al. 1988). Overstretching of the alveolar membrane by gas trapped in alveoli causes microscopic lung trauma (Fung et al. 1988). Hemorrhaging and edema in the lungs has been shown to positively correlate with peak blast overpressure (Elsayed 1997). Cited as the second most sensitive organ (tympanic membrane of the ear) to blast overpressure, primary blast lung injury is considered the most serious injury due to internal hemorrhage and hypoxia, which can lead death when severe (Elsayed 1997). On a macroscopic scale, pulmonary contusions are often seen as the soft tissue of the lungs interacts with the rigid rib cage and costal spaces. Injury mechanism to the lungs is highly dependent upon orientation of the specimen to the blast wave origin. Research in PBLI

usually treats the lungs as a continuous organ, so susceptibility of individual lobes to injury has not been ascertained in rodents or humans (Skotak et al. 2013).

2.2.3 Incidence of Primary Blast Lung Injury

The first informal reporting of lung injury from the "wind of (cannon) ball" was found around the 1800s (Blane 1785, Forbes 1812). Lung hemorrhage due to blast was one of first findings and one of the first pre-clinical blast experiment was performed in 1957 (Clemedson 1957). PBLI is a major cause of immediate mortality following IED strikes (Yeh and Schecter 2012). PBLI is particularly more frequent when exposure occurs in enclosed spaces. Fatal injury percentage is significantly increased when soldiers were exposed to the blast wave in vehicle compared to on foot, in terms of PBLI (Singleton et al. 2013). This phenomenon is speculated to occur in vehicle due to multiple reflections of the shock wave inside the vehicle once the vehicle shell is breached, i.e. underbody blast. In recent Israeli conflicts, half of all civilians injured in terrorist bombings suffered acute lung injury, which required immediate treatment (Aschkenasy-Steuer et al. 2005, Bala et al. 2010). Blast lung injury and thoracic trauma is common and almost always causing fatalities after blast exposures during terrorist activities (Marti et al. 2006, Turegano-Fuentes et al. 2008). It is also known that currently used treatments for lung and brain injury following BOP exposure can often contradict each other, so finding new treatments for lung injury is necessary for improving clinical interventions for cases of blast polytrauma (Hicks et al. 2010). From 2003 to 2009 for U.K. soldiers involved in military conflicts, less than 50% of patients that exhibited evidence of PBLI survived to reach a medical facility. Out of those that did survive, eighty percent required immediate ventilation support (Smith 2011). The need for a first responding treatment is vital in order to increase the chance patients with PBLI can survive to receive the needed intervention. The incidence of blast lung injuries seen in theatre increased from the Iraqi conflict to the war in Afghanistan for troops, demonstrating a growing clinical burden (Smith 2011). In many hospitals, physicians have the resources to adequately treat blast lung trauma, so having acute treatment to prolong survival in the prehospital stage would allow patients the opportunity for life-saving care (Ritenour and Baskin 2008).

2.2.4 Pre-clinical Blast Lethality Research

Blast lethality due to lung injury has been investigated since the late 1960s. Bowen et al. conducted multi-species blast experiments with a large sample size of over 2,000 subjects

(Bowen 1968, Bowen et al. 1968). This series of tests established the Bowen curves, which constitute the blast lung lethality thresholds of man, and were the first to highlight body mass as a scaling parameter for blast lung injury. While this still serves as a benchmark, there is more need of characterizing lethality risk for unscaled rodent studies

A thorough literature review was conducted in order to identify overpressure ranges previously used for rat experimentation. Few published reports have used rat models to investigate PBLI. Moreover, the experimental set-up greatly varies between research groups, which lead to conflicting results. Collectively, overpressures ranging from 62 - 136 kilopascals (kPa) have been investigated with variable time points for survival (Elsayed 1997, Gorbunov et al. 1997, Gorbunov et al. 2004). However, there are reported results of exposing rats to extremely high overpressures in the range of 550 - 827 kPa (Cooper et al. 1991, Irwin et al. 1998). A general consensus is that ranges between 60-100 kPa peak overpressure produces low level blast injury, ranges between 100-140 kPa produces moderate level blast injury and >180 kPa produces severe blast injury. To further the confusion, there is a lack of adequate evidence documenting the exact pressure wave pulse across the entire range of published results. This is a critical element because the time duration of exposure is a well-known characteristic of most other injury phenomena and likely plays a role in tissue damage. In conclusion, there is not an established lung injury threshold for transitioning between the overpressure levels.

Choosing studies for comparison of lethality must be methodical and precisely done to construct an appropriate threshold. The different modes of injury procurement vary widely and the injury model intended is important for consideration. Many methods have been utilized to create blast-induced lung injury, including percussive nail guns, high-energy explosives, and compressed-air driven shock tubes (Badami et al. 2007, Chavko et al. 2008, Chai et al. 2013). Since the shock tube method can have the most consistency and is most similar to the method used in the experimental study at hand, only shock tube and blast wave generator studies were included in comparing lethality risk thresholds. Only blast-induced lung models were included, since blast-induced brain injury models often utilize drastically different settings, including overpressure values and orientation of specimen. Also, the recorded values of overpressure need to be static overpressure since that is the load bearing parameter commonly used in reporting of blast magnitude. All studies that utilized pharmacological interventions or other protective

measures, such as vests covering the thorax, were excluded. Overall, thirteen additional studies that used around 330 rats were included in lethality risk comparison to the current experiment work (Bauman et al. 1997, Elsayed 1997, Gorbunov et al. 1997, Elsayed et al. 2000, Gorbunov et al. 2003, Gorbunov et al. 2004, Chavko et al. 2006, Gorbunov et al. 2006, Chavko et al. 2008, Flierl et al. 2008, Seitz et al. 2008, Chai et al. 2013, Skotak et al. 2013). All studies either used compressed air or helium to drive the shock tube for BOP administration. Table 3 signifies current lethality research of small animal models due to primary blast injury that was used for comparison:

Table 3. Small Animal PBLI Studies

Author	Orientation to Blast	Method on Primary Blast	Peak Overpressure	Lethality Rate
Chai, et al.	Suspension mounts (left side towards blast source)	Combined-compression explosive column (explosives)	61.00	0
Skotak, et al.	Prone position, attached to bed	Helium-driven shock tube	130.00	0
			190.00	30%
			230.00	0
			250.00	24%
			290.00	100%
Chavko, et al.	side exposed	compressed-air driven shock tube	165.00	35%
Chavko, et al.	side exposed	compressed-air driven shock tube	120.00	10%
Gorbunov, et al.	side exposed	compressed-air driven shock tube	118.00	8%
Gorbunov, et al.	side exposed	compressed-air driven shock tube	118.00	25%
Gorbunov, et al.	side exposed	compressed-air driven shock tube	86.00	0%
	side exposed	compressed-air driven shock tube	112.00	0%
Seitz, et al.	supine position, thorax	compressed-air driven shock tube	76.00	10%
	supine position, thorax	compressed-air driven shock tube	76.00	10%
Flierl, et al.	Thorax	compressed-air driven shock tube	73.00	5%
Elsayed, et al.	side exposed	compressed-air driven shock tube	62.00	0%
Elsayed, et al.	side exposed	compressed-air driven shock tube	62.00	0%

			136.00	0%
Bauman, et al.	side exposed	compressed-air driven shock tube	129.00	50%
			83.00	0%
Gorbunov, et al.	side exposed	compressed-air driven shock tube	62.00	0%

2.3 Methods

2.3.1 Animal Procedures and Blast Overpressure Exposure

The Virginia Tech Institutional Animal Care and Use Committee approved experimental protocols described herein. Prior to all experiments, male Sprague Dawley rats (~325 g, ~3 months old, Harlan Labs, San Diego) were acclimated to a 12 hour light/dark cycle with food and water provided ad lib. Male rats at this age were selected for easy comparison to other blast injury rodent models. Animals (n=26) were exposed to a single incident pressure profile resembling a 'free-field' blast exposure within the 130 to 190 kPa range, selected according to literature values for rodent lethality from PBLI.

Prior to blast exposure, rats were anesthetized with a ketamine/xylazine solution, in accordance with the rodent weight, to have sedation over the entire time point of one hour. The shock front and blast overpressure were generated by a custom-built ABS with an end wave eliminator (ORA Inc. Fredericksburg, VA) located at Center for Injury Biomechanics of Virginia Polytechnic Institute and State University (Hockey et al. 2013). The driver and test section were separated by acetate membrane, which creates the blast wave upon burst. Contrary to other blast simulators, the Advanced Blast Simulator has an end wave eliminator attached to the test section that diffuses the shock wave, ensuring the animal is only exposed once to the wave. A peak static overpressure was produced with compressed helium and calibrated acetate sheets (Grafix Plastics, Cleveland, OH) that were varied to produce a range of BOP. Pressure measurements were collected at 250 kHz using a Dash 8HF data acquisition system (Astro-Med, Inc, West Warwick, RI) and shockwave profiles were verified to maintain consistent exposure pressures between subjects. Peak overpressures were calculated by determining wave speed (m/s) at specimen position. A mesh sling was used to hold the animal during the exposure that allowed for minimal hindrance of the wave through the tube in addition to holding the animal in a prone position with

the right side of the thorax facing the shock wave driver. Peak overpressure is followed by an exponential decay (2.5 ms positive duration) and a short negative phase. A representative blast wave profile is seen at the bottom (170 kPa).

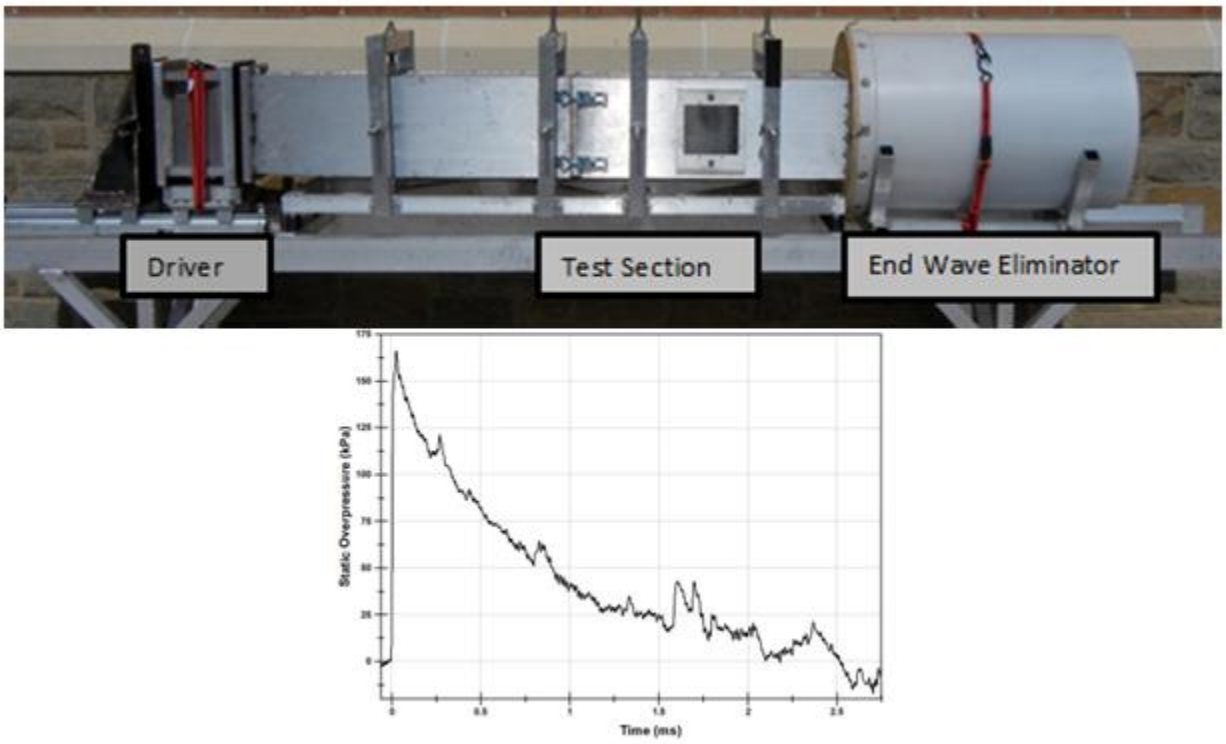

Figure 9. (Top) Advanced Blast Simulator. (Bottom) Representative Blast Wave Profile

After the blast exposure, animals were removed, returned to a warm pad and injected with sterile phosphate buffered saline (500 microliters (µls)) via tail vein injection, crucial for simulating any post-exposure injection. All large organs were immediately collected in animals that did not survive the blast exposure. Animals that survived the one-hour time assessment were sacrificed by transcardial perfusion with ice-cold phosphate buffered saline (PBS) and 4% paraformaldehyde.

2.3.2 Lung Injury Severity

Examining macroscopic images of the lungs after blast gives insight into mechanism of lung contusion after sustaining blast exposure to the thorax. Imaging of the lungs occurred immediately after removal from the specimen. Macroscopic damage and gross characteristics

were noted to determine any landmarks associated with increased peak overpressure and to investigate if specific injury patterns could be determined.

2.3.3 Lung Histology

After collection, lungs were stored in a 4% paraformaldehyde fixative solution. After 48 hours in fixative, the lungs were placed in 30% sucrose solution for tissue sectioning preparation. Lungs were separated into cassettes with each lobe isolated for analysis. Samples were then cut (8 micrometers (μm)) and stained with hematoxylin and eosin (H&E) to predict injury extent. Images were taken of three regions of interest in each lung tissue section at 10X magnification (Zeiss AxioCam ICc 1). These three images were converted to black and white and optical density readings were collected in order to determine the level of hemorrhaging in the lung tissue using Image J software (NIH, Bethesda, MD). Global assessment of all lobes was done to show internal hemorrhage after blast compared to sham.

2.3.4 Statistical Analysis

A one-variable linear logistic regression was performed on the experimental data obtained in this study in terms of static overpressure (SOP). Even though it has been suggested that a non-linear form is needed for short-duration blasts, using unscaled rodent tests and a consistent method of BOP stimulus (shock tube) provides for linear analysis (Bass et al. 2008). The model in equation form is:

Equation 6. Lethality Risk Logistic Regression

$$A = {}^{1}/_{(1+\exp(\beta_0+\beta_1*SOP))}$$

where A is the probability of lethality, SOP is the static overpressure, and parameters β0 and β1 are calculated and optimized. Logistic regression was completed using Matlab (Version R2012a, MathWorks, Natick, MA).

The model was assessed using the C-statistic or the area under the receiver operating characteristic curve, which compares sensitivity to (1-specificity) of the data obtained. Analysis

was done similarly to other computations on lethality risk (Bass et al. 2008). Statistical analysis of the coefficients was also performed in Matlab examining contribution to the model. Microsoft Excel was used to calculate a linear fit (R2) of the histological results.

2.4 Results

2.4.1 Lung Injury – Gross Observations

It was observed that the median lobe in all animals demonstrated noticeable macroscopic hemorrhaging. With increased overpressure magnitude, there was an increase in the number of lung lobes that were affected and appeared hemorrhaged. Figure 10 provides examples of macroscopic lung images. The images correspond to increasing level of BOP: A -156 kPa, B – 162 kPa, C – 180 kPa, D -182 kPa, and E - sham (0 kPa).

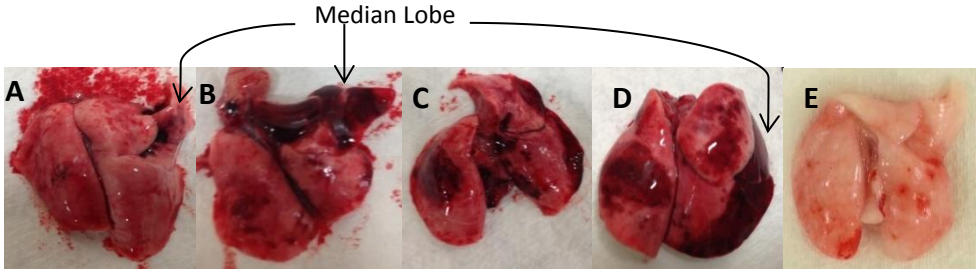

Figure 10. Macroscopic Images of Lungs Post-Blast

Results are consistent with other studies testing effects of blast peak pressure on lung injury severity (Skotak et al. 2013).

Marking of contusion against rib cage in the left lung were seen in blast exposure to right side of animal (Figure 11). This is reportedly due to decompression of the lungs against the rib cage during the negative phase of the blast wave. Traditional explanation of "rib markings" is now believed to be intercostal space markings (Clemedson 1950). It was also reported that these markings are not of hemorrhage but consist on collapsed alveoli (Fung 1985).

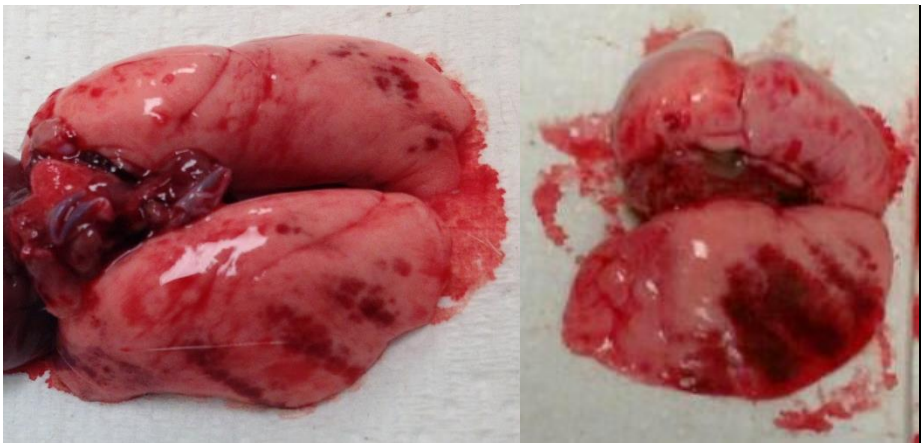

Figure 11. "Rib markings" after blast exposure directed to the thorax.

Another frequent finding was that a large hemorrhage was sustained on the left lobe and accompanied by contusion along the edge of all right lobes, especially the middle and lower lobes (Figure 12). Similar findings were reported as overpressure levels increased in a rat model of blast polytrauma (Skotak et al. 2013).

Figure 12. Lung contusion after blast exposure around 195 kPa static overpressure.

2.4.2 Internal Hemorrhage – One Hour Outcomes

Animals given varied degrees of BOP were analyzed and grouped according to outcome (survival and non-survival). The bronchiole in Figure 13-A2 is filled with blood indicated severe hemorrhaging and possible hemothorax.

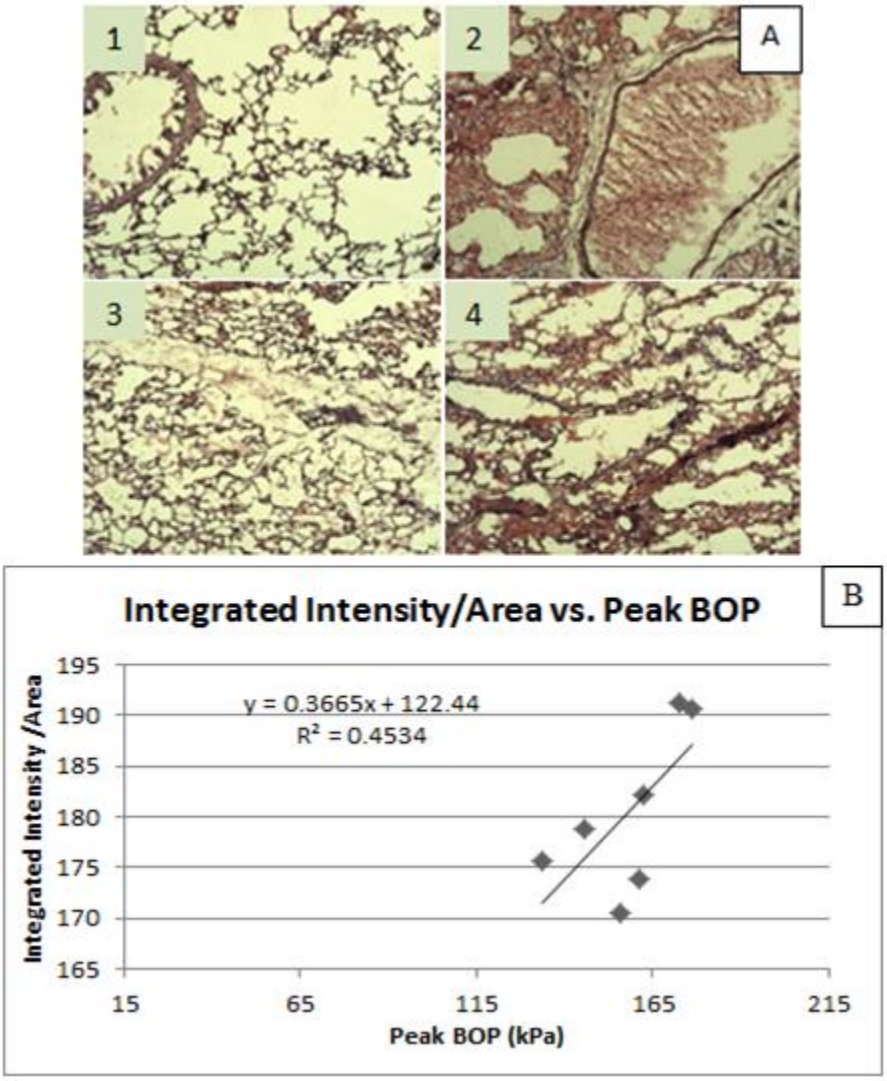

Figure 13. (A) H&E Staining of the Median Lobe Post-Blast. (B) Integrated Intensity/Area vs. Peak BOP

In Figure 13, images 1 and 3 were taken from an animal in a lower pressure group (130 kPa) that remained alive following the blast. Images 2 and 4 were from an animal in a higher pressure group (175 kPa) which died within the one hour time frame following blast. Integrated

intensity normalized to the area of the image was used to characterize the amount of bleeding within the median lobe.

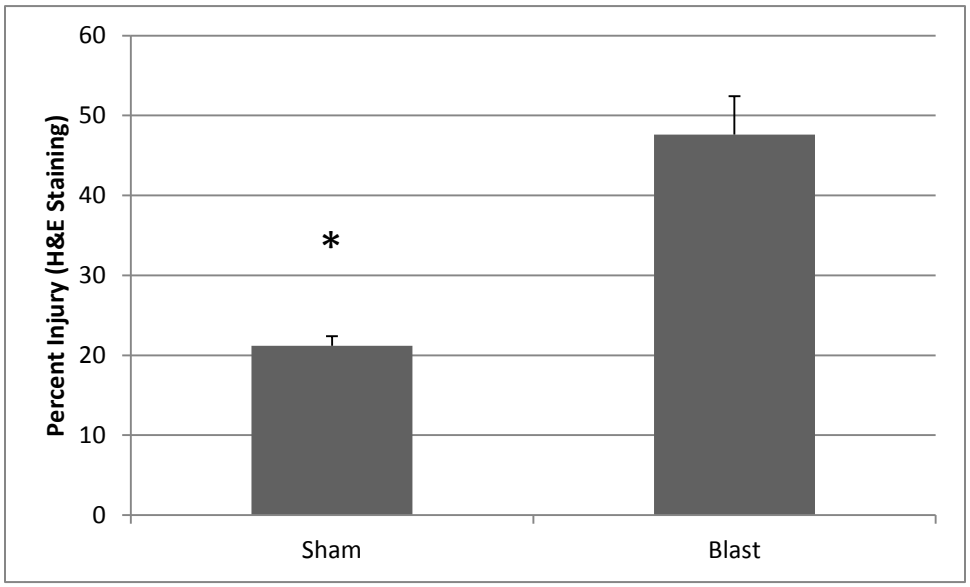

Figure 14. Sham vs. Blast for global hemorrhaging in all lung lobes. *p<0.05

Assessing three sections of each lobe (five) in rats with and without side-on blast exposure, H&E staining is significantly different in the Injury Only group at one hour compared to sham (Figure 14).

2.4.3 Lethality Risk for Blast Lung Injury

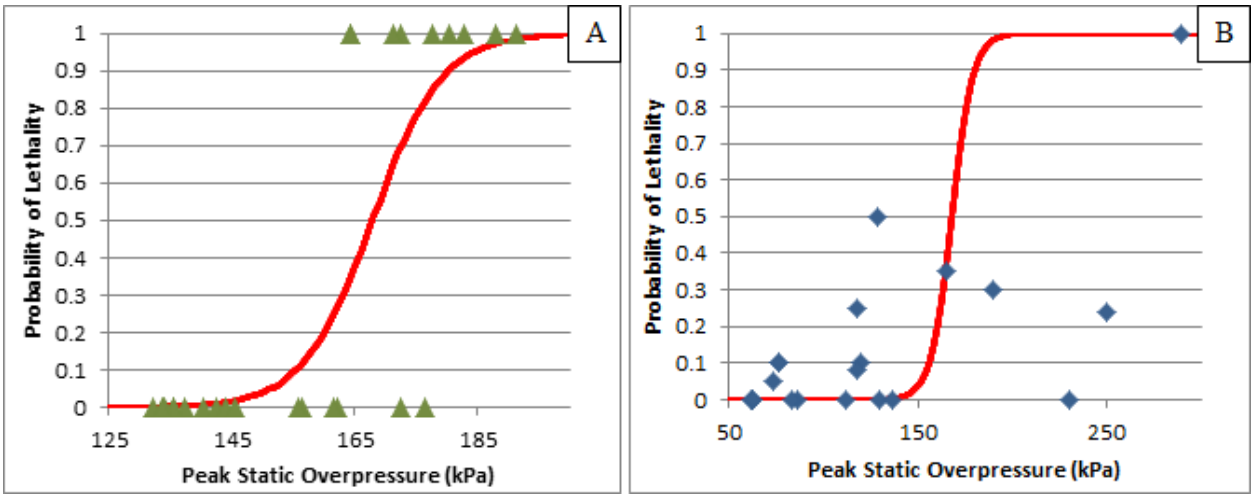

Figure 15. (A) Probability of Lethality vs. Peak BOP - Experimental Results. (B) Comparison from the Literature

The value for the parameters were: $\beta 0 = -29.82$ and $\beta 1 = 0.178$ and the p-value to determine the contribution of each parameter is 0.018 and 0.0178, respectively. The value for area under the curve (AUC) was 0.951 for the experimental data, which is considered a strong representation, and was 0.95 for the literature data.

2.5 Discussion

Examining the mechanism of lung injury from blast exposure is useful in determining causes of mortality, namely hypoxia. Inability to prevent hemorrhaging in the lungs causes immediate mortality after the blast. Injury can often be caused by blunt impact with the rib cage or rapid compression/decompression of lung tissue (Clemedson 1956, Sasser et al. 2006). It is speculated that orientation of the body to the blast wave played a significant role in this injury progression, and BOP exposure directed towards the sternum of the rat would have a different cascade of macroscopic trauma. Examining macroscopic lung trauma showed that the median lobe was progressively injured as peak BOP was increased, while other lobes, such as the upper right lobe and the left lobe, sustain external trauma as peak BOP reaches higher levels (Figure 10). Continuing with the observation that the middle lobe on the right side was increasingly affected by overpressure, it was also observed that histological analysis of this median lobe showed a linear increase of hemorrhaging compared to peak BOP. The H&E results coincide with macroscopic observations, while also providing a basis for further detailed studies on microscopic injury progression. Macroscopic and histological findings in this study resembled clinical symptoms seen in the human PBLI, such as hemothorax, pulmonary contusion, and interstitial emphysema (Mackenzie and Tunnicliffe 2011).

Injury severity can be portrayed in a variety of ways, one being lethality prevalence. According to previous studies, the span of 140 kPa to 180 kPa side exposure in rats marks the transition from moderate to severe PBLI, which corresponds to the entire range of lethality probability in the risk curve (Figure 15). The fifty percent lethality point is 168 kPa according to the developed risk curve with the ten percent lethality point at 155 kPa and the ninety percent lethality point at 180 kPa, so there is an operating range of 25 kPa between these marks. Orientation to the shock front of the blast wave is crucial in examining the mechanism of injury

to the lungs. In Figure 15, there are some discrepancies in the threshold for injury in comparison to other researchers. This was to be expected since a variety of methods are used. In this study, the duration of the blast wave had a linear correlation with peak overpressure. With a standard primary blast wave that has consistency and obeys the general tendencies of a Friedlander waveform, duration is a function of the peak overpressure. Since these go hand-in-hand, there was not any examination of lethality risk based on duration and/or impulse. When creating a threshold for blast injuries, it is important to know the parameters that are crucial for creating the injury. In all studies concerning this injury mode, peak overpressure had the strongest correlation with the survival outcome.

2.6 Conclusions

Lethality risk curves will serve to give guidance for further lung injury treatment studies. Also, observations on the development of gross trauma to lungs as corresponding to peak BOP could have implications to the response of larger specimens. Even though many experiments have pinpointed several markers associated with PBLI, there is a vast amount of effort that is needed to fully characterize the injury, as well as to develop therapeutics to combat sustained symptoms after initial trauma. Having a standard lethality risk curve is crucial for constancy among blast research and will be beneficial to all mechanistic or treatment-oriented blast-induced lung injury studies.

2.7 Limitations and Future Directions

The polytrauma model was characterized to provide static overpressure ranges for certain lethality risks. While the establishment of a unique injury model will provide a basic framework for other polytrauma model experiments or pre-clinical therapeutic testing, there are limitations that can be addressed by future studies. The model proposed has the animal in a side impact orientation with the shock front impacting the animal's right side. While this is a relevant injury modality to blast exposure in soldiers, more investigation is needed to examine how different orientations (exposure to animal's left side or front thorax) effect lethality risk. In addition to orientation, inhalation/exhalation status can also have an effect on lethality during blast exposure but this was not controlled in this study. The status can potentially play a large role in amount of hemorrhaging sustained, given that during inhalation more air can be trapped in the lungs causing more damage. While ventilation is not possible with our blast simulator set-up, the high

n in each group should ensure similar injury patterns for each blast level. Also, to fully characterize the acute systemic effects of lung trauma, evaluating serum biomarkers within the first hour is crucial to understanding specific biological mechanism that are at play. Another way to assess global hemorrhage is the measure wet/dry ratios of the lungs after blast.

Chapter 3: Secondary Mechanisms of Blast Polytrauma

3.1 Introduction

The objective was to assess the role of hypoxia and systemic injury mechanisms in blast-induced polytrauma. Among mechanisms that have the potential to play a role in polytrauma, downstream neurological regulators of hypoxia and BBB disruption are of interest in this study. Hypoxia likely contributes to the injury progression after primary blast exposure when impairment of the pulmonary gas exchange in the lung has occurred, resulting in secondary effects on cerebral vasculature (DeWitt and Prough 2009, Kirkman and Watts 2011). Primary blast can also cause BBB disruption which can lead to a myriad of molecular cascades (Chodobski et al. 2011). This cyclical relationship is elucidated with the finding that BBB disruption is biphasic, occurring at multiple time points after injury (Baskaya et al. 1997).

3.1.1 Statement of Problem

As polytrauma is increasing in prevalence due to terrorism activities, there has been a lack of characterizing the neuropathological aspects of blast polytrauma. Understanding specific mechanisms in this unique injury mode can impact the approach to treating polytrauma. While polytraumatic injury can be complex, the time course of systemic inflammation and other systemic effects on the brain can be crucial to therapeutic intervention and pre-hospital management. Examining markers that are found in isolated BINT can help correlate to neurotrauma sustained after polytrauma but this is only one layer to this complex trauma. Examining how systemic pathology after lung injury impacts neuropathology is crucial to understanding mechanisms of blast-induced polytrauma.

3.1.2 Significance

Even though hypoxia inducible factor-1α (HIF-1α) has been shown to play a role in TBI and cerebral ischemia, few studies have examined its role after BINT and it has not been investigated in relation to BPT (Ahmed et al. 2015, Liu et al. 2015). HIF-1α, the oxygen sensitive unit of HIF-1, is a mediator of disruption of the BBB and has been shown to have detrimental effects on injury pathology in the brain (Ogunshola and Al-Ahmad 2012). This injury pathway in the amygdala can potentially lead to neurologic impairment, such as anxiety (Sajja et al. 2015). Characterizing the role of secondary markers in BPT pathology would

contribute to understanding of injury pathways, such as BBB dysfunction and lead to novel therapeutic options.

3.2 Literature Review

3.2.1 Polytrauma Models

Small animals models designed for investigation of lung injury and neurotrauma sustained from blast exposure are scarce in the literature (Skotak et al. 2013). Primary blast exposure has been correlated with varying TBI injury severities (Mishra et al. 2016). This model includes consideration for physiological and lung injury criteria. There is a lack of identifiable polytraumatic-specific injury markers. Blood-brain barrier damage, signified by immunoglobulin G (IgG), has been characterized in blast trauma but exact mechanisms have not been elucidated (Skotak et al. 2013). In a lateral exposure to unanesthetized rodents, pulmonary hemorrhage was reported after 116 kPa exposure in addition to motor function impairment and absence of axonal injury (Ahlers et al. 2012).

Another blast polytrauma model was created by exposing the animal to blast wave directed at the thorax (Simard et al. 2014). This model relies on the "vascular pulse" blast injury mechanism where blast overpressure causes pressure differentials in vasculature and produces a wave to the cerebrovasculature. Lung injury and perivenular neuroinflammation was found in this study (Simard et al. 2014), highlighting the importance of systemic circulation in polytrauma.

3.2.2 Secondary Mechanisms of Polytrauma

In addition to blood-brain barrier damage that occurs during polytrauma, hypoxic conditions are ever present when lung injury has occurred. HIF-1α is a transcription factor that is involved in several injury modalities where hypoxia occurs, including TBI (Li et al. 2013). HIFs are heterodimeric transcription factors composed of an oxygen-sensitive α-subunit and a constitutively expressed β-subunit. Under normoxia, the HIF-1α subunit is constitutively transcribed but constantly targeted degradation through hydroxylation of conserved proline residues by prolyl hydroxylase domain (PHD) enzymes leading to recognition by von Hippel-Lindau (VHL) protein, ubiquitination and subsequent degradation by proteasome (Fandrey and Gassmann 2009). As oxygen tension drops, the PHD enzymes are inhibited and the lack of

hydroxylation results in cytoplasmic stabilization of the α-subunits. After phosphorylation, HIF-1α translocates to the nucleus and dimerizes with HIF-1β (also known as aryl hydrocarbon receptor nuclear translocator (ARNT)) and co-activators such as p300 forming a functional HIF-1 transcription factor. HIF-1 then binds to hypoxia-responsive elements in the promoter regions of its many targets inducing expression of genes involved in cellular adaptation to hypoxic stress by regulating erythropoiesis, angiogenesis, proliferation and cellular metabolism in order to reduce oxygen consumption and increase oxygen delivery to tissues (Engelhardt et al. 2014).

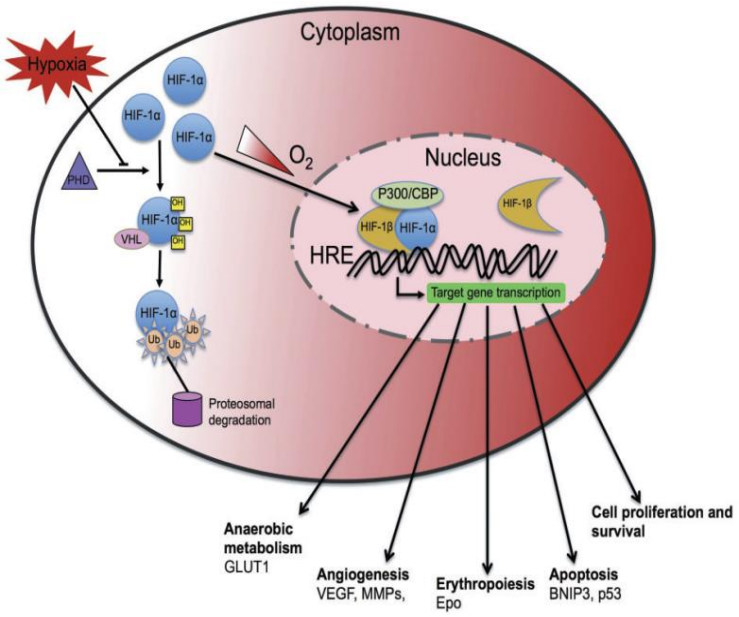

Figure 16. Schematic Diagram Illustrating the Mechanism of HIF-1 Regulation Under Normoxic and Hypoxic Conditions (Engelhardt et al. 2014). Engelhardt, S., S. Patkar and O. O. Ogunshola (2014). "Cell-specific blood-brain barrier regulation in health and disease: a focus on hypoxia." Br J Pharmacol 171(5): 1210-1230. *Fair use

Delayed opening of the BBB, that is, only after HIF-1α was already stabilized, suggested barrier stability is mediated via one or more HIF-1α effectors (Engelhardt et al. 2014). Vascular endothelial growth factor (VEGF), a downstream factor, can cause a leaky BBB (Engelhardt et al. 2014). Inhibition of HIF-1α has been reported to reduce BBB damage and improve recovery from cerebral ischemia in rats (Yeh et al. 2007, Ogunshola and Al-Ahmad 2012), possibly by reducing levels of VEGF, and attenuating the expression of caspase-3 and p53, which are key molecules in the apoptosis pathway (Chen et al. 2009). Mild TBI rat models have reported increased levels of VEGF were seen five days post-injury in the amygdala (Kamnaksh et al.

2011). Overall, BBB disruption is based on many factors during and after hypoxia with enhanced production of VEGF and inflammatory cytokines constituting on-going pathways (Kaur and Ling 2008).

3.3 Methods

3.3.1 Experimental Set-ups

3.3.1.1 Mild Neurotrauma Injury

All the experiments are in accordance with The Virginia Tech Institutional Animal Care and Use Committee and all the experimental protocols described herein have been approved. Prior to all experiments, male Sprague Dawley rats (~325 g, Harlan Labs, San Diego) were acclimated to a 12 hour light/dark cycle with food and water provided ad lib. As described previously, the shock front and dynamic overpressure were generated using a custom-built Advanced Blast Simulator (200 cm × 30.48 cm × 30.48 cm) that consists of a driving compression chamber attached to a rectangular transition and testing chamber with an end wave eliminator (ORA Inc. Fredericksburg, VA) located at the Center for Injury Biomechanics of Virginia Tech University. A passive end-wave eliminator was installed at the venting end of the ABS, which minimizes the shock wave outflow by means of a specially designed plate system. Patterns in the EWE plate system were created to mirror reflected shocks and rarefactions, which tend to 'cancel' each other and diminish unwanted effects within the test section. A peak static overpressure was produced with compressed helium and calibrated acetate sheets (Grafix Plastics, Cleveland, OH). Pressure measurements were collected at 250 kHz using a Dash 8HF data acquisition system (Astro-Med, Inc, West Warwick, RI) and peak overpressures were calculated by determining wave speed (m/s) at the specimen position. A mesh sling was used to hold the animal during the exposure that allowed for minimal hindrance of the wave through the chamber and shock wave profiles were verified to maintain consistent exposure pressures between subjects. The animals were anesthetized with 3% isoflurane before being placed in a rostral cephalic orientation towards the shock wave. Whole body exposure is considered "on-axis" with the animal facing rostral cephalic orientation towards the blast. This exposure has minimal effect on the lungs of the animals, as the shock streamlines around the body. Thus, resulting exposure in this study creates a relatively specific brain injury and minimal poly-organ trauma. Animals were randomly separated into two groups based on time points (n = 8/group).

Two groups were euthanized seven days following blast or control. Blast groups were exposed to a single incident pressure profile resembling a 'free-field' blast exposure, single Friedlander-like waveform that is in mild-moderate range at 17 psi (117 kPa) with a positive duration of 2.5 ms, while the control groups underwent same procedures with the exception of blast exposure.

3.3.1.2 Polytrauma Injury

The Virginia Tech Institutional Animal Care and Use Committee approved experimental protocols described herein. Prior to all experiments, male Sprague Dawley rats (~325 g, Harlan Labs, San Diego) were acclimated to a 12 hour light/dark cycle with food and water provided ad lib. Animals were exposed to a single incident pressure profile resembling a 'free-field' blast exposure at a range of 170 to 210 kPa (24.5 to 30.5 psi) peak overpressure with 2.5 ms positive phase duration to ensure severe levels of PBLI.

Using the following settings, necessary sample size was calculated: Power $(1-\beta) \geq 0.8$; $\alpha \leq 0.05$; Groups: 2; Minimum detectable difference in means (d) = 15%; Expected standard deviation (s) = 12%. Using power and α values, C = 7.85.

$n = 1 + 2C(\frac{s}{d})^2 = 1 + 2(7.85)(\frac{12}{.15})^2 =$11.05. (Dell, Holleran; 2002)

Power Analysis determined that 11-13 animals per group were needed.

All animals were randomly assigned to one of two groups: Blast Injury (n=13) and Sham (n=11). Prior to blast exposure, rats were anesthetized with a ketamine/xylazine solution, in accordance with the rodent weight, for sedation during blast. The shock front and blast overpressure were generated by a custom-built ABS with an end-wave eliminator (ORA Inc. Fredericksburg, VA) located at the Center for Injury Biomechanics at Virginia Tech (Figure 9). The ABS consists of a driving compression chamber attached to rectangular test section chamber with an end-wave eliminator.

A peak static overpressure was produced with compressed helium and calibrated acetate sheets (Grafix Plastics, Cleveland, OH). Pressure measurements were collected at 250 kHz using a Dash 8HF data acquisition system (Astro-Med, Inc, West Warwick, RI) and peak overpressures were calculated by determining wave speed (m/s) at the specimen position. A mesh sling was used to hold the animal during the exposure that allowed for minimal hindrance of the wave

through the tube, in addition to holding the animal in a prone position with the right side of the thorax facing the shock wave driver. The animal was not allowed to impact any solid surface in order to prevent secondary injuries and this was confirmed using high-speed video (Phantom Miro eX2, Vision Research). Motion analysis is found in Appendix A. Sham animals underwent all procedures except for blast exposure.

3.3.2 Open Field Test

Seven days post-injury, used for examining subacute changes, animals underwent an open field thigmotaxis assessment (Huang et al. 2013, Darwish et al. 2014). Briefly, an opaque black acrylic box with dimensions 80 x 80 x 36 cm was used for the task. Animals were acclimated in the open field box before the injury and two days after injury. The acclimation ensures that any anxiety-like traits would be due to the blast and subsequent injury progression. Activity changes were detected using EthoVision XT™ software tracking. Thigmotaxia, preference of proximity to walls, can expose fear of open, lit spaces and is displayed in animals with anxiety. Time spent along the chamber wall reflects an increased level of anxiety and is a common method of determining anxiety levels (Darwish et al. 2014). Rats were videotaped for five minutes and avoidance of center square activity (i.e. anxiety-related behavior) was measured by determining the amount of time and frequency of entries into the central portion of the open field.

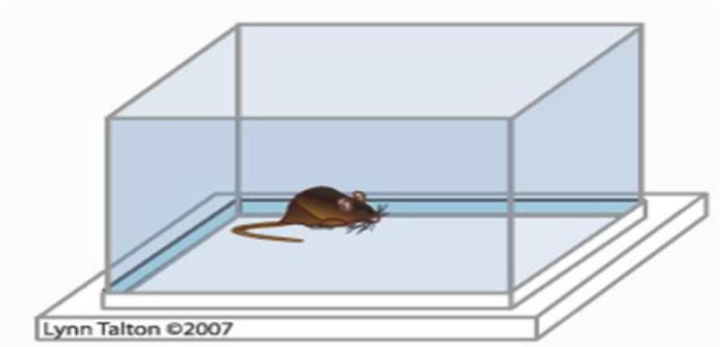

Figure 17. Representation of the Open Field Arena

3.3.3 Tissue Processing

After seven days, animals were euthanized by transcardial perfusion of saline and 4% paraformaldehyde. Following collection, brains were stored in a 4% paraformaldehyde fixative solution. After 48 hours in fixative, the whole brains were placed in 30% sucrose solution for

tissue sectioning preparation. Whole brains were embedded in Tissue-Tek® optimal cutting temperature embedding medium (Sakura Finetek USA, Inc., Torrance, CA) for cryostat processing in the coronal plane. Samples were then cut (40 µm) and sections containing amygdala nuclei were isolated (Bregma: -2.28 mm).

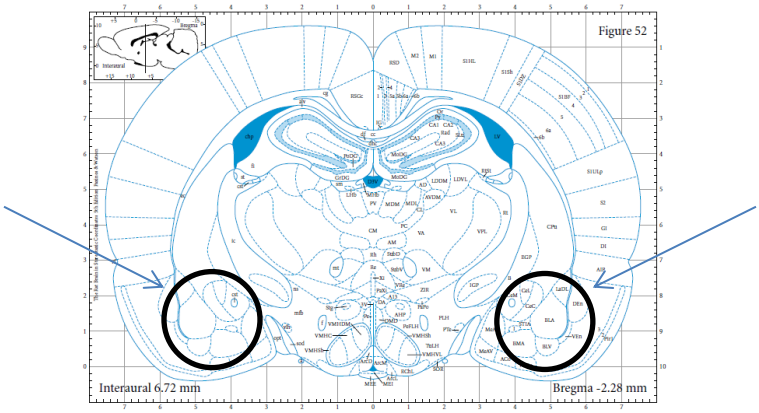

Figure 18. Amygdalar Representative Section (Paxinos 2006) Paxinos, G. a. W., C. (2006). "The rat brain in stereotaxic coordinates." Elsevier 6th edition. *Fair Use.

3.3.4 Immunofluorescent Staining

Immunohistochemistry was performed on amygdalar sections to evaluate levels of markers: glial fibrillary acidic protein (GFAP), Caspase-3, ionized calcium-binding adaptor molecule 1 (IBA-1), SMI-71, HIF-1α, and VEGF. SMI-71 is an established antibody against rat endothelial barrier antigen (Lin and Ginsberg 2000, Pelz et al. 2013). Samples were rinsed three times with PBS and incubated in 2% bovine serum albumin (BSA) in PBS for one hour at room temperature. Sections were then incubated with a primary antibody (Appendix C); anti-GFAP (1:500; Invitrogen, Carlsbad, California), anti-caspase-3 (1:500; Cell Signaling Technologies, Danvers, Massachusetts), anti-IBA-1 (1:500; Biocare Medical, Concord, California), anti-SMI-71 (1:250; Covance, Princeton, New Jersey), anti-HIF-1α (1:250; Novus Biologicals, Littleton, Colorado), or anti-VEGF (1:250; Santa Cruz, Dallas, Texas) overnight at 4ºC. Both primary antibodies were only labeled separately on different amygdalar sections. After a PBS wash, the samples were incubated for 1.5 hours with fluorescein isothiocyanate (FITC) anti-rat, Alexa Fluor 555 anti-rabbit, Alexa Fluor 488 anti-mouse or Alexa Fluor 594 anti-mouse. After three PBS washes (five minutes each), samples were mounted, air dried and coverslipped with prolong antifade gold reagent with 4',6-diamidino-2-phenylindole (DAPI; Invitrogen, Carlsbad, CA).

Sections were examined under Zeiss fluorescence microscope at 20X magnification under appropriate fluorescent filters and images were taken by Zeiss AxioCam ICc 1. For all images, quantification (ImageJ software; NIH, Bethesda, MD) was based on fluorescence intensity after thresholding to eliminate background color.

3.3.5 Flurojade C Protocol

Sections of the amygdala were stained with Fluorojade-C (FJC) to identify degenerating neurons. This was completed with a kit from Biosensis (Thebarton, South Australia).Tissue sections were mounted on gelatin coated slides and dried. They were then incubated in the solution of NaOH (Solution A) in 70% ethanol for five minutes. The sections were then transferred to 70% ethanol and distilled water for two minutes each. The sections were then incubated in a solution of potassium permanganate (Solution B) in distilled water and rinsed in distilled water. They were then incubated in a solution of FJC (Solution C) and DAPI (Solution D) in distilled water. Sections were then rinsed in distilled water thrice, air-dried, and placed on slide warmer until fully dry. The dry slides were cleared in xylene and mounted with DPX (Sigma-Aldrich Co. Ltd, St. Louis, MO). Sections were examined at 20X on a Zeiss microscope, and analysis was conducted. FJC+ neurons were counted by blinded technicians and the results were quantified.

3.3.6 Detailed ImageJ Analysis

Image analysis consisted of several steps. First, the image was split into three different color channels: red, green, and blue. Depending on what secondary antibody was used (red or green), that color channel was chosen for further analysis. The background was subtracted using a rolling ball radius of twenty pixels.

When quantification of cell types (astrocytes and microglia) is performed, the ImageJ output variable used was the mean pixel value. This is simply used to stand for the overall fluorescent intensity of an image and divide it by the number of pixels in that image. In a sense, the output number is the average fluorescent intensity per pixel (a number between 0 and 255). The neuroglia stains are quantified in this manner, since these cell types can be activated or not.

When quantification is based on presence of a protein (SMI-71 and HIF-1α), the ImageJ output variable used was percent area. A threshold was then applied to the image, which teased

out the relevant signal from the left-over background. After processing each image, the output variable of "Percent Area" gives an indication of the amounts of pixels with signal divided by the total amount of pixels. For SMI-71, two images were taken at 20X for each hemisphere for each tissue section analyzed (three per animal).

3.3.7 Statistical Analysis

Statistical differences between the treatment groups were assessed with analysis of variance, or ANOVA, using LSD post-hoc test. All statistical analysis was performed using JMP Pro 10 (SAS Institute, Cary, NC) and $p < 0.05$ considered statistically significant. Unless indicated otherwise, data are presented as mean ± standard error of the mean, or SEM.

3.4 Results

3.4.1 Anxiety Assessment

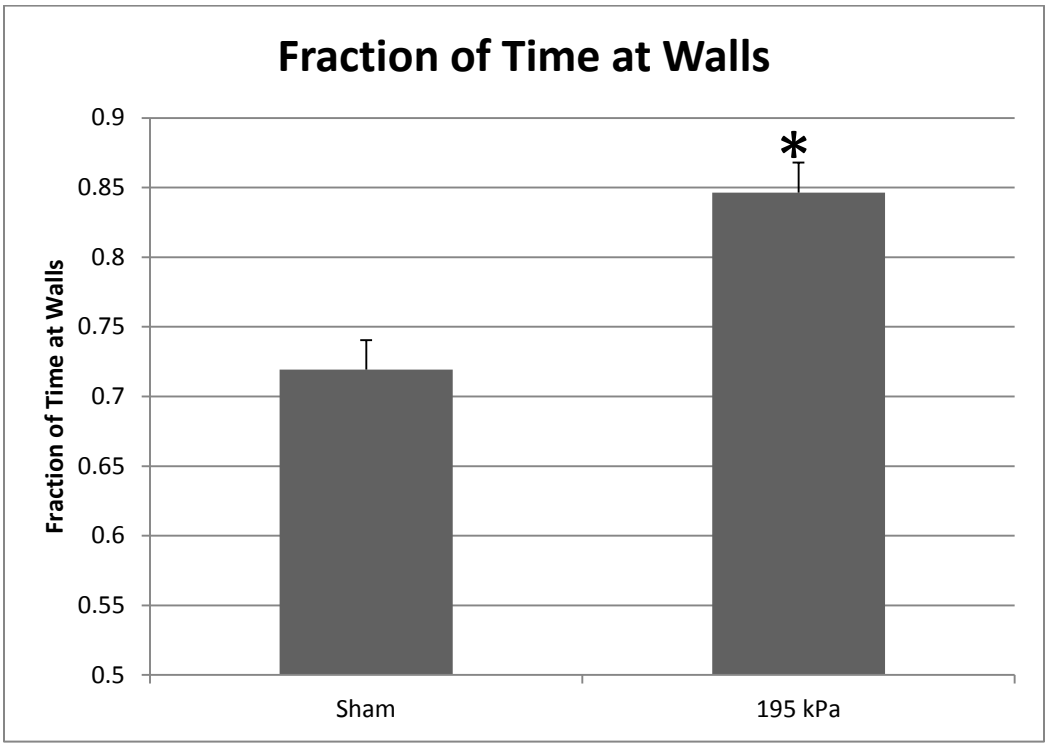

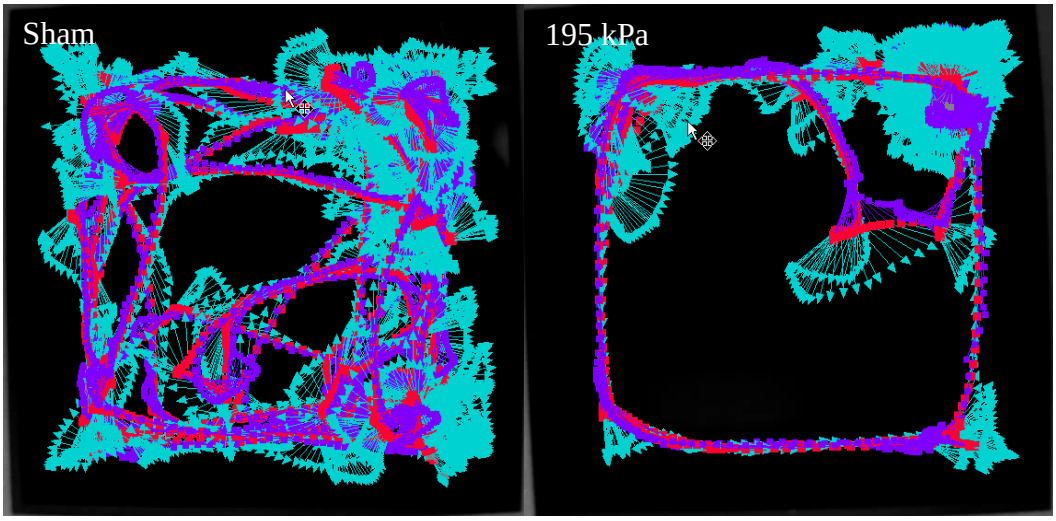

Figure 19. Fraction of time spent at the walls of the open arena was significantly higher in the 195 kPa BPT group compared to sham ($p<0.05$). Representative images show animal tracking over five minutes.

The fraction of time spent at the walls of the open field box for the blast injury group was significantly increased ($p<0.02$) compared to sham (Figure 19). Representative image of animal activity over the five minute period in the open arena demonstrates global exploration by the sham group and proximity to the walls in the BPT group (Figure 19). This display of anxiety-like behavior in the blast group could be the neurological manifestation of injury pathology.

3.4.2 Astrocyte Activation

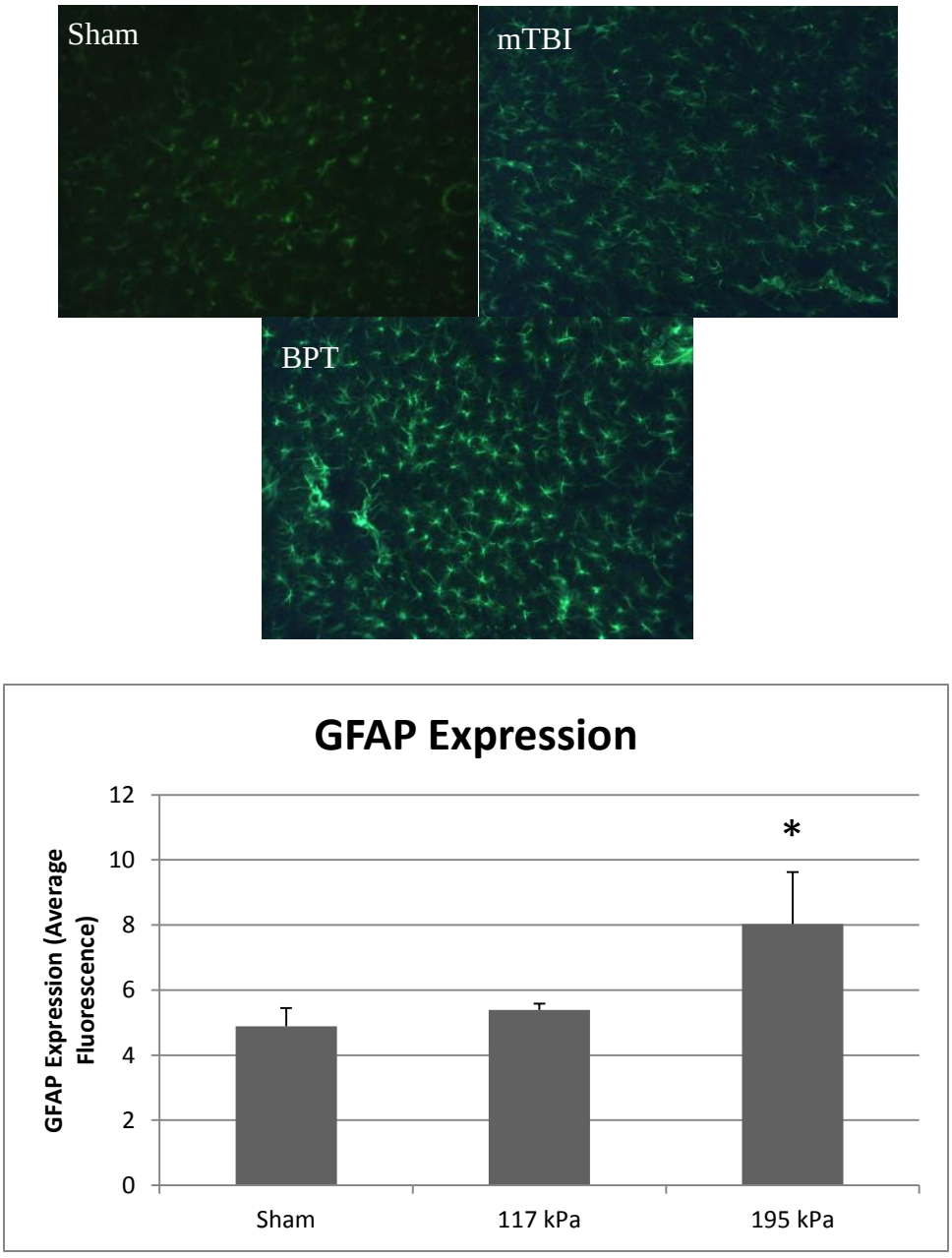

Figure 20. Representative images show reactive glia present seven days after blast in the 195 kPa group. GFAP expression, examining astrocytosis, was significantly different in the 195 kPa BPT group compared to sham ($p<0.05$).

While only slight elevation in seen in the 117 kPa group (n=6) compared to sham, the 195 kPa BPT group is significantly different compared to sham (Figure 20). Images show similar

number of astrocytes in all groups but more GFAP expression and swelled processes in the BPT group.

3.4.3 Apoptosis

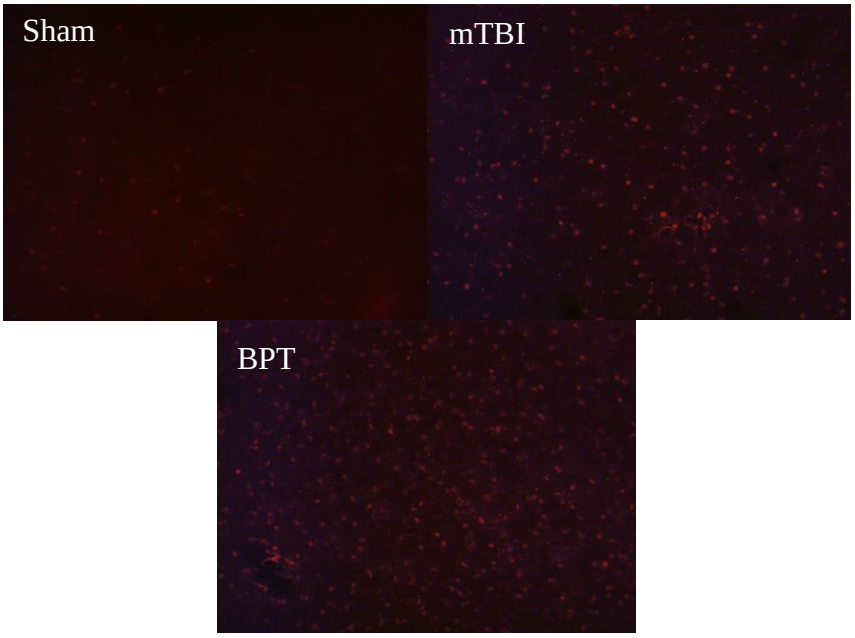

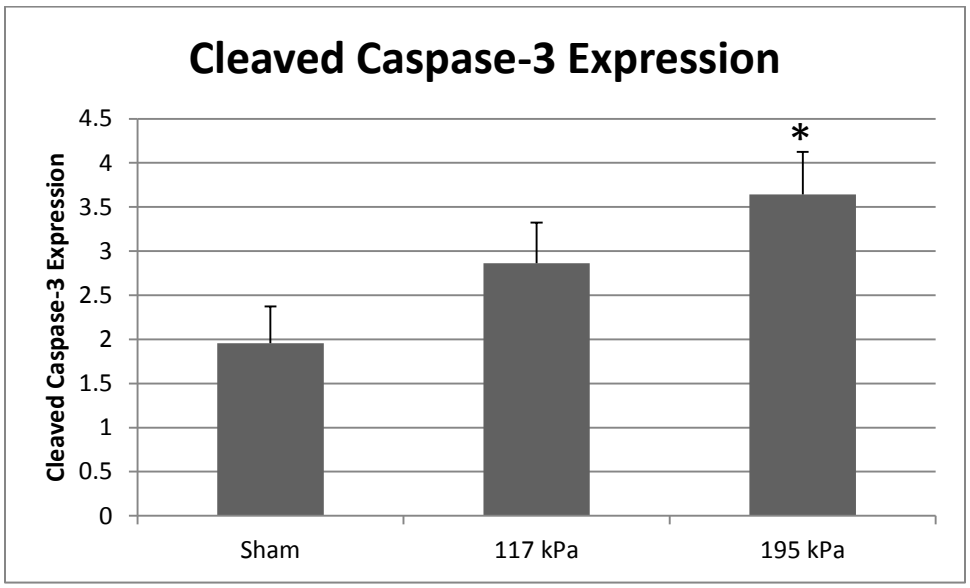

Figure 21. Representative images show higher number of cells undergoing apoptosis in the 117 and 195 kPa blast groups. Cleaved Caspase-3 expression was significantly different in the 195 kPa BPT compared to the sham group ($p<0.05$).

Expression of cleaved caspase-3, indicative of apoptosis, was elevated in both blast groups, although only significantly different in the BPT 195 kPa group (Figure 21). Amygdalar images show much higher number of apoptotic cells in the blast groups compared to sham.

3.4.4 Microglia Activation

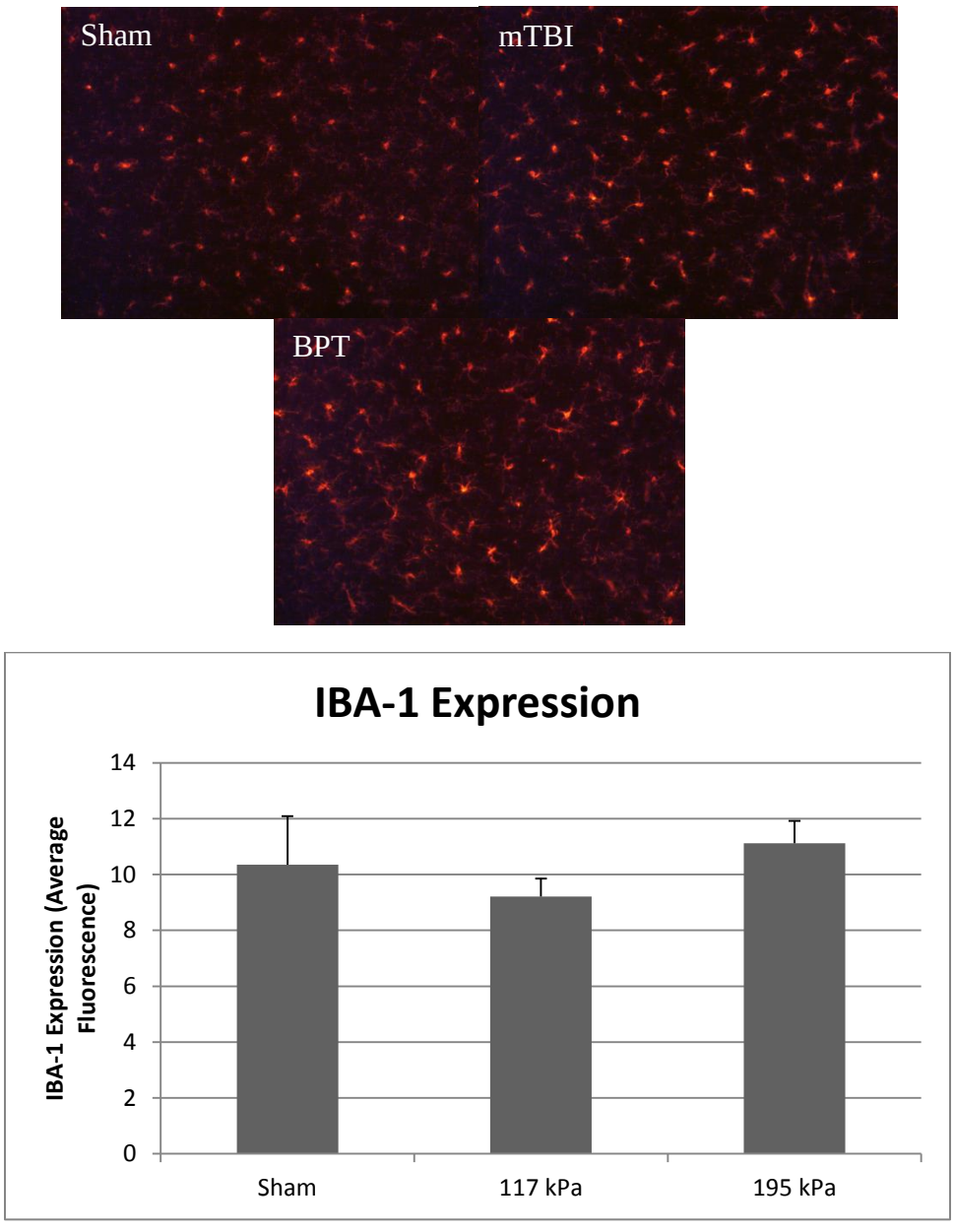

Figure 22. Images show similar counts of microglia. IBA-1 expression, marking microglia, in the amygdala. Among all groups, there was no significant difference.

Although there is no significant difference between the 195 kPa BPT group and sham, there is slight elevation in IBA-1 expression in the 195 kPa group compared to sham (Figure 22).

3.4.5 Blood-brain Barrier Disruption

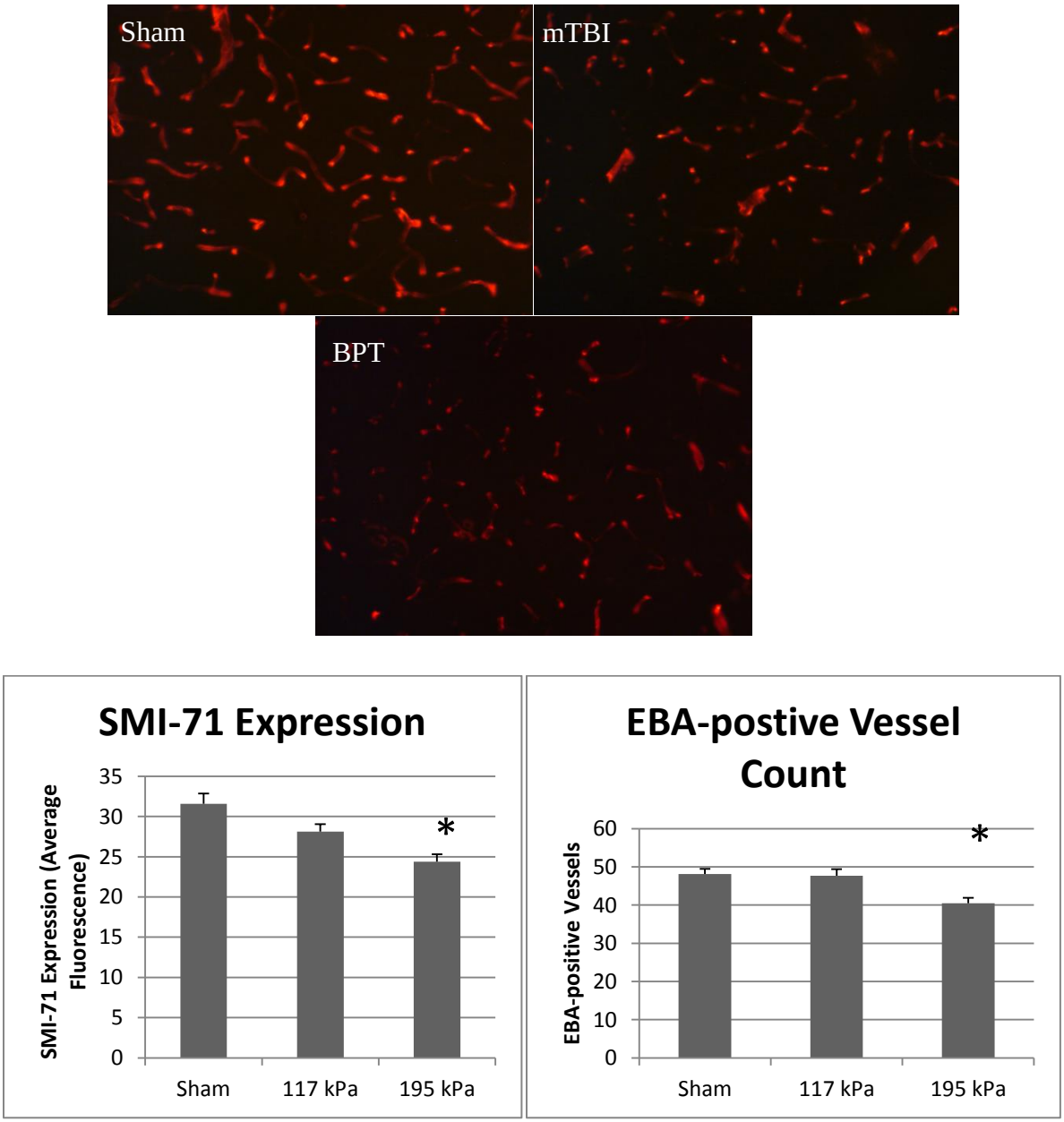

Figure 23. Representative images show lower number of vessels with EBA (BBB competent) in the 195 kPa BPT group. SMI-71 average fluorescence and marking of EBA+ vessels both show significant difference in the 195 kPa BPT group compared to sham ($p<0.05$).

The expression of SMI-71 was decreased in the blast injury group, which has been shown previously to signify a compromised BBB (Westin et al. 2006), compared to the sham group (p-value < 0.001). This antibody binds to EBA, which is not present in vessels with BBB disruption (Pelz et al. 2013). Figure 23 depicts the decreased staining found within the injury group compared to sham, due to decrease vessel count with EBA expressed.

3.4.6 HIF-1α Expression

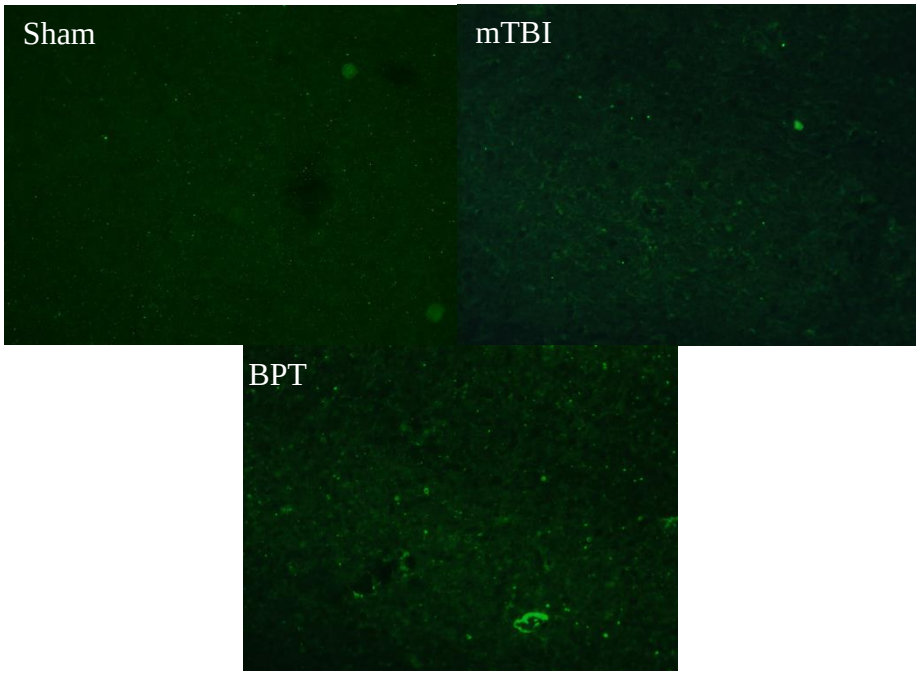

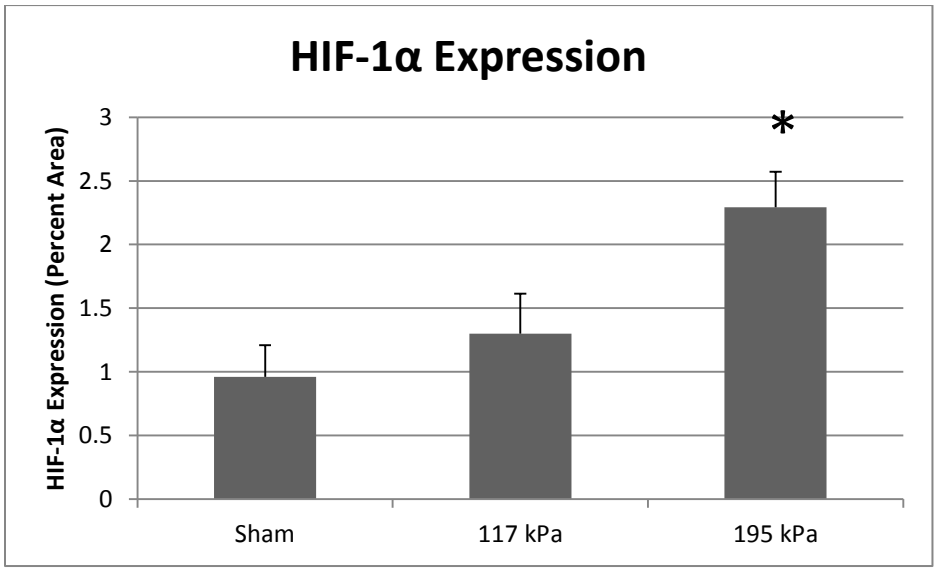

Figure 24. Representative images show HIF-1α expressed in more cells in the 195 kPa group. HIF-1α expression in the amygdala. There was significant difference ($p<0.05$) between the 195 kPa BPT group and the sham group.

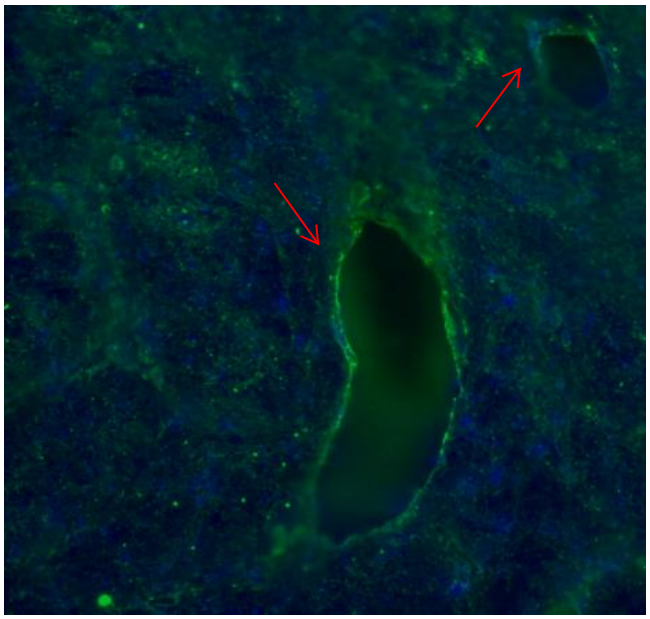

Figure 25. HIF-1α is co-localized with DAPI around the vessels in the 195 kPa group.

For the blast injury group, HIF-1α expression was increased in the amygdala at seven days post-blast compared to the sham group (Figure 24). All analysis only examined protein expression. In Figure 25, HIF-1α is co-localized with DAPI around major vessels, showing that hypoxia is potentially being sensed first due to low blood oxygen concentration and this could be an on-going mechanism.

3.4.7 VEGF Expression

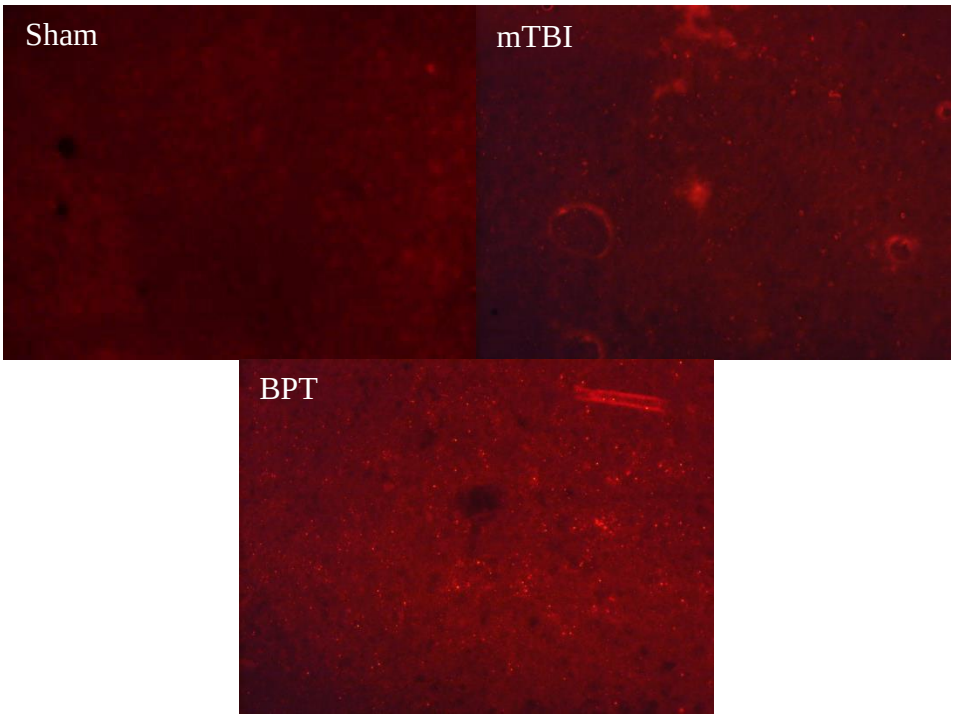

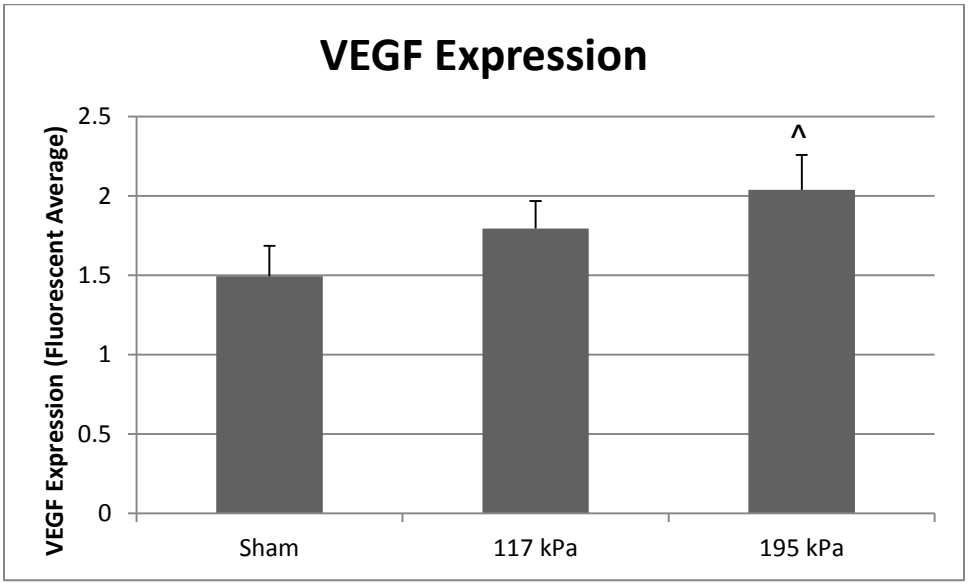

Figure 26. VEGF Expression in the amygdala. The 195 kPa BPT injury was elevated although not statistically different compared to sham (p=0.064). Representative Images of VEGF expression in the amygdala.

Expression of VEGF was elevated though not statistically different in the 195 kPa group compared to sham (Figure 26).

3.4.8 FJC+ Neuronal Count

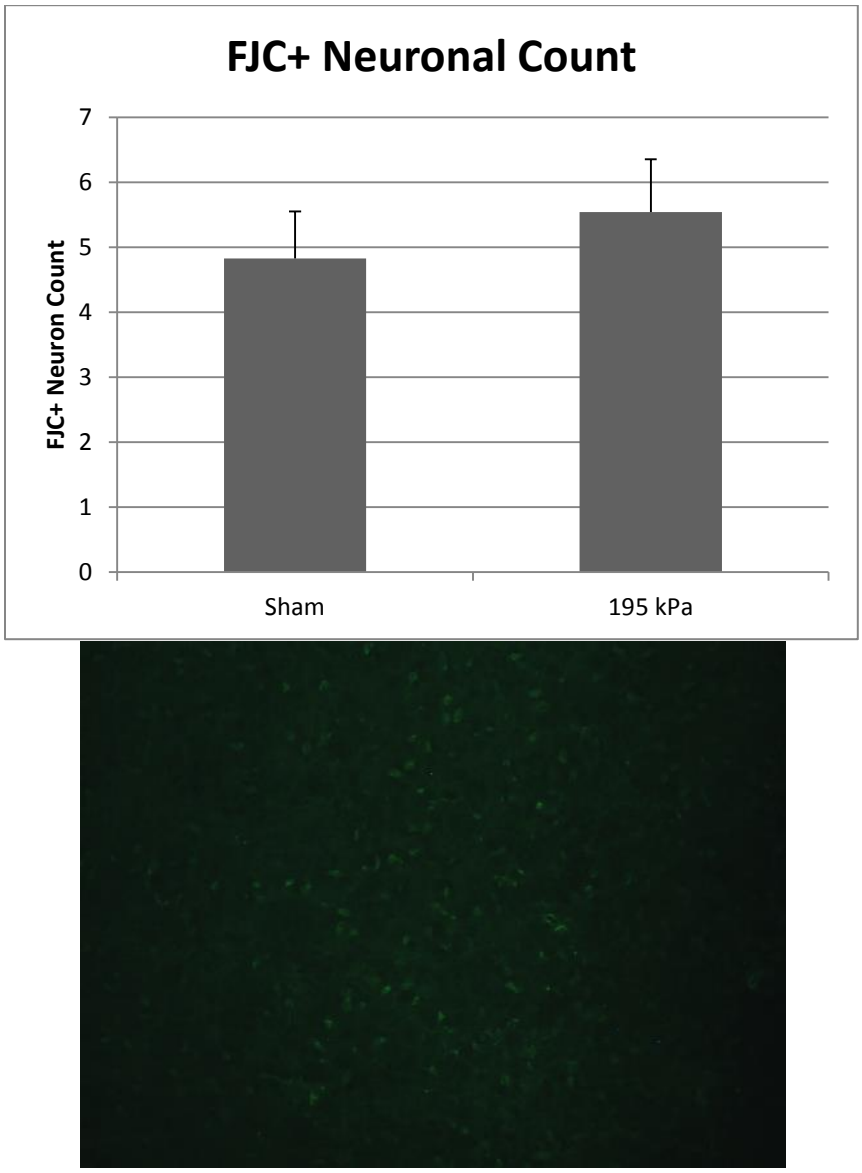

Figure 27. FJC+ Neuronal count was elevated, although not significantly different at seven days post-blast. Image depicts amygdala from the 195 kPa BPT group with abundant FJC+ neurons, though this was not common.

FJC+ neuronal count was not statistically different compared to sham at seven days post-blast (Figure 27).

3.5 Discussion

The polytrauma injury model established in this chapter has neuropathology unique compared to the mild neurotrauma model. While there is some overlapping pathology between the injury models assessed in this chapter, injury markers in general are exacerbated in the polytrauma model. Elevated GFAP expression and cleaved caspase-3 have been reported over the course of multiple time points after blast in the amygdala (Kamnaksh et al. 2011, VandeVord et al. 2012). Higher expression of GFAP and cleaved caspase-3 in the 195 kPa BPT model shows that there is more astroglial reactivity and apoptosis with higher injury severity. While differences in IBA-1 are not seen in this model, activation-specific antibodies, such as CD68 or CD11b, could be investigated to assay microglia activation after BPT. IBA-1, which is involved in phagocytosis and actin reorganization in microglia, is constitutively expressed in microglia and is elevated when microglia are activated but an antibody, like CD68, would be more sensitive as it has a distinct role in phagocytosis during the activation process. There is a potential that microglia at seven days post-blast are in a retracted process activation state (Huber et al. 2016) and this morphology would be difficult to quantify with IBA-1.

A major finding was that BBB disruption, highlighted by a reduction in EBA+ vessels at seven day post-injury, plays a distinct role in BPT injury pathology. Disruption of the BBB is a common finding in models of polytrauma but the exact mechanisms have not been deduced (Skotak et al. 2013, Simard et al. 2014, Mishra et al. 2016). This could be a crucial upstream event in an on-going injury cascade, involving hypoxia indicator and BBB disruption (Figure 28). Even though no significant difference was found between VEGF staining in blast polytrauma compared to sham, this factor could still play a role in the pathology at different time points. The role of VEGF, a downstream factor in injury cascades, in BBB disruption has been established in models of brain injury (Okada et al. 1998, Skold et al. 2005). Elevated VEGF levels have been reported in the amygdala at seven days after blast exposure (Kamnaksh et al. 2011). As VEGF is a potential downstream marker after HIF-1α presence, it is possible that VEGF is expressed either before or after the seven day time point. After multiple blast exposure, VEGF levels in plasma were upregulated at two hours after multiple injuries but not at 22 days post-injury (Kamnaksh et al. 2012). In a repeated mild blast TBI model, long lasting (42 days post-injury) elevated levels of HIF-1α and VEGF in plasma were reported and due to hypoxia at time of injury (Ahmed et al. 2013). HIF-1α has been shown to play a distinct role in apoptosis

and BBB disruption after TBI in several models (Higashida et al. 2011, Li et al. 2013). Acute presentation of hypoxic factors would validate the findings of secondary mechanisms that are at play seven days post-blast. More studies need to be completed to fill in these knowledge gaps.

Although the majority of the BPT amygdalar sections did not express high levels of FJC+ neurons, a few animals had aberrant levels of FJC+ neurons (Figure 27). FJB+ neuronal levels have been reported inconsistently in models after blast (3-14 days) (de Lanerolle et al. 2011, Li et al. 2013, Sajja et al. 2015). Neurodegeneration at seven days after blast polytrauma could be in the late stage but is not seen as a consistent finding in this study. More studies will be needed to determine chronic emergence of pathology.

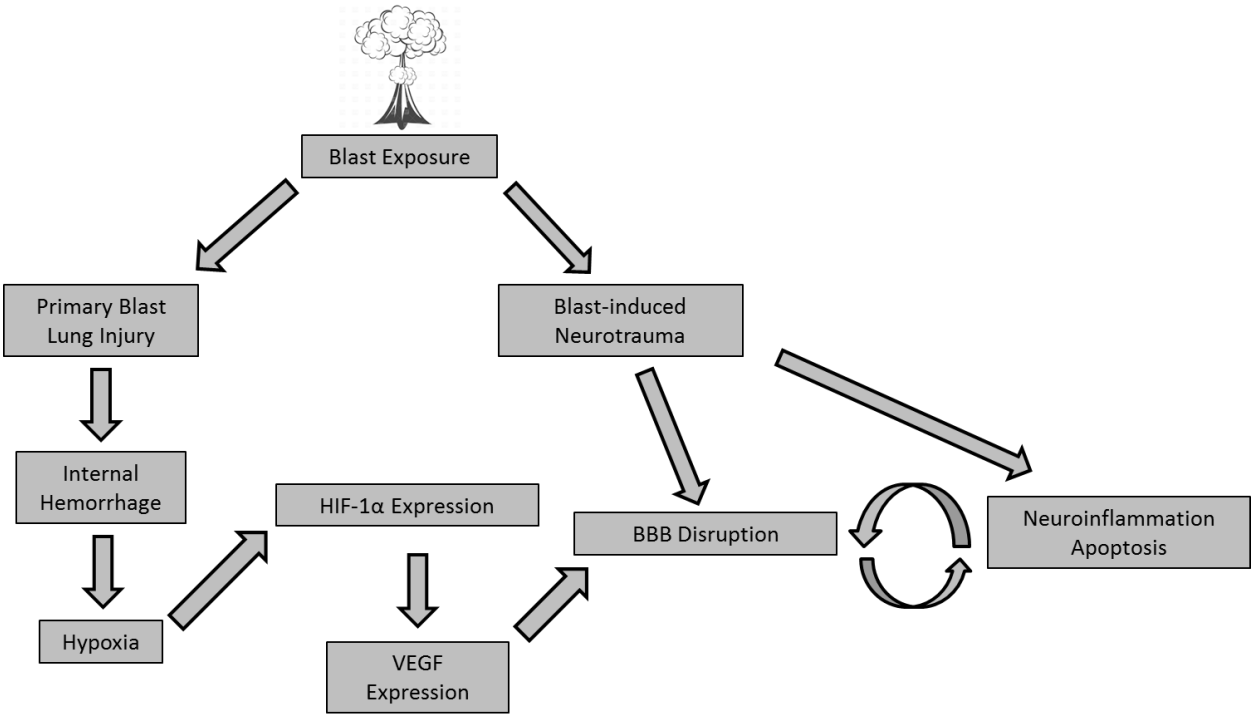

Figure 28. Speculated Blast-induced Pathology Diagram

The mechanics of how primary blast exposure specifically injures the brain, usually in an inhomogeneous way, is poorly understood and is likely to be dependent upon orientation to the blast. Some studies speculate that vascular surge, or venous pressure pulse that is transmitted to the brain through the jugular veins after blast exposure to the thorax, is the main mechanism of blast-induced brain injury (Bauman et al. 2009, Simard et al. 2014). While this may play a role, extensive evidence has been provided that skull dynamics contributes to the injury (Bolander et

al. 2011, Leonardi et al. 2011, Dal Cengio Leonardi et al. 2012, Hampton and VandeVord 2012, Gean 2014). Vibration of the skull from the shock wave causes secondary brain tissue displacement and injury stems from susceptibility of the viscoelastic brain to shear forces (Moss et al. 2009, Bolander et al. 2011, Leonardi et al. 2011). Other potential mechanisms of blast wave transmission to the brain include overpressure entering the orifices of the skull, acceleration of the head, and impaired cerebrovascular reactivity (Cockerham et al. 2009, Svetlov et al. 2010, Alford et al. 2011, Abdul-Muneer et al. 2013, Gullotti et al. 2014).The neuroanatomical position of the amygdala inside the rat brain makes it susceptible to skull flexure injury of the ventral side of the skull due to high static overpressure. This model could be utilized to further investigate which mechanisms play the most important role in blast transmission to the brain, as likely it is a combination of several factors that induce injury. Isolating blast exposure to either the thorax or the head is difficult due to animal positioning inside the tube and any rigid fixture to shield a portion of the body could likely create injury unrepresentative of primary blast.

The mechanism in which the energy of the blast wave interacts with the skull and the resultant high speed compression interfaces with brain tissues of varying properties, e.g. density, is not fully understood. One hypothesis mentioned in Kuehn, et al. (Kuehn et al. 2011) is that the exhaustion of energy at density boundaries can cause injury in tissue. Multiple studies have confirmed that microcontusion and microhemorrhaging of the blood-brain barrier (BBB) occurs with a lower threshold of 200 kPa peak overpressure in direct cranial and lateral blast exposure models (Kuehn et al. 2011, Yeoh et al. 2013). While shearing of vessels can cause microhemorrhaging, there is currently no definitive vascular map that would point out increased vasculature in any specific brain region, such as the amygdala. There is some evidence citing increased vascular sensitivity of the amygdala due to a stimulus of stress, with increased vascular hypertrophy in the amygdala. This indicates increased regulation of neural networks that would be more susceptible to vascular mechanisms (Neigh et al. 2010).

3.6 Conclusion

While many overlapping mechanisms in blast polytrauma coincide with that of blast-induced neurotrauma, specific markers, such as BBB dysfunction and hypoxic factors, can play a larger role in neuropathology. BBB dysfunction plays a major role in mechanisms at seven days post-blast and can exacerbate downstream pathways to produce more devastating outcomes. It is

shown that BPT has a unique pathology and should have a different therapeutic approach compared to BINT.

3.7 Future Directions

While these findings give a general view of mechanisms present at this time point, more detail is needed to investigate specific pathways after BPT. More studies examining microglia activation and neuroinflammatory processes at different time points are needed. Also, determining which components of the BBB are disrupted could point to how it is being damaged and at what point it is involved in injury pathology.

In addition to the effect on acute lung trauma, the primary injury mechanisms of blast-induced neurotrauma can be influenced by orientation of the animal within the blast tube. Acute hypoxemia can produce immediate cerebrovascular pathology. As evidence is seen at later stages in this model (Chapter 3), more investigation of acute manifestation of BINT is needed.

Expansion of physiology recording is needed to see how long hypoxia is present after initial injury. This could solidify hypoxia as a major concern after systemic injury. More studies are needed to examine the time course of when systemic and secondary markers are first present after injury. This will also give an idea of the best time window for therapeutics designed to mitigate early factors in place to aggravate injury pathology at later stages. Assessing BBB disruption at several time points will show if this is bi-modal, tri-modal, or even a continuous occurrence after BPT.

To validate and expand of the proposed pathway in BPT, a series of tests with HIF-1α and VEGF knockout mice will be conducted to elucidate if hypoxia upregulates HIF-1α and that induces VEGF expression to exacerbate BBB disruption. Appropriate controls will be tested as well to determine the significance of these factors.

As astrocytosis and BBB disruption are mechanisms present in this injury model, more investigation of overlapping pathology between astrocytes and the BBB is needed. Astrocytic end-feet coverage is important to BBB function and health. Astrocytic dysfunction can lead to debilitating consequences, such as major depressive disorder (MDD) (Rajkowska et al. 2013). Preliminary images have been examined (Figure 29) but quantitative analysis is needed.

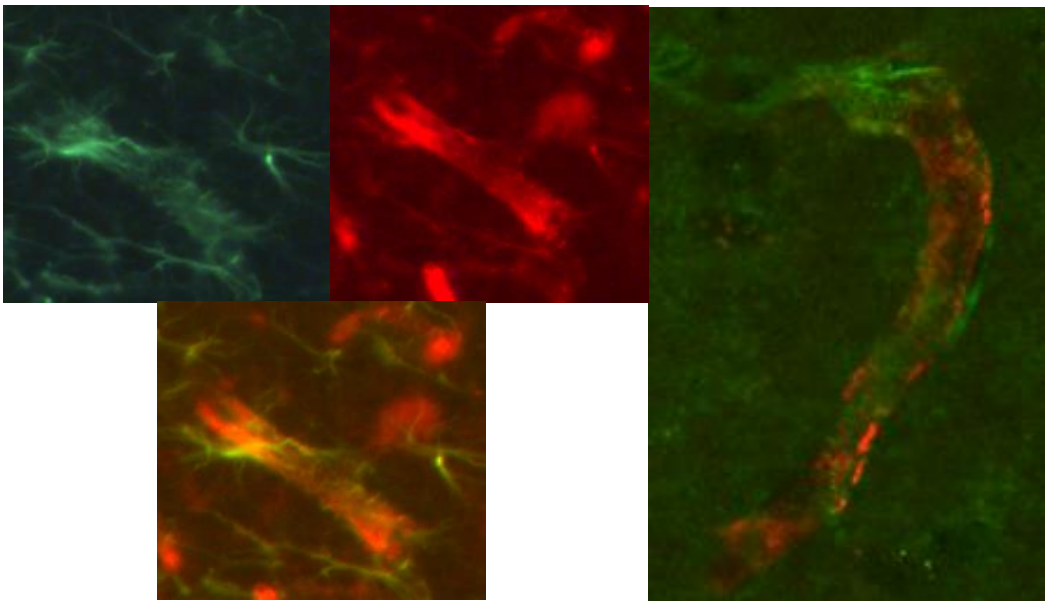

Figure 29. Left - Overlap of GFAP and SMI-71 in the amygdala. Right – Overlap of aquaporin-4 and SMI-71.

Chapter 4: Hemostatic Nanoparticles

This section has been adapted from Hubbard, et al. "Steroid-Loaded Hemostatic Nanoparticles Combat Lung Injury after Blast Trauma" *ACS Macro Letters*, 2015. 4(4): 387-391.

This data is a result of collaboration with Case Western Reserve University. The nanoparticles and treatments were synthesized and developed by Dr. Margaret Lashof-Sullivan and other collaborators at Case Western.

4.1 Introduction

Due to the lack of therapies that specialize in mitigating internal hemorrhage after trauma, our efforts focused on synthesizing functionalized nanoparticles to target and assist clotting to reduce internal bleeding. The functionalized nanoparticles were composed of a block copolymer, poly(lactic-co-glycolic acid)-poly(l-lysine)-poly(ethylene glycol). These particles are conjugated with the peptide, glycine-arginine-glycine-aspartic acid-serine (GRGDS), to enable binding with the glycoprotein IIb/IIIa receptor found on activated platelets (Bertram et al. 2009). Because these particles are based on poly(lactic-co-glycolic acid) (PLGA), they lend themselves to application as a drug delivery vehicle that leverages their entrapment in the clots for local delivery.

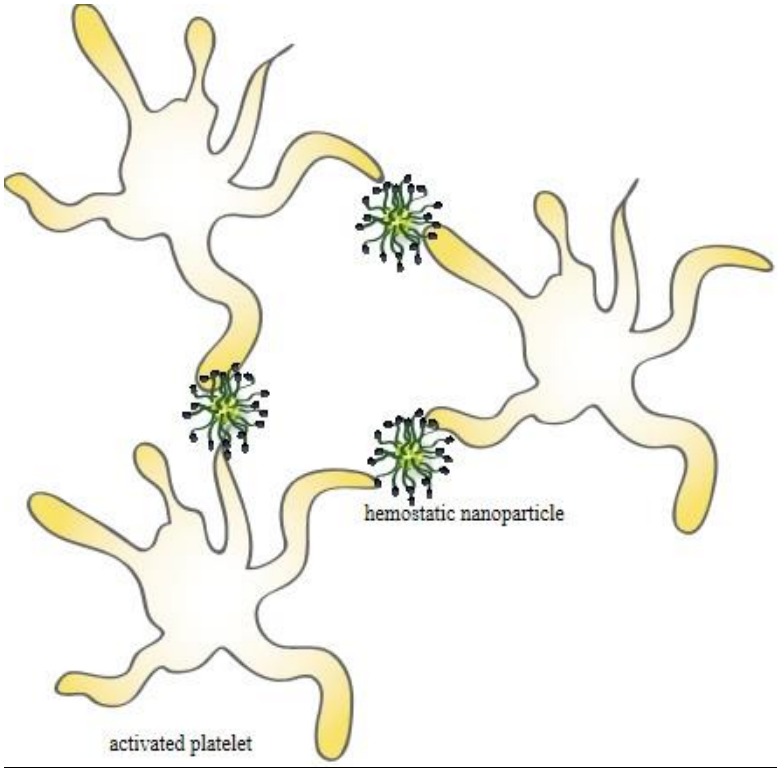

Figure 30. Schematic of the interaction of hemostatic nanoparticles with activated platelets to aid in formation of the platelet plug.

4.2 Current Anti-hemorrhage Therapeutics

There are limited options readily available for treatment of internal hemorrhage. Hemorrhage is a leading cause of preventable death on the battlefield (Champion et al. 2003). The gold standard in the military for controlling compressible hemorrhage is tourniquets, which uses compression to mitigate bleeding. While there are some current strategies for non-compressible intracavitary bleeding, there is a critical need for improvements to these options. One current option is platelet derived hemostatic agents which provide a substitute for apheresis platelets that have a limited shelf life of five days (DoD 2014). *Thrombosomes* are modified platelets, administered by IV injection, that function to initiate and amplify hemostasis by producing thrombin and converting fibrinogen to fibrin to form stable clots. However, this option is still under development (Fitzpatrick et al. 2013). *Tranexamic acid,* an antifibrinolytic drug used for patients with hemophilia, has been re-purposed to treat traumatic hemorrhage but is also in the early stage of development (Hunt 2015). Another option is the *wound stasis system.* This system is a combination of liquid phases that react to form expanding foam inside the body that

absorbs blood and applies pressure at injury site. A disadvantage of this system is that it needs to be surgically removed (DoD 2014). *X-Stat* hemostatic dressing halts bleeding with the application of mini-sponges that have a tamponade-like effect at site of injury but it requires an open wound to be applied (DoD 2014). *Quikclot Combat Gauze* is comprised of kaolin-impregnated rayon and polyester hemostatic dressing, which accelerates clotting by activating factor XII of the coagulation cascade, and is used in all branches of the U.S. military. It is relatively inexpensive and contains no animal or human proteins so adverse reactions are limited. However, it treats mainly compressible hemorrhage and it is not used in absence of open wounds (Gegel et al. 2013). *NovoSeven*, or recombinant coagulation factor VIIa, can be administered IV and used to promote clotting by bypassing the need for factor VII and activating factor X. Downfalls of *NovoSeven* include risk of unwanted blood clots and immunogenic complications due to reactions with animal proteins (mouse, hamster, and cow), as well as being very expensive (Bertram et al. 2009). While these treatments provide some options to mitigate traumatic bleeding, there is no standard and all have drawbacks. Some suit specific applications with open wounds or are for use in hospitals but not one of these products can solely contribute to prolonged survivability; next generation hemostatic agents are needed (DoD 2014).

4.3 Therapeutic Effect of Hemostatic Nanoparticles in Other Injury Models

Hemostatic particles have proven to mitigate internal bleeding in several models of bleeding (Bertram et al. 2009, Shoffstall et al. 2012, Shoffstall et al. 2013, Lashof-Sullivan et al. 2014, Lashof-Sullivan et al. 2016). In a rodent model of lethal liver trauma, hNP were found to reduce blood loss following liver injury and increase survival from 40% in controls to 80% in animals given hNP after injury (Shoffstall et al. 2012). Another study of lethal liver trauma in rodents was conducted to demonstrate increased efficacy with higher concentration of the targeting peptide (GRGDS) and resulted in a similar increase in survival (92% to 45%) for hNP compared to controls (Shoffstall et al. 2013). A rodent model of major femoral artery injury was initiated to examine bleeding time after administration of hNPs (Bertram et al. 2009). As a proof-of-concept, agents were administered prior to injury and bleeding time after hNP administration was reduced 45% compared to Injury Only controls and reduced 25% more than NovoSeven. In a model of blast polytrauma, hemostatic nanoparticles (hNPs) were shown to increase survival and reduce lung injury without long-term complications (Lashof-Sullivan et al. 2014). The effect

on acute blast exposure implicates that recovery will lead to better subacute outcomes. hNPs have far reaching applications for internal bleeding after car crashes or blast exposure.

4.4 Therapeutic Effect of Dexamethasone in Other Injury Models

Dexamethasone was determined to be a suitable steroid-link for this hNP treatment due to its anti-inflammatory properties and non-effect on coagulation. Dexamethasone has been shown to reduce lung injury, monitored by leukocyte infiltration and hemorrhage, clinically as well as in a rodent model of acute lung injury (Araz et al. 2013). In a lung injury model, dexamethasone in conjunction with targeting nanogels, has been shown to alleviate pulmonary inflammation one day after administration (Coll Ferrer et al. 2014). Sustained delivery of dexamethasone from coated nanoparticles has been shown to be necessary to elicit biological effects (Lo et al. 2010). By reducing the effects of pro-inflammatory cytokines responsible for tissue damage after injury, dexamethasone is an attractive option for treatment of PBLI, and the drug lends itself to encapsulation in a hemostatic nanoparticle formulation to aid recovery following injury.

The therapeutic effect of dexamethasone has been previously examined in brain injury models (Shain et al. 2003, Lee et al. 2014, Hue et al. 2015). It has been shown to reduce programmed cellular death, or apoptosis, due to hemorrhage in the brain while also inhibiting inflammation after injury (Lee et al. 2014). Dexamethasone has been shown to reduce inflammation due to amyloid beta in the cerebrovasculature, in relation to Alzheimer's disease (AD) (Previti et al. 2006). A recent review by Obermeier et al. described the only applicable BBB therapeutic as glucocorticosteroid (GC) treatment (Obermeier et al. 2013). Dexamethasone, an anti-inflammatory GC, has been shown to inhibit matrix metalloproteinase (MMP) levels and consequently improve vessel wall integrity by preserving BBB components (Forster et al. 2007). In an *in vitro* model of primary blast injury, BBB restoration occurred *via* glucocorticoid receptor signaling by dexamethasone (Hue et al. 2015). Dexamethasone has also been shown to attenuate astrocytosis after peripheral injection and local delivery through polymers (Shain et al. 2003).

4.5 Methodology of Synthesis

4.5.1 Particle Synthesis

PLGA-PLL-PEG-GRGDS block copolymer for the hemostatic nanoparticles and PLGA-PLL-PEG-GRADSP were synthesized using protocols described previously (Bertram et al. 2009, Shoffstall et al. 2012, Shoffstall et al. 2013). In brief, the triblock polymer was synthesized using stepwise conjugate reactions. The PLGA was coupled to poly(ε-cbz-L-lysine) (PLL-cbz; PLL with carbobenzoxy-protected amine side groups). The conjugation was confirmed by UV-vis spectroscopy. After the PGA-PLL-cbz was deprotected with HBr, the free amines of the PLL-NH3 were reacted with CDI-activated PEG in a 5:1 molar excess (Hermanson 1996).

The GRGDS was conjugated to PEG-PLGA (or the conservatively substituted GRADSP) as described previously (20). In brief, the peptide was conjugated by dissolving the PLGA-PLL-PEG (1 g) in anhydrous dimethyl sulfoxide (DMSO) to a concentration of 100 mg/mL and the oligopeptide (25 mg) was dissolved in 1 mL of DMSO and added to the stirring polymer solution. The free amine of the oligopeptide then reacted with free end of the CDI-activated PEG. The mixture reacted for 3 h, and was then transferred to dialysis tubing (SpectraPor, 2 kFa molecular weight cutoff) and dialyzed for 4 h before being snap-frozen in liquid nitrogen and lyophilized (Shoffstall et al. 2013).

To form particles, the polymer was dissolved at a concentration of 20 mg/mL in acetonitrile containing coumarin-6 (C6), a fluorescent dye used to track the particles after injection (loaded at 1% wt/wt). This dye has been previously shown to release <0.5% of the initial loading by 24 h and 1.5% by 7 d. This solution was added dropwise to a volume of stirring PBS twice that of the acetonitrile (Cheng et al. 2007). Precipitated nanoparticles form as the water-miscible solvent is displaced.

4.5.2 Coacervate Precipitation

Coacervate precipitation was adapted from D'Addio and performed as previously described (Bertram et al. 2009, D'Addio et al. 2010). Briefly, one mass equivalent of dry poly(acrylic acid) (PAA) was added to the stirring nanoparticle solution. Then, a solution of 1% PAA was added until flocculation occurred. The flocculated nanoparticles were then collected by centrifugation. After rinsing, they were suspended in approximately 10 mL deionized water,

snap-frozen, and lyophilized for three days. Nanoparticles were resuspended at 20 mg/mL in Lactated Ringer's solution and briefly sonicated.

4.5.3 Nanoparticle Characterization

Nanoparticles were characterized for diameter using dynamic light scattering (DLS) (90Plus; Brookhaven Instruments) and scanning electron microscopy (Hitachi S4500). DLS data were represented as the effective diameter as calculated using the 90Plus software. The PEG corona of the nanoparticles as well as presence of dexamethasone was characterized by NMR (600-MHz Varian Inova NMR spectrometer). Data were collected with particles suspended in deuterated water (D2O) and again with particles dissolved in deuterated chloroform (CDCl3).

4.6 Methodology of Hemostatic Dexamethasone-Loaded Nanoparticles

4.6.1 Polymer Synthesis

PLGA-PLL-PEG-GRGDS block copolymer was synthesized as previously described (Shoffstall et al. 2013). Briefly, poly(lactic-co-glycolic acid) (PLGA resomer 503H) and poly(ε-cbz-L-lysine) (PLL-cbz) PLL with protected amine side groups (Sigma P4510) were coupled and conjugation was confirmed using UV-vis. The amine side groups were deprotected with HBR, and the free amines reacted were reacted with CDI-activated poly(ethylene glycol) (PEG). The copolymer PLGA-PLL-PEG (with CDI activated PEG end groups) was then reacted with the peptide GRGDS (or the control peptide GRADSP) in DMSO and purified by dialysis.

4.6.2 Nanoparticle Formation

The steroid, dexamethasone, was dissolved in acetonitrile at a concentration of 4 mg/mL. Particles for biodistribution were instead made by dissolving the fluorescent marker coumarin (C-6) at 0.2 mg/mL. The block copolymer, PLGA-PLL-PEG-GRGDS, was then dissolved at a concentration of 20 mg/mL in the dexamethasone (or C-6) acetonitrile solution. This solution was added dropwise to a volume of stirring PBS. Nanoparticles were then collected by coacervate precipitation as described below.

4.6.3 Coacervate Precipitation

This was performed as described in 4.5.2.

4.6.4 Nanoparticle Characterization

This was performed as described in 4.5.3.

4.6.5 Dexamethasone Release Study

A release study was performed to determine how dexamethasone is be eluted from the particles. Particle samplers were incubated at 37^{O}C in PBS. The samples were centrifuged to remove the supernatant at regular intervals. This supernatant was analyzed using Uv-Vis spectroscopy at 241 nm to determine dexamethasone concentration. The particles were then suspended in additional PBS and returned to the incubator. Supernatant samples were taken over a 13 week time period to calculate the cumulative dexamethasone release. Initial loading was determined by fully dissolving particles in DMSO and centrifuging to remove the supernatant. The supernatant was analyzed by Uv-Vis spectroscopy to determine the initial dexamethasone concentration of the particles.

4.6.6 Biodistribution

Animals given a dose of particles containing C-6 (particles for biodistribution) were euthanized at one hour following blast. Organs, including kidneys, lungs, liver, spleen, and brain, were collected and lyophilized for the biodistribution assay. The dry weight of the whole organ was recorded, and a 100-200mg sample of the organ was homogenized (Precellys 24). 1 mL of acetonitrile was then added and samples were incubated at 37 ^{o}C for 24 hours. A quantity of particles to determine loading was also dissolved in 1 mL of acetonitrile and incubated for 24 hours. This dissolved the nanoparticles remaining in the tissue and released the C-6 contained in the particles. The samples were centrifuged and the supernatant was collected for analysis on HPLC (Shimadzu) with fluorescence detection (450/490nmex/em). The C-6 concentration in the organs was then compared to the loading concentration to determine how much of the particle dose was found in each organ.

4.7 Results

4.7.1 SEM Image of Nanoparticles

A representative scanning electron microscope, or SEM, image of the particles (Figure 31AB) shows that the treatment is a spherical nanoparticle of approximately 500 nm in size. This sizing measurement is confirmed by dynamic light scattering (DLS) measurement (Figure 31C).

A

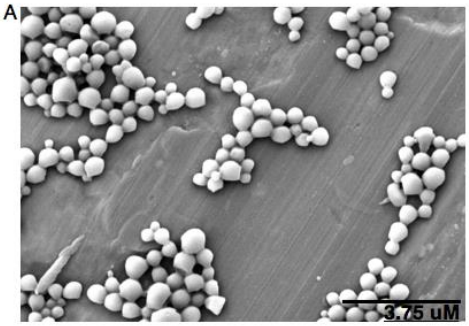

B

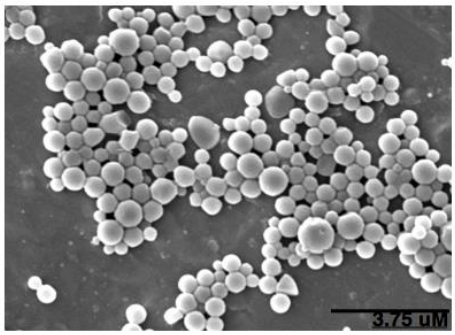

C

Nanoparticle Formulation PLGA-PLL-PEG-X	DLS Mean Diameter (nm +/- SD)	SEM Mean Diameter (nm +/- SD)
X= GRGDS+DEX hDNP treatment	484 +/- 78	504 +/- 113
X= GRADSP+DEX cDNP treatment	553 +/- 132	555 +/- 125

Figure 31. (A) SEM of hemostatic dexamethasone loaded nanoparticles (hDNPs) (B) SEM of control dexamethasone loaded nanoparticles (cDNPs) (C) Particle size as measured by SEM and DLS.

4.7.2 NMR

Nuclear magnetic resonance (NMR) data indicated that the poly(ethylene glycol) (PEG) arms form a corona when suspended in aqueous solution, indicated by in increased size of the PEG peak ($\delta = 3.21$) in deuterated water (D2O) in relation to other peaks. In addition the dexamethasone peak ($\delta = 1.68$) were visible in deuterated chloroform (CDCl3) indicating that the dexamethasone is encapsulated by the particles. Total loading of the dexamethasone is 22 ug/mg.

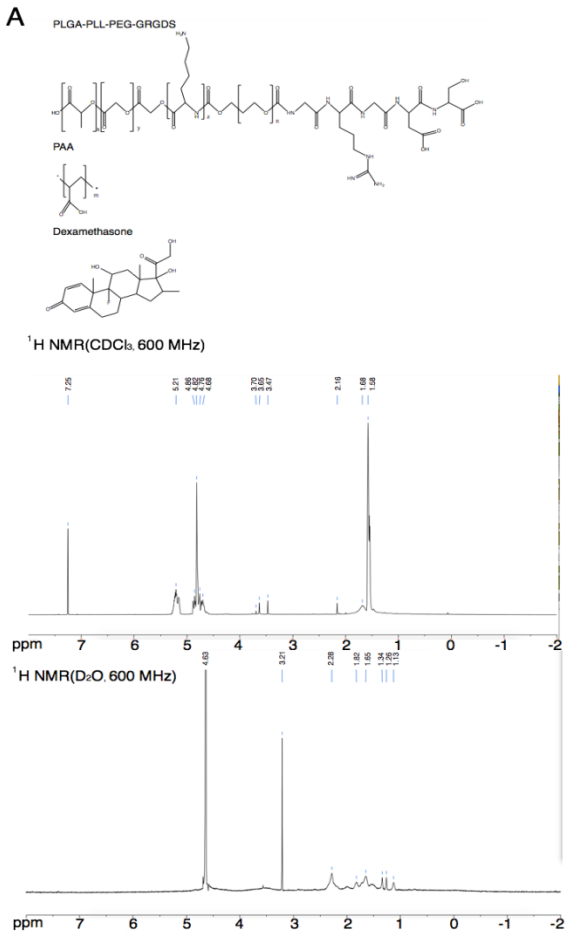

Figure 32. Molecular structure of nanoparticles as well as dexamethasone. Characterization of the nanoparticles by NMR in deuterated chloroform and deuterated water, showing the presence of the PEG corona.

4.7.3 Dexamethasone Release

Release data showed that the majority (70%) of the dexamethasone is released within the first 24 hours of incubation (Figure 33). This is beneficial in our injury model since it releases over the first day to help acutely but it is not exhausted all in the first hour. After 63 days, 95% of the loaded dexamethasone has been released.

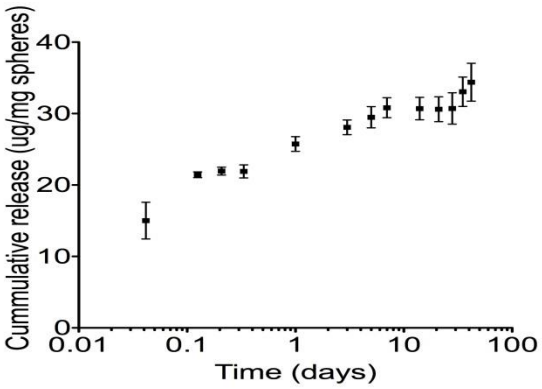

Figure 33. Release of dexamethasone from hemostatic nanoparticles over time.

4.7.4 Biodistribution

Biodistribution data show the vast majority of the injected dose seen in organs is located in the right lung. This coincides with lung injury data in Chapter 2.

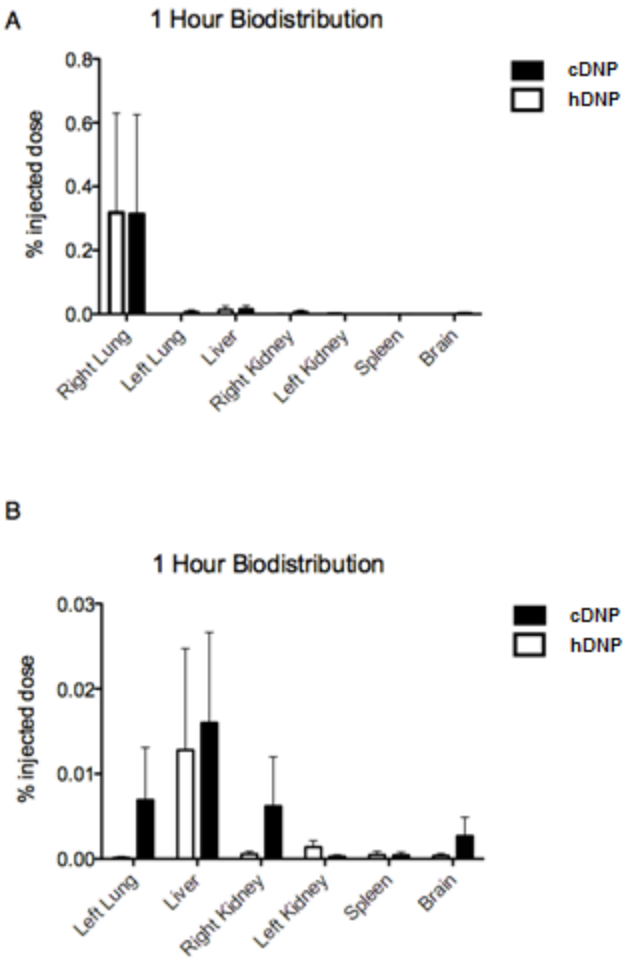

Figure 34. (A) One hour biodistribution study for hDNP and cDNP (hDNP, n=6; cDNP, n=8). Results show that vast majority of the nanoparticle accumulation is in the right lung for both hDNP and cDNP. (B) Zoom view for one hour biodistribution study on all organs examined except for the right lung.

4.7.5 Confirmation of Injection

Evans blue dye was injected to confirm injection of nanoparticles. This dye was seen where injured was sustained, even secondary injury from acetate shrapnel (Figure 35).

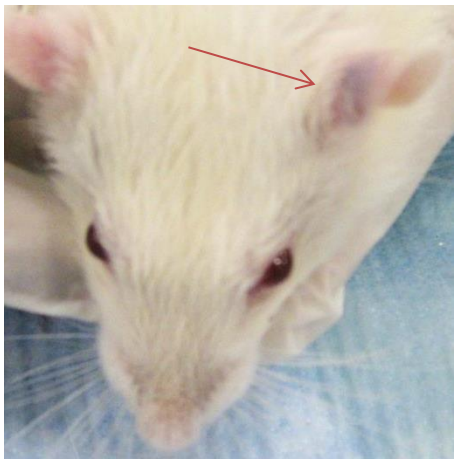

Figure 35. Evans Blue found in ear after with small laceration

Evans blue dye was also found in the lungs, as expected with the extent of injury sustained. Figure 36A contains lungs exposed to 179 kPa static peak overpressure and injected with hDNP while Figure 36B contains lungs exposed to 200 kPa static peak overpressure and injected with cDNP.

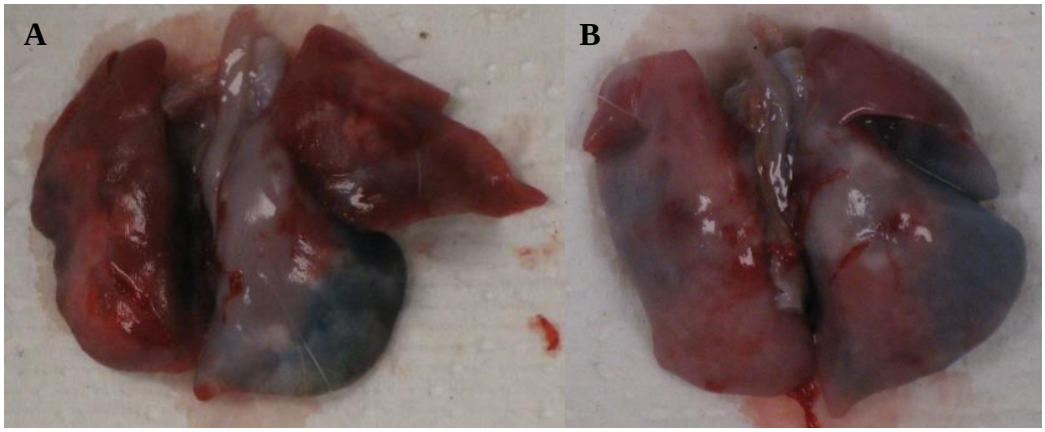

Figure 36. Evans Blue found in the lungs after administration of treatment

4.8 Discussion and Conclusion

The size of the nanoparticles with dexamethasone loaded was 500 nm, which is too large to cross the blood-brain barrier. If there was microhemorrhaging present in the BBB, there could be direct action of the nanoparticles in the brain. The dexamethasone release curve shows that

there is an initial burst released followed by the majority released in the first day. Dexamethasone is steadily released until day ten, so there is some long-term therapy.

Biodistribution data show that most of the injected nanoparticles are located in the lungs one hour after injury and injection. This is due to localized hemostasis where most of the acute hemorrhaging occurs. A small percentage is found in the brain suggesting some therapeutic action initially at one hour but nanoparticle location can change over time. Injection confirmation was macroscopically analyzed by adding Evans blue dye to the nanoparticle injection. The blue dye was found in the lungs at seven days after injury.

The characterization of the nanoparticles shows the functionality and properties that make the hemostatic nanoparticles a viable option for therapeutic after injury. Localization and release profile of dexamethasone give immediate therapy as well as prolonged release to assuage injury and secondary mechanisms.

Chapter 5: Investigation of the Therapeutic Effects of Hemostatic Nanoparticles after Blast Polytrauma: Lung Pathology

This section has been adapted from Hubbard, et al. "Steroid-Loaded Hemostatic Nanoparticles Combat Lung Injury after Blast Trauma" *ACS Macro Letters,* 2015. 4(4): 387-391.

This data is a result of collaboration with Case Western Reserve University. The nanoparticles and treatments were synthesized and developed by Dr. Margaret Lashof-Sullivan and other collaborators at Case Western. All immunohistochemistry and behavior, as well as experiment testing, was performed at Virginia Tech.

5.1 Introduction

5.1.1 Statement of Problem

PBLI is a significant cause of death due to internal hemorrhage following detonation of improvised explosive devices (Yeh and Schecter 2012). Explosions account for the majority of injuries in the current military conflicts (Ramasamy et al. 2008). There is a severe lack of treatments for traumatic injuries, especially for on-site administration. A readily assessable treatment to decrease mortality of those who suffer from internal trauma is needed. Moreover, it is vital that treatment must occur within the first hours following injury to increase survival (ATLS 2004). Our blast trauma rodent model can be utilized as a tool to assess novel nanotherapeutics (Hubbard et al. 2014). There is a clear call for therapeutic intervention for treating lung injury and internal hemorrhage immediately after blast exposure (Huller and Bazini 1970, Clifford 2004).

5.1.2 Significance

In response to the lack of therapeutics for internal bleeding following a traumatic event, hemostatic dexamethasone nanoparticles (hDNP) were synthesized to help alleviate internal hemorrhaging and were evaluated after PBLI. Increased survival has been shown in a mouse model as a result of hDNP administration, citing a direct effect of improved the coagulation process mediated by the nanoparticle (Lashof-Sullivan et al. 2014). This is the first study to assess hDNP in a rodent model of blast trauma. In addition to effects on survival and acute

hemorrhaging, recovery using physiological parameters and immunohistochemistry in the lung will provide indication of subacute (seven days post-injury) benefits from therapeutic intervention. hDNPs are hypothesized to fill the need as a therapeutic for internal bleeding mitigation, also aiding concerns that arise from blood loss (Champion et al. 2003). hDNP have the potential to alleviate physiological impairment caused by blast injury and reduce lung injury damage.

5.2 Literature Review

5.2.1 Physiology and Internal Bleeding after Primary Blast Lung Injury

Changes in physiological parameters have been reported following PBLI, such as oxygen content and heart rate. Hypoxemia has been observed post-blast, monitored by a reduction in partial pressure of oxygen (PAO2), due to pulmonary hemorrhage leading to a ventilation-perfusion mismatch (Irwin et al. 1997, Knoferl et al. 2003). Apnea concomitant with oxygen desaturation is a common outcome found in animal studies of PBLI (Mayorga 1997).

Some of the first pre-clinical experimental findings of intra-alveolar hemorrhage and alveolar-capillary rupture were cited in studies of blast lung injury with right lateral blast exposure (Fung 1984, Jaffin et al. 1987, Brown et al. 1993). Brown, et al. found that pathological conditions in the lung after blast injury progressed over time, such that lobes which did not present with hemorrhage at 30 minutes post-injury showed edema and hemorrhage at one day post-injury (Brown et al. 1993). Studies have confirmed findings of hemorrhage and edema, as well as examined markers of inflammation and oxidative damage (Elsayed and Gorbunov 2003, Chavko et al. 2006). Hemorrhage in the lungs has been well documented in models of PBLI (Brown et al. 1993, Zhang et al. 1996, Bauman et al. 1997, Elsayed et al. 1997, Cernak et al. 2001, Knoferl et al. 2003, Chavko et al. 2006). It has been reported that blast exposure as low as 62 kPa can cause infiltration of red blood cells (RBCs) in the alveolar spaces and biochemical changes in the lungs (Elsayed and Gorbunov 2007). A PBLI model with BOP ranging from 12.5 to 16.25 kPa produced lesions in the left lobe as well as bilateral traumatic pulmonary hemorrhage (Gorbunov et al. 2003). Researchers induced PBLI in order to examine the effects of varied overpressures and lung recovery post-blast; however, methodologies have not been standardized (Chavko et al. 2006, Skotak et al. 2013). Our previous study provided more

thorough evidence that contusion and hemorrhaging in the left lobe was correlated with a higher incidence of lethal outcomes (Hubbard et al. 2014).

5.2.2 Lung Pathology after Primary Blast Lung Injury

Animal models of PBLI have been studied in order to analyze inflammatory, anti-oxidant, and other physiological characteristics of the injury (Elsayed et al. 1997, Irwin et al. 1997, Elsayed et al. 2000, Elsayed and Gorbunov 2003, Knoferl et al. 2003, Liener et al. 2003, Gorbunov et al. 2006, Flierl et al. 2008, Seitz et al. 2008, Chavko et al. 2009). Limited research has been conducted with the objective of investigating pharmaceutical treatments geared towards mitigating PBLI (Chavko et al. 2008, Chavko et al. 2009). Although there is little data on the pathology of PBLI, apoptosis and inflammation are two observed activated signaling pathways documented. It has been shown that apoptosis, as well as necrosis, was elevated in low oxygen environments (Michiels 2004, Lee et al. 2012). As described in Seitz, et al., apoptosis of alveolar type 2 cells contributed to the loss of epithelial cells following lung contusion (Seitz et al. 2008). In a study by Liener, et al., apoptosis was identified as a cellular mechanism after pulmonary contusion (Liener et al. 2003).

The pro-inflammatory response has been characterized with increased levels of myeloperoxidase at one day and chemokine, intercellular adhesion molecule-1(ICAM-1), increased at two days post-blast (Chavko et al. 2006). Recent efforts have also looked at the combined effects of blast and burn exposure on lethality and inflammatory cytokines (Chai et al. 2013). Inflammatory cytokines, such as tumor necrosis factor-α (TNF-α) and interleukin-6 (IL-6), have been examined in a model of PBLI. Knoferl, et al. demonstrated that levels of TNF-α and IL-6 were elevated three hours post-blast in blood plasma due to the thoracic trauma (Knoferl et al. 2003). Injury-induced cytokines are known to contribute to tissue damage (Brown et al. 1993). TNF-α has been shown to induce apoptosis leading to cleavage of DNA into fragments (Rath and Aggarwal 1999). These studies provide evidence that inflammation is a key mediator for injury progression in the lungs and is a likely contributor to PBLI pathology.

5.3 Methods

5.3.1 Experimental Set-up

The Virginia Tech Institutional Animal Care and Use Committee approved experimental protocols described herein. Prior to all experiments, male Sprague Dawley rats (~325 g, Harlan Labs, San Diego) were acclimated to a 12 hour light/dark cycle with food and water provided ad lib. Animals (n=65) were exposed to a single incident pressure profile resembling a 'free-field' blast exposure (range of 170 to 190 kPa).

Using the following settings, necessary sample size of the seven day study was calculated: Power (1-β) ≥ 0.8; α ≤ 0.05; Groups: 5; Minimum detectable difference in means (d) = 20%; Expected standard deviation (s) = 10%. Using power and α values, C = 7.85.

$n = 1 + 2C(\frac{s}{d})^2 = 1 + 5(7.85)(\frac{.10}{.20})^2 =$10.8. (Dell et al. 2002)

Power Analysis determined that a minimum of 10-12 animals per group were needed for the seven day post-blast study.

For the one hour study, all animals were randomly assigned to one of five groups: hNP, control nanoparticles (cNP), Lactated Ringer's (LR), Injury Only (IO), and sham (n=6/group). For the seven day study, all animals were randomly assigned to one of five groups: hDNP, control dexamethasone-loaded nanoparticles (cDNP), Lactated Ringer's (LR), Injury Only (IO), and sham (N = 23, 20, 22, 12, and 18, respectively).

Prior to blast exposure, rats were anesthetized with a ketamine/xylazine solution, in accordance with the rodent weight, for sedation during blast and the one hour post-blast monitoring. The shock front and blast overpressure were generated by a custom-built ABS (ORA Inc. Fredericksburg, VA) located at the Center for Injury Biomechanics at Virginia Tech. The ABS consists of a driving compression chamber attached to rectangular test section chamber with an end-wave eliminator as shown in Figure 9.

A peak static overpressure was produced with compressed helium and calibrated acetate sheets (Grafix Plastics, Cleveland, OH). Pressure measurements were collected at 250 kHz using a Dash 8HF data acquisition system (Astro-Med, Inc, West Warwick, RI) and peak overpressures

were calculated by determining wave speed (m/s) at the specimen position. A mesh sling was used to hold the animal during the exposure that allowed for minimal hindrance of the wave through the tube, in addition to holding the animal in a prone position with the right side of the thorax facing the shock wave driver. The animal was not allowed impact any solid surface in order to prevent secondary injuries.

Immediately after blast exposure, animals were injected with treatment (hDNP, cDNP, LR, or IO; 500 μL total volume) via tail vein injection. The injected treatment also included Evans blue which binds to albumin in the blood circulation (Chapter 4.7.5). This addition helped us visualize the injection and provided for macroscopic visualization of albumin-Evans blue infiltration after hemorrhage. The hDNP and cDNP groups were dosed at 4 mg/kg of the nanoparticles suspended in LR. A physiological monitoring system (Nonin PulseSense VET Pulse Oximeter, #033692, Henry Schein Inc.) was used to collect physiological parameters such as heart rate and oxygen saturation at one hour post-blast. The minimum recording for HR and oxygen saturation was documented for analysis. Sham animals underwent all procedures except for blast exposure and tail vein injection.

5.3.2 Tissue Processing

To assess acute hemorrhage, a subset of animals (n=6/group) were euthanized by transcardial perfusion of saline and 4% paraformaldehyde at one hour post-blast. After seven days, the rest of the animals were euthanized by transcardial perfusion of saline and 4% paraformaldehyde. Following collection, lungs were stored in a 4% paraformaldehyde fixative solution. After 48 hours in fixative, the lungs were placed in 30% sucrose solution for tissue sectioning preparation. Lungs were separated into cassettes with each lobe isolated for analysis and embedded in Tissue-Tek® optimal cutting temperature (O.C.T.) embedding medium (Sakura Finetek USA, Inc., Torrance, CA) for cryostat processing. Samples were then cut (8 μm) and stained with hematoxylin and eosin (H&E) to predict injury extent. Images were taken of three regions of interest (Okeda, Okada) in each lung tissue section at 10X magnification (Zeiss AxioCam ICc 1). The images were converted to black and white and optical density readings were collected in order to determine the level of hemorrhaging in the lung tissue using Image J software (NIH, Bethesda, MD). The percent injured area was calculated in each lobe and significance was determined and reported as mean ± SEM.

5.3.3 Immunofluorescent Staining

Immunohistochemistry was performed on lung tissue for TNF-α (an inflammatory cytokine) and cleaved caspase-3 (early apoptosis marker). Pre-mounted samples were frozen overnight and then rinsed three times with PBS and incubated in 2% BSA in PBS for one hour at room temperature. The histological sections labeled with primary antibodies were taken from the mid-point of the respective lobe for consistency. Sections were then incubated with a primary antibody (anti-cleaved caspase-3 (Cell Signaling Technologies, Danvers, Massachusetts) or anti-TNF-α (Abnova, Taipei City, Taiwan) at 1:500 overnight at 4ºC. All sections were only labeled with one primary antibody. After a PBS wash, the samples were incubated for 1.5 hours with Alexa Fluor 555 anti-rabbit IgG antibody or Alexa Fluor 488 anti-mouse IgG antibody (1:500; Cell Signaling, Danvers, MA). After a PBS wash, samples were air dried and coverslipped with prolong antifade gold reagent with 6-diamidino-2-phenylindole (DAPI; Invitrogen, Carlsbad, CA). Sections were examined under Zeiss fluorescence microscope at 20X magnification (three images per tissue section) under appropriate fluorescent filters and images were taken by Zeiss AxioCam ICc 1. Fluorescence intensity of acquired digital images was quantified by ImageJ software (NIH, Bethesda, MD).

5.3.4 TUNEL Assay

Terminal deoxynucleotidyl transferase dUTP nick end labeling (TUNEL) was performed to assess DNA fragmentation associated with apoptotic signaling cascades. In situ cell death detection kit (Roche Diagnostics, Indianapolis, Indiana) was utilized to mark DNA strand breaks fluorescently. This TUNEL technique was quantified using the Zeiss fluorescence microscope (three images per tissue section) and the intensity was determined using ImageJ.

5.3.5 Statistical Analysis

Statistical differences between the treatment groups were assessed with analysis of variance using LSD post-hoc test. All statistical analyzes were performed using JMP Pro 10 (SAS Institute, Cary, NC) and $p < 0.05$ considered statistically significant. Unless indicated otherwise, data are presented as mean ± standard error of the mean, or SEM.

5.4 Results

5.4.1 Survival

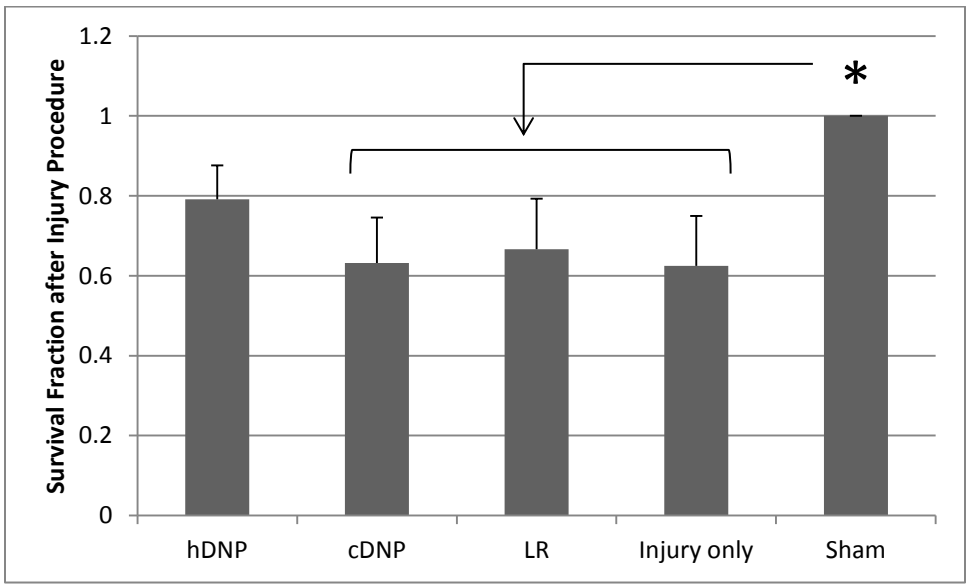

Figure 37. Survival at seven days post-blast. The sham group is significantly different compared to Injury Only, LR, and cDNP groups ($p<0.05$), but not to the hDNP group.

For seven day survival, the sham group was significantly different ($p<0.05$) from all groups except for the hDNP groups (Figure 37). The Injury Only group had 60% survival while hDNP survival approached 80%.

5.4.2 Physiology

There was a significant difference between the hDNP and the other blast groups (cDNP, LR, and IO) in terms of minimum oxygen saturation during the one-hour post-blast monitoring period (p-value < 0.05). (Figure 38A) When evaluating the acute heart rate response following injury, similar trends were observed as the hDNP group was higher when compared to the cDNP group. (Figure 38B)

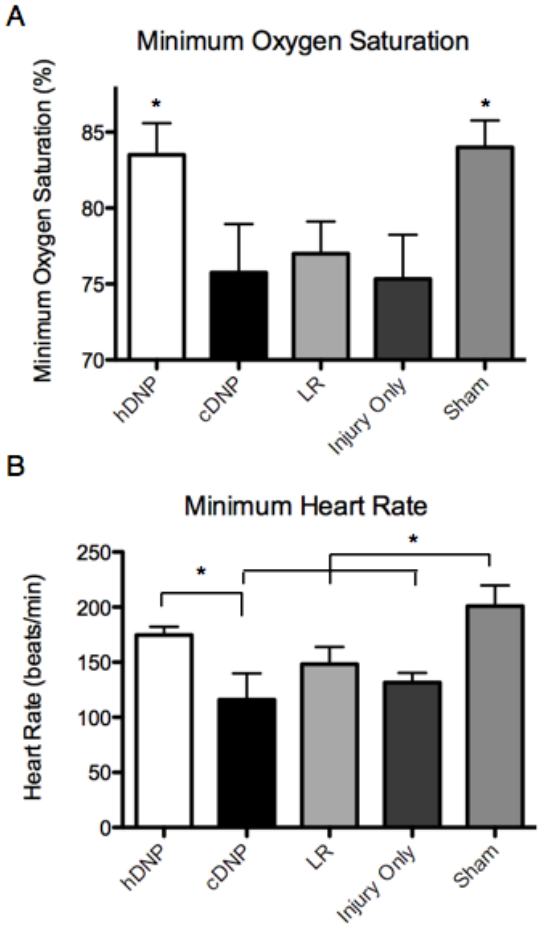

Figure 38. (A) Oxygen saturation for treatment groups (B) Heart rate for treatment groups (* - p-value < 0.05)

5.4.3 Lung Hemorrhage – One Hour

For the one hour study, hemostatic nanoparticles without dexamethasone were evaluated to determine the therapeutic effect of hemostasis. Lung hemorrhage at one hour post-injury was significantly lowered ($p<0.05$) after hNP treatment compared to cNP, LR, and Injury Only (Figure 39).

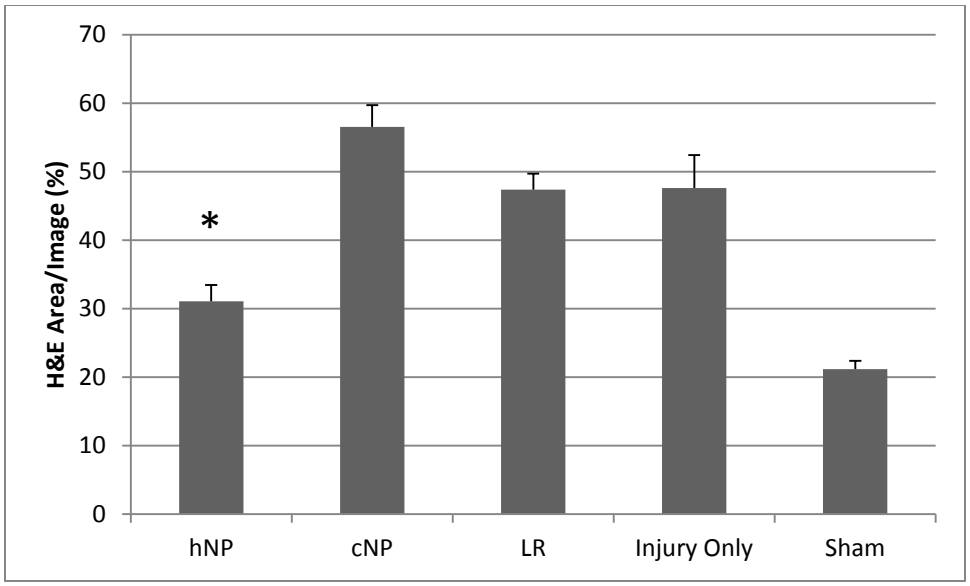

Figure 39. Percent area of hemorrhage and interstitial edema, constituting lung injury. Numbers include normal lung structure of alveolar walls. (* - p-value < 0.05)

5.4.4 Lung Hemorrhage – Seven Days

Figure 40 displays representative images of H&E staining in the lung cross-section. The hDNP and sham groups have significantly lower hemorrhage levels compared to the cDNP and Injury Only groups (* $p < 0.05$) at seven days after blast (Figure 40). Staining represents (A) hDNP (B) cDNP (C) LR (D) IO and (E) Sham.

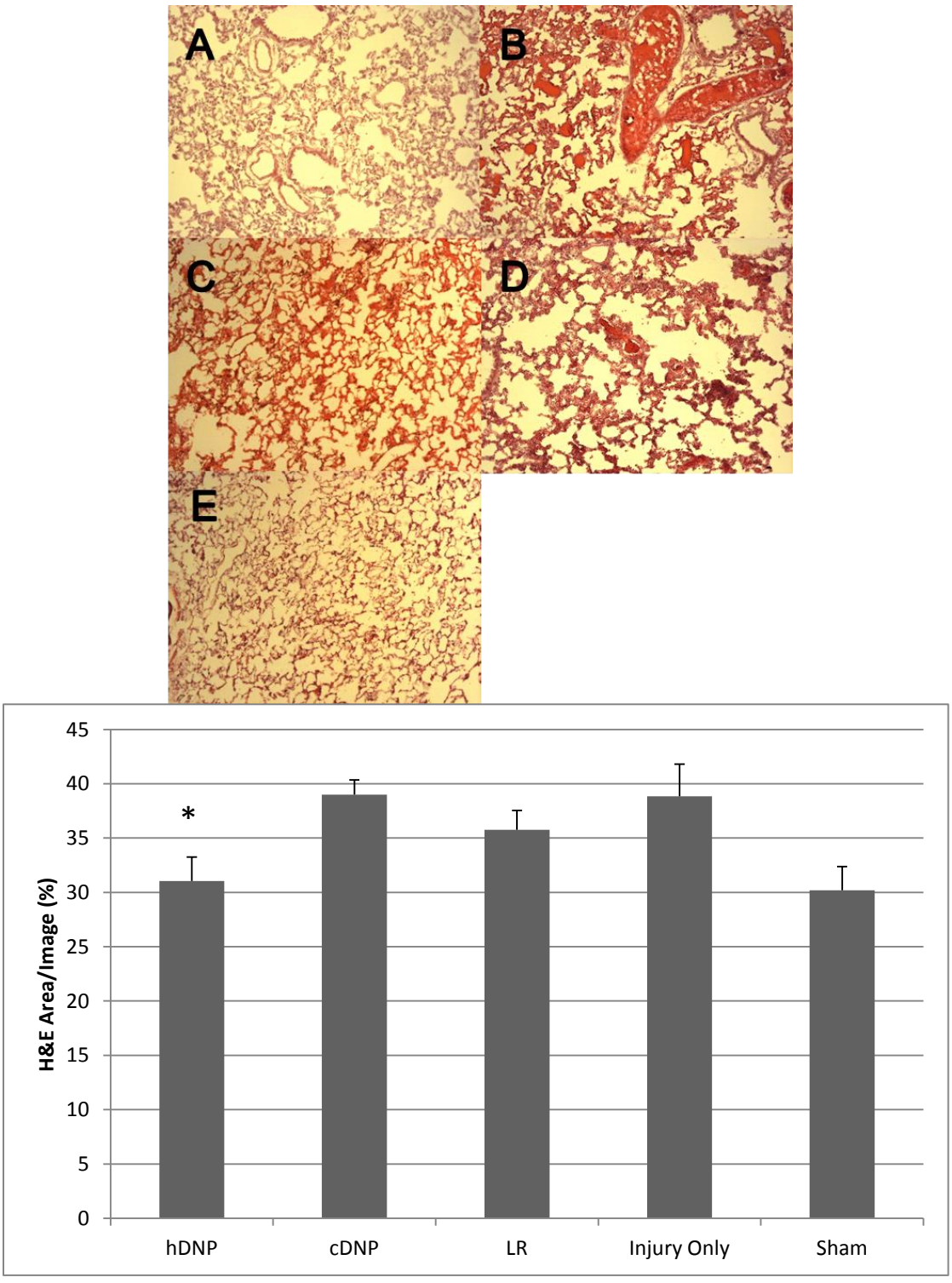

Figure 40. Representative images of H&E stained tissue which were used to assess internal hemorrhage in the left lobe after blast. hDNP was statistically significant compared to cDNP and Injury Only ($p<0.05$).

5.4.5 Caspase-3 Staining

Figure 41 shows representative images from cleaved caspase-3 immunofluorescence on the left lobe. The hDNP group had significantly lower amount of early stage apoptosis compared to the other blast groups (cDNP, LR, and IO) at the seven day time point after injury ($p<0.05$).

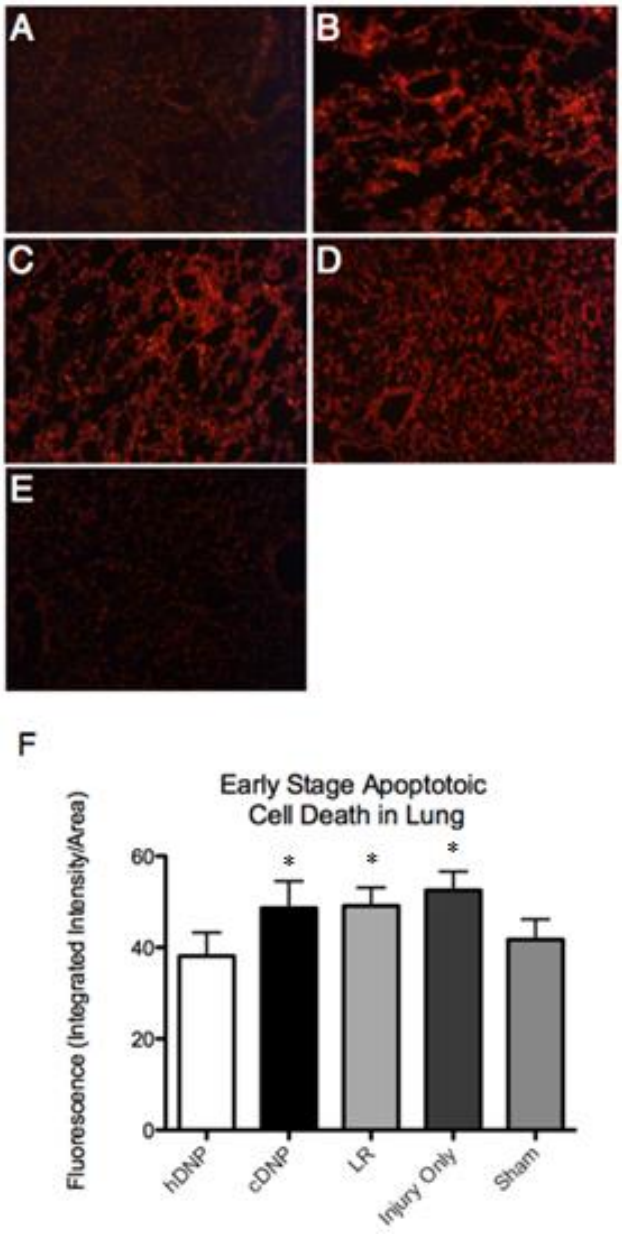

Figure 41. Representative images of cleaved caspase-3 staining for (A) hDNP (B) cDNP (C) LR (D) IO and (E) Sham. (F) The cDNP, LR, and IO groups have significantly elevated levels compared to the hDNP and sham groups at seven days after blast (* - $p<0.05$).

5.4.6 TNF-α Staining

Figure 42 shows representative images from TNF-α staining. For percent area of TNF-α fluorescence, the hDNP and sham group were significantly reduced compared to the other blast groups (cDNP, LR, and IO) at the seven day time point ($p<0.05$).

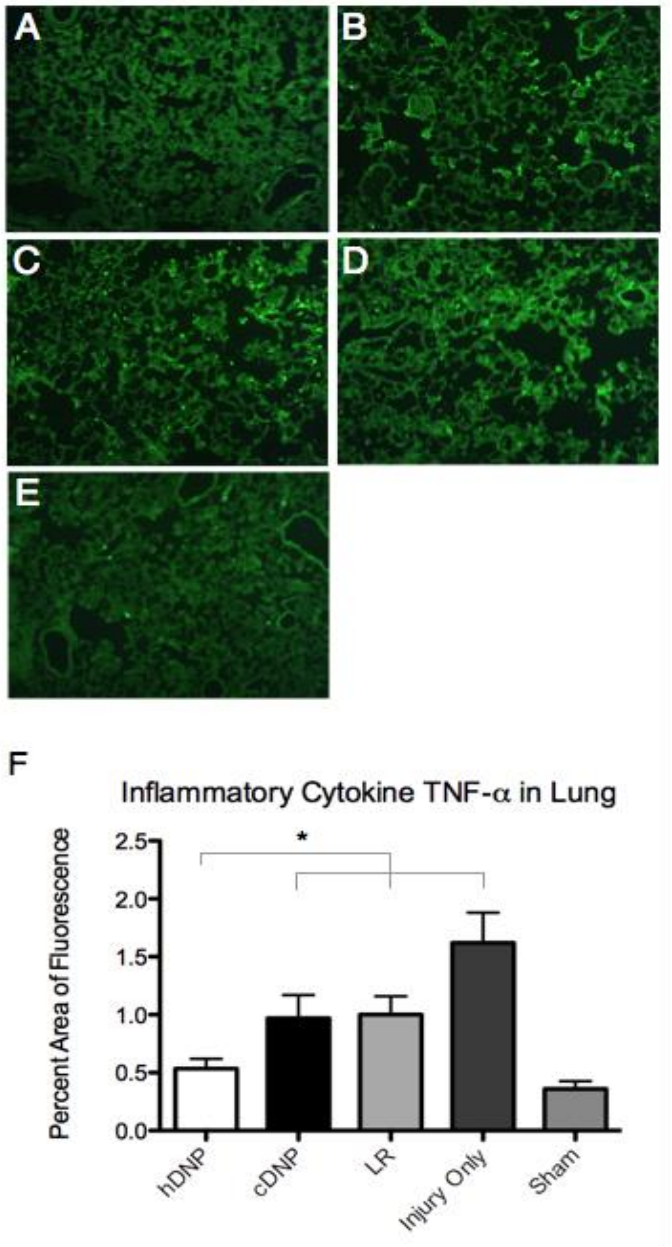

Figure 42. Representative fluorescent images of TNF-α. (A) hDNP (B) cDNP (C) LR (D) IO and (E) Sham (F) The average percent area of the TNF-α fluorescence. (* - p<0.05)

5.4.7 TUNEL Assay

Figure 43 shows representative images from the TUNEL assay on the lung tissue. The hDNP group had a significantly lower amount of late stage apoptosis compared to the other blast groups (cDNP, LR, and IO) at the seven day time point after injury ($p<0.05$).

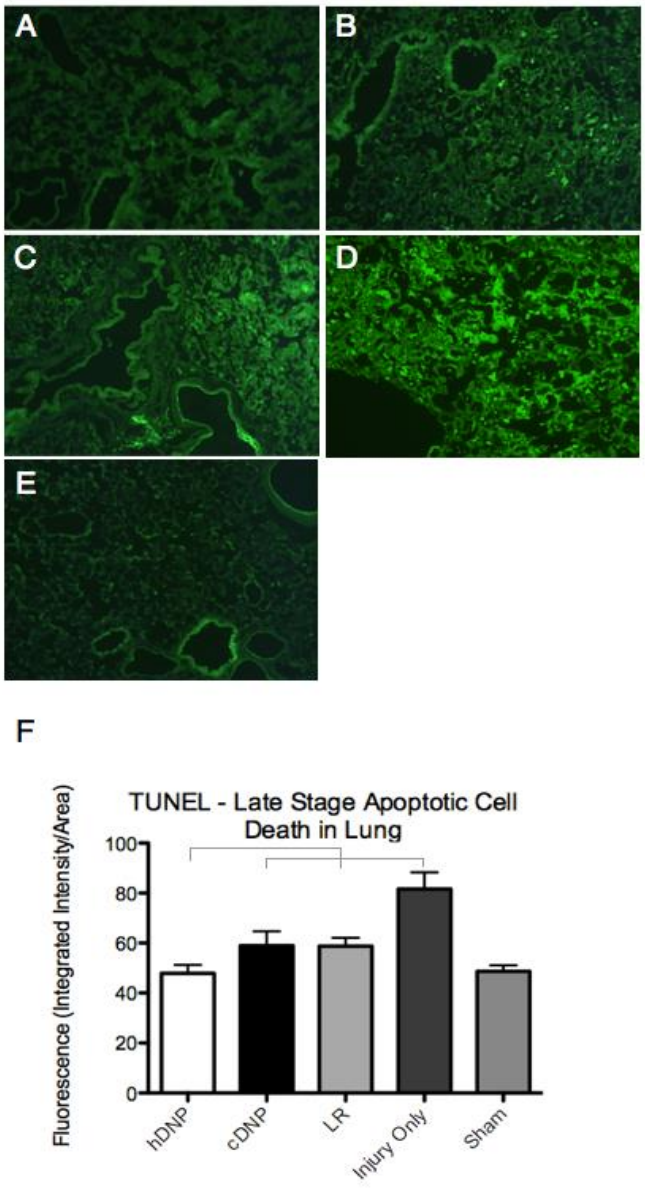

Figure 43. Representative TUNEL staining for (A) hDNP (B) cDNP (C) LR (D) IO and (E) Sham. (F) The hDNP group and sham group are significantly different compared to the cDNP, LR, and IO groups at seven days after injury (* $p<0.05$).

5.5 Discussion

Treatment with hDNP improved outcomes in acute measures of lung injury. Reduced levels of oxygen saturation after lung trauma are harmful to survival as well as tissue health. There was a significant difference between the hDNP and the other blast groups (cDNP, LR, and IO) in terms of minimum oxygen saturation during the one-hour post-blast monitoring period ($p < 0.05$) (Figure 38A). This suggests that animals treated with hDNP experience a more immediate level of recovery in terms of supplying oxygen to the body. As commented on in Brown, et al., the compensatory response during lung contusion of the undamaged areas of the lung played an important role in combating hypotension and apnea after initial trauma (Brown et al. 1993, Irwin et al. 1999). When evaluating the acute heart rate response following injury, similar trends were observed as the hDNP group was higher when compared to the cDNP group. (Figure 38B) Physiology after blast was beneficially influenced by administration of hDNP but not cDNP.

Previously, a PBLI model was shown to produce lesions in the left lobe as well as bilateral traumatic pulmonary hemorrhage (Gorbunov et al. 2003) . Contusion and hemorrhaging in the left lobe has been correlated with a higher incidence of lethal outcomes in preliminary studies (Hubbard et al. 2014). Figure 40 demonstrates that the hDNP treatment, as well as the uninjured sham group, had significance when compared to the cDNP, LR, and Injury Only groups, which may also help account for a better outcome in oxygen saturation. Injury-targeting by hDNP is crucial to form enhanced clots in the injured lungs and promote physiologic recovery in the acute stage.

Pathology in the lung after blast has been examined previously (Elsayed et al. 1997, Gorbunov et al. 1997, Gorbunov et al. 2004, Chavko et al. 2006, Gorbunov et al. 2006). One mechanism of lung injury progression suggests that the amount of free actin in the circulation from dying cells that can obstruct circulation in the lungs and destroy pulmonary endothelium (Chavko et al. 2006). This mechanism could pose a delayed response of apoptosis in the lungs and can show how assuaging the injury in the acute stages can alleviate ensuing cellular degradation. Delayed pulmonary injury can be indirectly due to extravasated blood components (Brown et al. 1993, Gorbunov et al. 1997). Apoptotic markers, TUNEL and cleaved caspase-3, were measured to provide a representation of various stages within the apoptosis cascade. Lee, et

al. has shown that apoptosis is elevated in low oxygen environments (Lee et al. 2012). Apoptosis is a consistent finding after blast-induced lung contusion (Liener et al. 2003, Seitz et al. 2008). Knowing that apoptosis of epithelial cells are a result of many post-injury mechanisms, decreased levels of early and late stage apoptotic signals with the hDNP group is a promising result, indicating that this treatment may have a protective effect on surviving cells after trauma.

Cytokines, such as TNF-α, can cause prolonged state of injury after trauma. In a brain ischemia-induced lung injury model, TNF-α positive epithelial cells were seen in lung tissue three days after injury (Liao et al. 2012). In a model of interleukin-2-induced microvascular lung injury, TNF-α was seen elevated in the lung tissue while having undetectable levels in blood serum indicating that local mechanisms are responsible for inflammation and injury progression (Rabinovici et al. 1996). In other models of lung disease, TNF-α protein levels in the tissue were seen at several weeks (Rube et al. 2002). Characterization of the currently tested nanoparticles showed that they can deliver a burst of dexamethasone at an injury site during the few hours after injury, which may also reduce the long-term inflammatory effects of PBLI (see Dexamethasone Release in Chapter 4.7.3). Decreased TNF-α levels at seven days indicates that the hDNP group is effective at mitigating inflammation as well as cellular injury cascades compared to controls after injury.

Multiple administrations of dexamethasone as treatment for lung injury have resulted in therapeutic benefits, reducing hemorrhage and anatomical implications of emphysema (Araz et al. 2013). These same curative effects can be seen in our study, but with only a single administration of hDNP. Targeting activated platelets creates efficiency of dexamethasone's therapeutic effect by local release in the lungs (Lashof-Sullivan et al. 2014). Administration of hDNP has the potential to be a viable option for open field trauma care because of its effectiveness in reducing lung damage and improving oxygen exchange as well as ease of delivery. Treatment with hDNP significantly decreased acute hemorrhaging and alleviated cellular damage of lungs at a subacute stage. The lower levels of TNF-α, accompanied by reduced levels of apoptosis in the hDNP group show a therapeutic effect at a delayed time point. Findings of increased oxygen saturation and lower cell death in the lungs for the hDNP group demonstrate promising therapeutic roles in trauma care.

5.6 Conclusion

Results from Elsayed, et al. (Elsayed and Gorbunov 2007) stress the need for initiating treatment within the first hour following blast exposure due to oxidative stress, pulmonary hemorrhage, and rupture of alveolar walls in the lungs. Due to the absence of therapeutics that target internal hemorrhage, administered nanoparticles are a potential venue to produce this rapid response in cases of PBLI. The way hDNP affects the interplay between physiological parameters, percent hemorrhage, and apoptosis after injury is crucial for survival and healing. Examining the effects of nanoparticles on other inflammatory cytokines in the lungs and blood plasma as well as factors involved with oxidative stress can further validate their performance as a post-injury therapeutic. hDNP administration after traumatic injury mitigates internal bleeding and improve lung pathologic outcomes in this model.

5.7 Future Directions

To fully characterize the injury and what therapeutic influence hemostatic nanoparticles have on the injury, additional investigation of inflammatory markers, such as interleukins, and markers of endothelial damage, such as ICAM-1, should be conducted. While the effect of hDNPs on general apoptosis and inflammation has been assessed in the left lobe, more detail into whether secondary injury is happening globally in the lung or locally is needed. Collecting blood for analysis at acute time points would give the ability to determine cellular mechanisms of apoptosis, such as free actin accumulation. In order to relate PBLI to systemic effects, biomarkers of inflammation and hemostasis should be assessed (Barnett and Ware 2011). The amount of neutrophils found after acute lung injury has been shown to correlate to tissue damage (Seitz et al. 2008, Grommes and Soehnlein 2011). Furthermore, ICAM-1 has been reported after acute lung injury and blocking its expression has ameliorated lung injury (Lundberg et al. 2001). Other endothelial dysfunction markers, such as endothelin-1 and von Willebrand factor, and evaluation of macrophage count in the lungs are crucial components of the injury response (Pittet et al. 1997). Additional inflammatory markers such as interleukin-8 and interleukin-6 constitute part of the inflammatory response after lung injury; additional predictors of endothelial permeability, such as angiopoietin-2, can be assessed (Knoferl et al. 2003, Barnett and Ware 2011). Examination of these markers would give a detailed characterization of the injury, as well as show the therapeutic mechanism of hDNP.

The time course of PBLI needs elucidating in order to further investigate the therapeutic window. Analysis with hemostatic nanoparticles without dexamethasone will pinpoint if dexamethasone release is required for the full therapeutic effect. This will be beneficial to highlight the importance of local release of dexamethasone. Physiology monitored at multiple time points after injury would be beneficial to characterizing recovery time after injury and hemostatic nanoparticle injection. Kirkman and Watts report that hypoxia after blast lung injury can worsen after several hours (Kirkman and Watts 2011). Clinical reports of blast lung trauma have examined hypoxemia becoming progressively worse over one to two days post-injury (Peitzman AB 2007). With these findings, assessing oxygen saturation every hour after blast for at least six hours would give a detailed pattern of the progression or regression of hypoxia. Also, examining oxygen saturation daily from day two until seven would give the time course of recovery.

Chapter 6: Investigation of the Therapeutic Effects of Hemostatic Nanoparticles after Blast Polytrauma: Amygdala Pathology

This data is a result of collaboration with Case Western Reserve University. The nanoparticles and treatments were synthesized and developed by Dr. Margaret Lashof-Sullivan and other collaborators at Case Western. All immunohistochemistry and behavior, as well as experiment testing, was performed at Virginia Tech.

6.1 Introduction

BINT is a debilitating condition developed after blast exposure and has increased incidence in the military. The specific pathways triggered and activated after injury are not fully understood. In addition, neurological deficits result from long-term pathology of BINT. As such, the amygdala, the fear/anxiety regulation center of the brain, was assessed as the therapeutic target for hDNP activity. The purpose of this aim is to investigate whether hDNPs could reduce cellular injury through polytraumatic mechanisms and improve neurological outcomes in a model of whole-body blast trauma.

6.1.1 Statement of Problem

According to the Defense and Brain Injury Center of the Department of Defense, the number of service members diagnosed with TBI has steadily increased in previous years. Even though diagnostics of TBI in military combat has advanced, there is a distinct lack of treatments for blast-induced neurotrauma that are FDA approved. The absence of FDA-approved treatments likely is a result of a lack of understanding of the intricate neuropathology after TBI. Furthermore, TBI is not a "one size fits all" term as each injury results from different mechanical insults and progresses in a unique pattern. BINT sustained as a part of a polytraumatic episode is complex and has unique pathology. Blast-related traumatic brain injury in military personnel leads to long-term effects on the nervous system and is widely recognized as a risk factor in developing neuropsychological and neurodegenerative disease (Elder 2015). While the primary concern after BPT is to increase acute survival, secondary outcomes, such as mental health impairment, can be mitigated early if treatment addresses acute neuropathology (Shetty et al. 2014).

6.1.2 Significance

In order to address the need for a multipurpose treatment for blast trauma, a nanotherapeutic was designed to benefit both acute survival and neurological outcome. Functionalized hemostatic nanoparticles offer a wide variety of advantages compared to alternatives, such as increased biocompatibility and targeting of the injury site (Bertram et al. 2009). Hemostatic nanoparticles have been shown to increase survival acutely in a mouse model of blast injury (Lashof-Sullivan et al. 2014). The acute recovery and anti-inflammatory actions of dexamethasone can enhance brain healing and mitigate secondary injury mechanisms. Currently, one recent study has highlighted the use of dexamethasone as a suitable treatment after blast, due to its beneficial effect on the BBB (Hue et al. 2015). As BBB dysfunction is a hallmark of BPT in this dissertation, this treatment could provide mitigation of secondary pathology in addition to alleviation of acute hypoxia. While hDNP have the potential to positively influence the subacute and chronic stages of injury, this has not been tested. An established polytrauma model that simulates severe injury, including PBLI and BINT, will be used to evaluate hDNP. It is possible that through prevention of both hypoxic and neuroinflammatory cascades, hDNP can mitigate cellular injury and improve cognitive outcomes.

6.2 Literature Review

6.2.1 The Amygdala

To focus on alleviating anxiety after blast trauma, the amygdala was a major focus of this investigation. The amygdaloid complex, located in the temporal lobe, exhibits structural diversity and consists of 13 nuclei. These are further divided into subdivisions that have extensive internuclear and intranuclear connections. In this classification, the amygdala nuclei are divided into three groups (Sah et al. 2003, Murphy et al. 2012)(Figure 44):

1) The deep or basolateral group, which includes the lateral nucleus, the basal nucleus, and accessory basal nucleus

2) The superficial or cortical-like group, which includes the cortical nuclei and nucleus of the lateral olfactory tract

3) The centromedial group composed of the medial and central nuclei

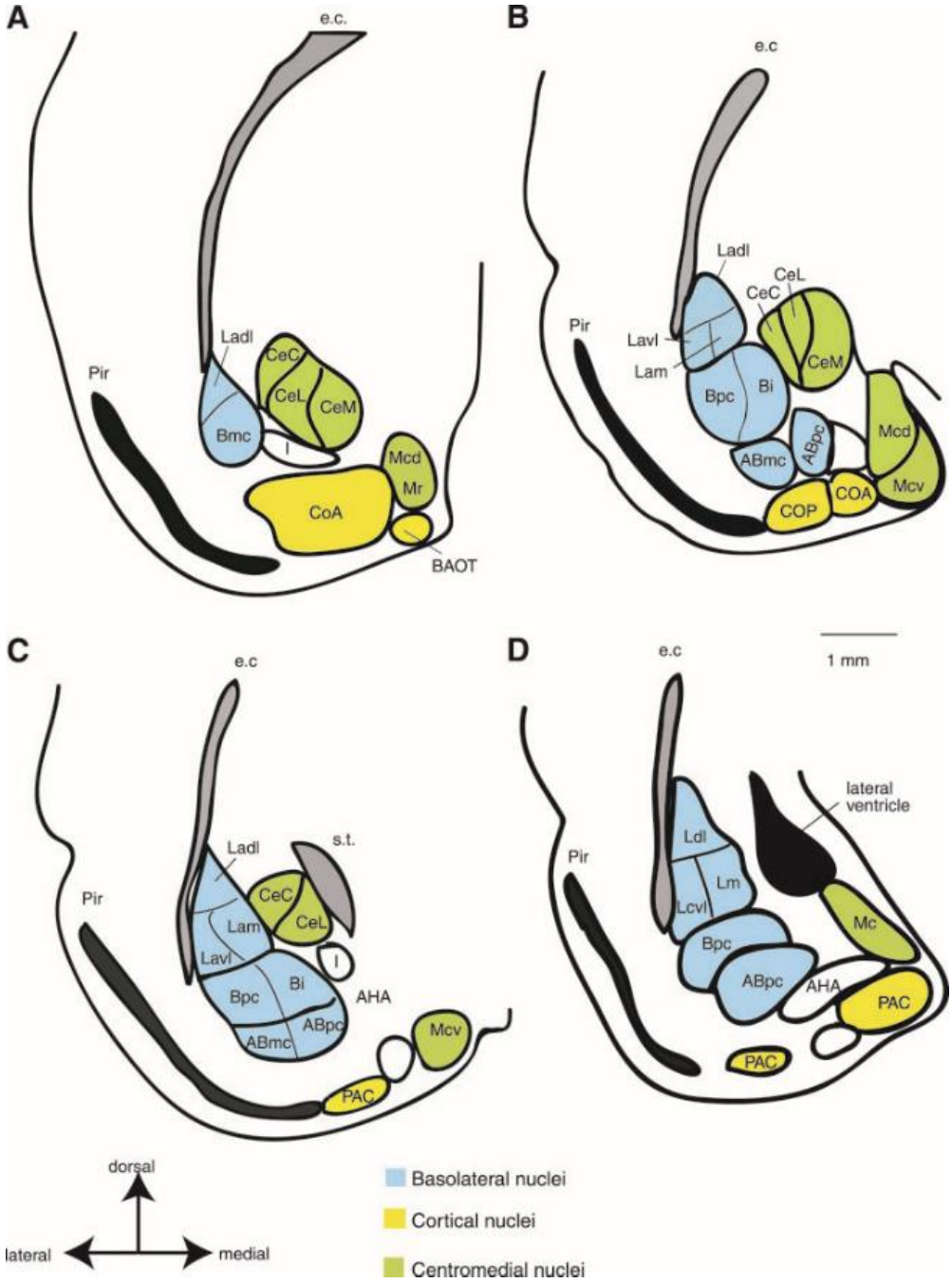

Figure 44. Nuclei of the Rat Amygdaloid Complex (Sah et al. 2003) ABmc, accessory basal magnocellular subdivision; ABpc, accessory basal parvicellular subdivision; Bpc, basal nucleus magnocellular subdivision; e.c., external capsule; Ladl, lateral amygdala medial subdivision; Lam, lateral amygdala medial subdivision; Lavl, lateral amygdala ventrolateral subdivision; Mcd, medial

amygdala dorsal subdivision; Mcv, medial amygdala ventral subdivision; Mr, medial amygdala rostral subdivision; Pir, piriform cortex; s.t., stria terminalis.

Sah, P., E. S. Faber, M. Lopez De Armentia and J. Power (2003). "The amygdaloid complex: anatomy and physiology." Physiol Rev 83(3): 803-834. *Fair use

In Figure 44, coronal sections are depicted from rostral (A) to caudal (D). The different nuclei are divided into three groups as described in text. Blue-shaded areas form part of the basolateral group, areas in yellow are the cortical group, and areas in green form the centromedial group.

6.2.1.1 Connections

The amygdala receives inputs from all sensory modalities: olfactory, somatosensory, gustatory and visceral, auditory, and visual. These inputs are largely from cortical and thalamic structures but also preside from memory-related structures. Inputs from the hypothalamus and brain stem are involved in behavior and autonomic system connections. The major source of sensory information to the amygdala is the cerebral cortex (Amaral et al. 2003, Davis et al. 2003). Electrical stimulation of amygdala produces fear in humans and animals (Sah et al. 2003).

Efferent outputs of amygdaloid nuclei have widespread projections to cortical, hypothalamic, and brain stem regions. Projections from the amygdala to cortical sensory areas originate in cortical and basolateral areas of the amygdala but are not profound. The perirhinal area, along with other areas in the frontal cortex that project to the amygdala, receive reciprocal connections from periamygdaloid cortex (Aroniadou-Anderjaska et al. 2007, Johansen et al. 2011).

6.2.1.2 Functions

The amygdala is involved in emotional responses, especially in fear and fear conditioning. These responses are characterized by freezing, release of stress hormones, and changes in blood pressure and heart rate which are elicited by activation of the autonomic and hormonal systems (Goldstein et al. 1996). Damage to this system can potentially initiate the neuropsycholigcal cascades in conditions such as PTSD, epilepsy, depression disorders, and TBI (Wilde et al. 2007, Johansen et al. 2011, Mahan and Ressler 2012). In some neurological disease,

such as TBI and PTSD, exacerbation of fear and anxiety through amygdalar hyperactivation occurs (Mahan and Ressler 2012, Walker et al. 2015).

6.2.2 Clinical Presence of Anxiety after Blast Exposure

Anxiety has been reported in military populations, both service members and Veterans (Armed Forces Health Surveillance 2013, Lovering et al. 2013, Kirsch et al. 2014). It has been shown that anxiety can affect performance in military tasks for service members (Nibbeling et al. 2014) Clinical studies have shown that the amygdala is hyper-regulated after blast-related TBI, possibly linking neuropathology with elevated levels of anxiety in Veterans (Matthews et al. 2012, Knutson et al. 2013). White matter integrity, assessed by diffusion tensor imaging, was reduced in individuals with major depressive disorder related to blast exposure (Matthews et al. 2012). For service members and Veterans with PTSD, MEG activity in the amygdala has been shown to positively correlate with PTSD symptom scores (Huang et al. 2014). PTSD is often accompanied by symptoms such as anxiety. Prevalence of self-reported and clinician-rated PTSD symptoms was higher in Veterans with a history of TBI (Davis et al. 2013). Smaller amygdala volume is also associated with PTSD in Veterans (Morey et al. 2012). From the studies presented, amygdala dysregulation likely can cause anxiety and PTSD-like symptoms.

6.2.3 Pre-clinical Assessments for Anxiety after Blast-induced Neurotrauma

The presence of anxiety-like behavior has been reported in animal models of BINT. In a repeated blast exposure model, it was shown that repeated stressors compiled with repeated blast exacerbated anxiety levels, measured by the elevated plus maze, immediately after exposure (Kamnaksh et al. 2011). Anxiety, assessed by light and dark box and open field exploration, has also been reported three and seven days after mild blast exposure (Park et al. 2013, Sajja et al. 2015). In a murine blast TBI model, anxiety was reported using the open field activity assessment at one week following a 170-275 kPa blast exposure (Heldt et al. 2014). A study examining the relation of blast exposure to PTSD in a rat model found increased anxiety parameters during the elevated zero maze assessment from repeated mild exposure, in the absence of psychological stressors (Elder et al. 2012). Chronic levels of increased stathmin-1, an essential protein in the proper development of fear responses, were reported at eight months after repeated mild blast exposure, which is responsible for fear responses (Elder et al. 2012). Anxiety and active avoidance were reported at one and three months after mild blast exposure, evidenced

by the light and dark box assessment (Sajja et al. 2015). In a rat model of mild blast TBI, minocycline, a non-steroidal anti-inflammatory drug, was administered and negated anxiety seen in injured animals at eight days post-injury, measured by the elevated plus maze (Kovesdi et al. 2012).

6.2.4 Amygdala Pathology after Blast-induced Neurotrauma

The amygdala has been studied in blast-induced TBI studies and has relation to anxiety-like behavior. Neuronal reduction within the amygdala and anxiety-like behavior was observed after 342-410 kPa blast exposure in a rodent model (Heldt et al. 2014). Also, elevated protein levels of tau and fetal liver kinase-1 (the receptor for VEGF) were observed in the amygdala after single mild blast exposure (Kamnaksh et al. 2012). Pressure dependence can also play a role in display of neurologic impairment and elevated glial activity and neurodegeneration (VandeVord et al. 2012). Five days after initiation of injury, astrocyte levels were increased within the amygdala in repeated mild TBI rat model along with increased levels of VEGF, which can be upregulated by hypoxic conditions and can regulate vascular permeability (Kamnaksh et al. 2011). Elevated levels of activated microglia and astrocytes have also been reported at seven days post-blast in the amygdala (Sajja et al. 2015). In a mild TBI model by Perez-Polo, et al., increased microglial activation was reported in the amygdala at six hours and 30 days after injury. They also observed BBB impairment in the hippocampus, but not the amygdala, at six hours after injury (Perez-Polo et al. 2015). Recovery of the BBB was noticed at 30 days after blast (Perez-Polo et al. 2015). At one and three months after mild blast exposure, astrocyte and microglia activation, as well as neuronal reduction, are reported (Sajja et al. 2015). These data provide evidence to help characterize amygdala pathology following blast exposure, yet little evaluation of treatment to alleviate this pathology has been conducted (Kovesdi et al. 2012).

6.3 Methods

6.3.1 Study Design

The purpose of this pre-clinical study was to examine the role of hemostatic nanoparticles loaded with dexamethasone in a rodent blast polytrauma model. Utilizing a side-thorax orientation in the Advanced Blast Simulator (ABS), the rodents sustained whole body blast exposure (Hubbard et al. 2014). hDNP were investigated based on their immediate ability to assuage internal hemorrhaging in the lungs, as well as secondary effects on mitigation of

neuropathology. The outcomes measured were survival percentages, behavioral assays, and immunohistology. Rodents were randomly placed into treatment groups with the experimenters blinded until statistical analysis was completed. Sample sizes were based on power analysis and previous studies that observed effects using the hemostatic nanoparticles (Bertram et al. 2009, Lashof-Sullivan et al. 2014). Due to slight variability in experimental blast procedures and the sensitive threshold by which lung injury can cause lethality, a lower threshold of 183 kPa (26.5 psi) static overpressure was applied to exclude animals from the study. This threshold was determined by the 50% lethality range of a weight-adjusted lethality curve established for this polytrauma model (Hubbard et al. 2014). Behavior and immunohistology outliers were excluded based on statistical analysis (± two standard deviations). For immunohistological assays, three brain sections per animal (four images at 20X per section) were taken and analyzed. Immunohistology for amygdala sections was quantified by investigators blinded to the treatment groups until statistical analysis.

6.3.2 Experimental Design

Detailed information for experimental procedures can be found in Hubbard, et al. (Hubbard et al. 2015). The Virginia Tech Institutional Animal Care and Use Committee approved experimental protocols described herein. Prior to all experiments, male Sprague Dawley rats (~325 g, Harlan Labs, San Diego) were acclimated to a 12 hour light/dark cycle with food and water provided ad lib. Animals were exposed to a single incident pressure profile resembling a 'free-field' blast exposure. The average peak static overpressure of the blast profile was at 191.1 ± 15.9 kPa (27.7 ± 2.29 psi) (BOP ± standard deviation) with positive duration at 2.475 ± 0.16 ms and positive impulse at 150.8 ± 13.8 kPa.ms (21.86 ± 2.00 psi.ms). After animals were excluded based on 183 kPa (26.5 psi) threshold, peak static overpressure was 196.7 ± 10.4 kPa (28.49 ± 1.5 psi). All animals were randomly assigned to one of seven groups: hemostatic nanoparticles (hNP), hemostatic dexamethasone-loaded nanoparticles (hDNP), control nanoparticles (cNP), control dexamethasone-loaded nanoparticles (cDNP), Lactated Ringer's (LR), Injury Only (IO) and sham. Prior to blast exposure, rats were anesthetized with a ketamine/xylazine solution, in accordance with the rodent weight, for sedation during blast. The shock front and blast overpressure were generated by a custom-built ABS with an end-wave eliminator (ORA Inc. Fredericksburg, VA) located at the Center for Injury Biomechanics at

Virginia Tech University. The ABS consists of a driving compression chamber attached to rectangular test section chamber with an end-wave eliminator.

A peak static overpressure was produced with compressed helium and calibrated acetate sheets (Grafix Plastics, Cleveland, OH). Pressure measurements were collected at 250 kHz using a Dash 8HF data acquisition system (Astro-Med, Inc, West Warwick, RI) and peak overpressures were calculated by determining wave speed (m/s) at the specimen position. A mesh sling was used to hold the animal during the exposure that allowed for minimal hindrance of the wave through the tube, in addition to holding the animal in a prone position with the right side of the thorax facing the shock wave driver. The animal was not allowed to impact any solid surface in order to prevent secondary injuries and this was confirmed using high-speed video (Phantom Miro eX2, Vision Research). After blast exposure, animals were immediately injected with test solution (hDNP, cDNP, or LR; 500 μL total volume) via tail vein injection, confirmed by Evans blue (Chapter 4.7.5). Sham animals underwent all procedures except for blast exposure and tail vein injection.

6.3.3 Open Field Test

At seven days after blast exposure, animals underwent an open field thigmotaxis assessment as a standard test to assess anxiety (Carola et al. 2002, Bailey and Crawley 2009). Briefly, an opaque black acrylic box with dimensions 80 x 80 x 36 cm was used for the task. Animals were acclimated in the open field box before the injury and two days after injury. The acclimation ensures that any anxiety-like traits would be due to the blast and subsequent injury progression. Activity changes were detected using EthoVision XT™ software tracking. Thigmotaxia, preference of proximity to walls, can expose fear of open, lit spaces and is displayed in animals with anxiety. Time spent along the chamber wall reflects an increased level of anxiety. Rats were videotaped for five minutes and avoidance of center square activity (i.e. anxiety-related behavior) was measured by determining the amount of time and frequency of entries into the central portion of the open field.

6.3.4 Novel Object Recognition

In order to assess spatial learning and short term memory, the animals underwent a Novel Object Recognition (NOR) test. The well-established NOR test was used to gauge rodent memory (Bevins and Besheer 2006, Davis et al. 2010). Briefly, animals undergo an acclimation

period two days prior to blast testing. This process was done to reduce stress and handling and increase familiarity with the testing environment (Besheer and Bevins 2000). Seven days following blast exposure, the animals underwent two trials with a delay of 20 minutes between each trial for short term memory evaluation. The first trial (T1) involved the exposure of animal to identical "familiar" objects for five minutes. In the second trial (T2), animals were exposed to a "familiar" object (same object used in the first task) and a "novel" object for five minutes. Trials took place in an opaque black acrylic box with dimensions 80 x 80 x 36 cm and animal behavior was tracked using EthoVision XT™ tracking software. Precautions were taken to clean the chamber between the trials and have the experimenter leave the room during the experiment (Bevins and Besheer 2006). For analysis, a discrimination index was calculated for each trial (time spent exploring the familiar object relative to the novel object divided by total time exploring objects during each trial). A ratio of 0.5 indicated equal exploration of both objects during the trial. Results were provided with statistical analysis of each assessment.

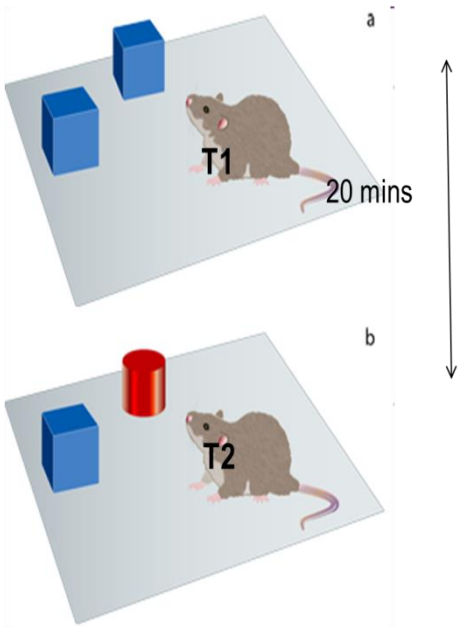

Figure 45. Novel Object Recognition Paradigm

6.3.5 Tissue Processing

At seven days, animals were euthanized by transcardial perfusion of saline and 4% paraformaldehyde. Following collection, brains were stored in a 4% paraformaldehyde fixative

solution. After 48 hours in fixative, the whole brains were placed in 30% sucrose solution for tissue sectioning preparation. Whole brains were embedded in Tissue-Tek® O.C.T. embedding medium (Sakura Finetek USA, Inc., Torrance, CA) for cryostat processing in the coronal plane. Samples were then cut (40 µm) and sections containing amygdala nuclei were isolated (Bregma: -2.28 mm).

6.3.6 Immunofluorescent Staining

Immunohistochemistry was performed on amygdalar sections (Bregma: -2.28 mm) to evaluate levels of: glial fibrillary acidic protein (GFAP; activated astrocytes), cleaved caspase-3 (C3; apoptosis), ionized calcium-binding adaptor molecule-1 (IBA; microglia), endothelial barrier antigen (EBA/SMI-71; BBB integrity), HIF-1α, and VEGF. Samples were rinsed three times with PBS and incubated in 2% BSA in PBS for one hour at room temperature. Sections were then incubated with a primary antibody (Appendix C); anti-GFAP (1:500; Invitrogen, Carlsbad, California), anti-caspase-3 (1:500; Cell Signaling Technologies, Danvers, Massachusetts), anti-IBA-1 (1:500; Biocare Medical, Concord, California), anti-SMI-71 (1:250; Covance, Princeton, New Jersey), anti-HIF-1α (1:250; Novus Biologicals, Littleton, Colorado), or anti-VEGF (1:250; Santa Cruz, Dallas, Texas) overnight at 4ºC. Both primary antibodies were only labeled separately on different amygdalar sections. After a PBS wash, the samples were incubated for 1.5 hours with Alexa Fluor 594 anti-mouse IgG antibody, Alexa Fluor 555 anti-rabbit IgG antibody, Alexa Fluor 488 anti-mouse IgG antibody, or FITC anti-rat IgG antibody (Invitrogen, Carlsbad, California). After three PBS washes (five minutes each), samples were mounted, air dried and coverslipped with prolong antifade gold reagent with 6-diamidino-2-phenylindole (DAPI; Invitrogen, Carlsbad, CA). Sections were examined under Zeiss fluorescence microscope at 20X magnification under appropriate fluorescent filters and images were taken by Zeiss AxioCam ICc 1. For all images, quantification (ImageJ software; NIH, Bethesda, MD) was based on fluorescence intensity after thresholding to eliminate background color.

6.3.7 Flurojade-C Staining

Sections of the amygdala were stained with Fluorojade-C (FJC) to identify degenerating neurons. This was completed with a kit from Biosensis (Thebarton, South Australia). Tissue sections were mounted on gelatin coated slides and dried. They were then incubated in the

solution of NaOH (Solution A) in 70% ethanol for five minutes. The sections were then transferred to 70% ethanol and distilled water for two minutes each. The sections were then incubated in a solution of potassium permanganate (Solution B) in distilled water and rinsed in distilled water. They were then incubated in a solution of FJC (Solution C) and DAPI (Solution D) in distilled water. Sections were then rinsed in distilled water thrice, air-dried, and placed on slide warmer until fully dry. The dry slides were cleared in xylene and mounted with DPX (Sigma-Aldrich Co. Ltd, St. Louis, MO). Sections were examined at 20x on a Zeiss microscope, and analysis was conducted. FJC+ neurons were counted by blinded technicians and the results were quantified.

6.3.8 Statistical Analysis

Statistical differences between the treatment groups were assessed with analysis of variance, or ANOVA, using LSD post-hoc test. All statistical analyzes were performed using JMP Pro 10 (SAS Institute, Cary, NC) and $p < 0.05$ considered statistically significant. Unless indicated otherwise, data are presented as mean ± standard error of the mean, or SEM.

6.4 Results

6.4.1 Anxiety Assay

Two days following blast exposure, hDNP treatment contributed to improved behavioral outcomes over baseline data, in terms of open arena exploration. hDNP significantly increased time spent in the center of the arena ($p<0.05$) compared to cNP, LR, and the IO groups (Figure 46A). At six days following blast exposure, the sham, hNP, and hDNP groups displayed significantly higher ($p<0.05$) exploration of the open center of the box compared to IO (Figure 46A). Prevalence for the walls, relating to the thigmotaxic paradigm, was seen more in IO compared to the hDNP group in animal tracking over five minutes (Figure 46BC) indicative that the treatment decreased anxiety-like behavior.

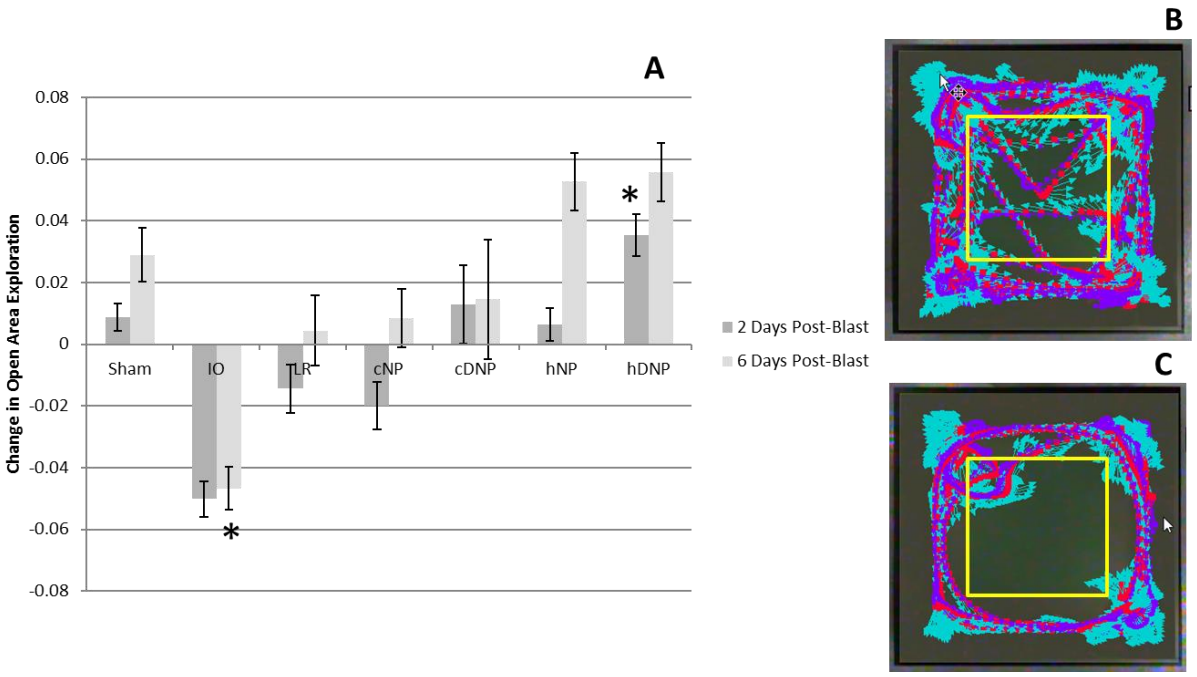

Figure 46. A) Rodents injected with hDNP display increased open area exploration over time after blast. At two days post-blast, hDNP is significantly different from IO, LR, and cNP groups (*p<0.05). At six days post-blast, the Injury Only group is significantly different from Sham, hNP, and hDNP groups (*p<0.05). (B) Representative rodent tracking for five minutes at six days post-blast in the hDNP group. (C) Representative rodent tracking for five minutes at six days post-blast in the IO group.

6.4.2 Novel Object Recognition

At seven days post-blast, the sham group was significantly higher in fraction of time spent around the novel object ($p<0.05$) compared to LR, cNP, and hNP, though not significant compared to hDNP (Figure 47). Tracking of the nose point over five minutes demonstrates the sham group investigating the novel object a higher fraction of time spent at objects than control groups.

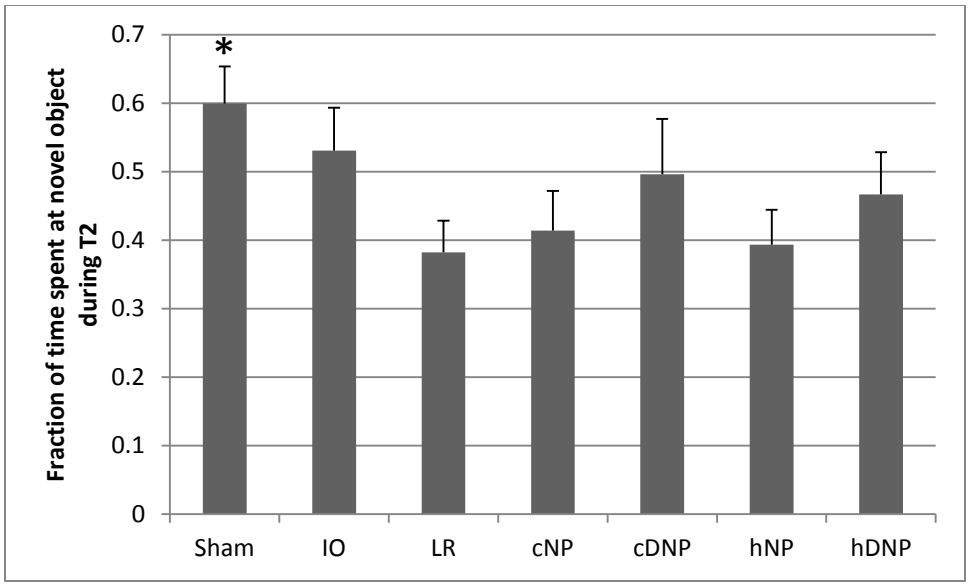

Figure 47. Fraction of time spent around the novel object in the T2 test.

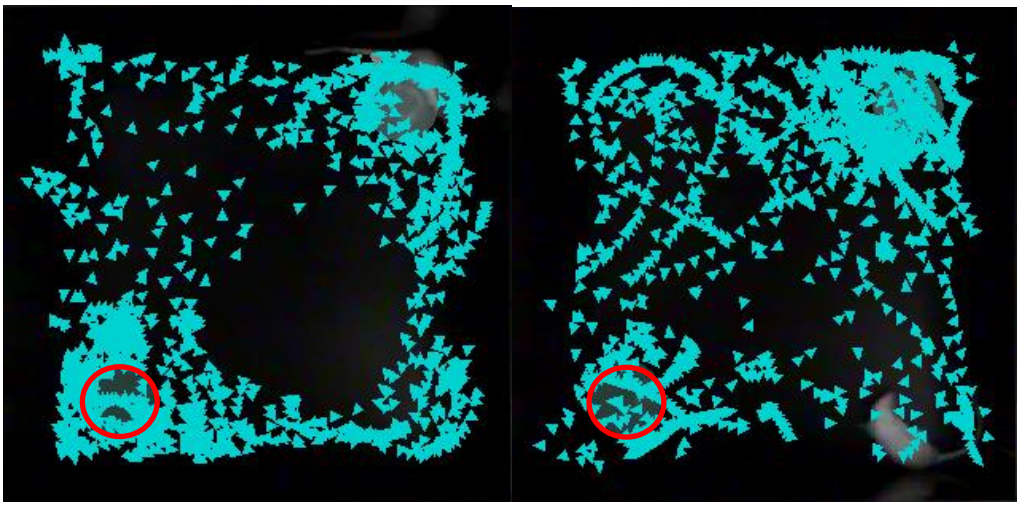

Figure 48. Animal tracking over five minutes. (Left) Sham animal spends more time with novel object (red circle). (Aggleton et al.) Animal spends less time around novel after injury and cNP treatment

6.4.3 Astrocyte Activation

Astrogliosis within the amygdala was significantly decreased after hNP treatment as compared to the IO ($p<0.05$) (Figure 50). The other control groups also presented with elevated GFAP levels, though not significantly different from hNP or hDNP. Images of GFAP staining in the amygdala depicted higher astrocytic activation with the IO compared to hNP (Figure 49), demonstrating that treatment with hNP reduced GFAP expression.

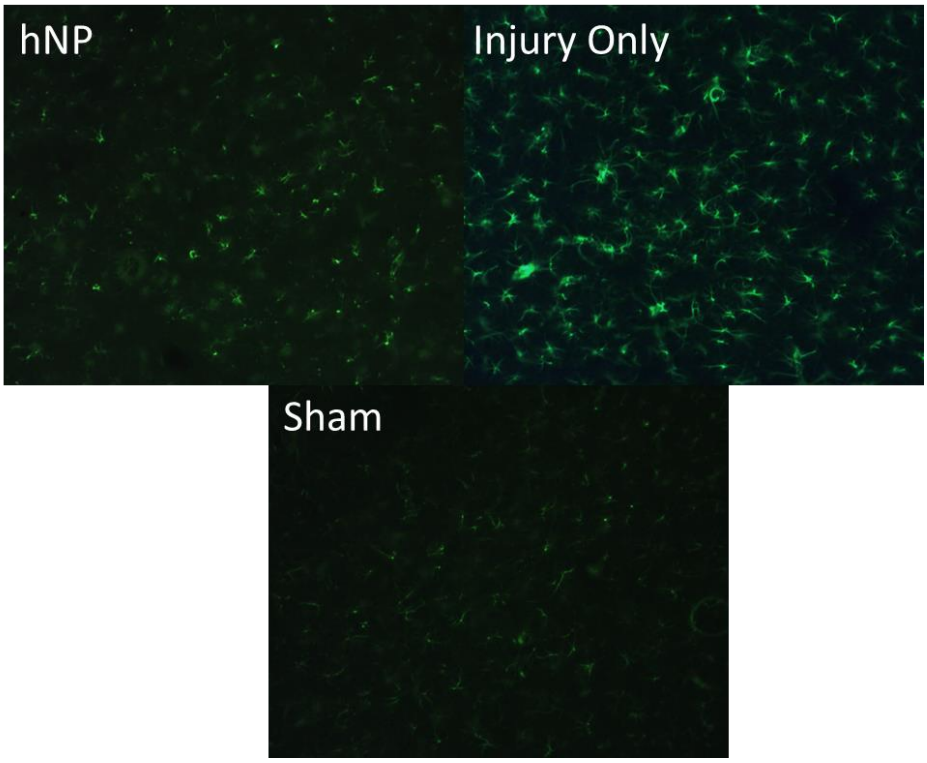

Figure 49. Representative images from the amygdala for GFAP (green images) from hNP, IO and Sham animals.

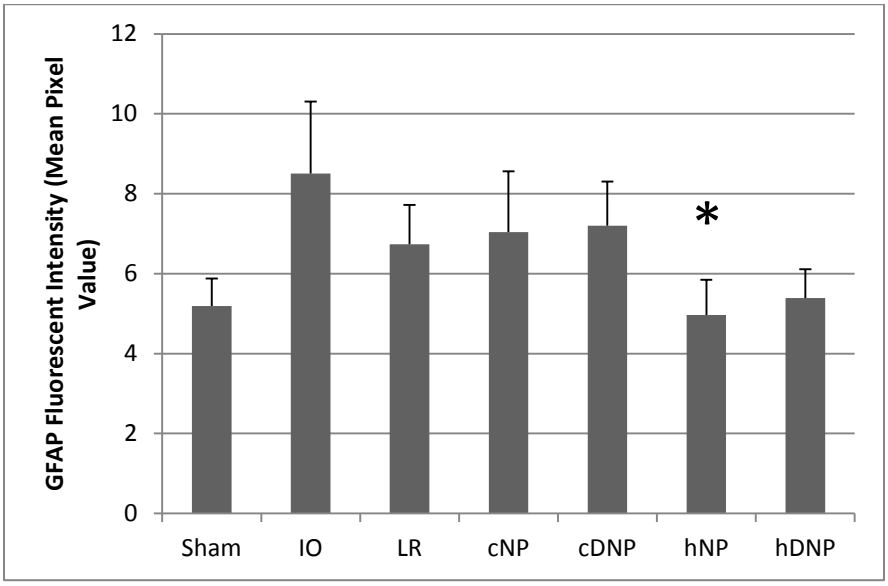

Figure 50. Fluorescent intensity of GFAP staining, a marker indicating astrocytic activation. At seven days post-blast, hNP is significantly different from the IO group (*p<0.05).

6.4.4 Apoptosis

Cleaved caspase-3 presence within the amygdala was significantly diminished with hDNP treatment as compared to the cNP and IO groups ($p<0.05$) (Figure 52). Representative images of cleaved caspase-3 levels in the amygdala depict more apoptosis occurring in the IO group compared to hDNP, showing less apoptosis in the amygdala after hDNP treatment (Figure 51).

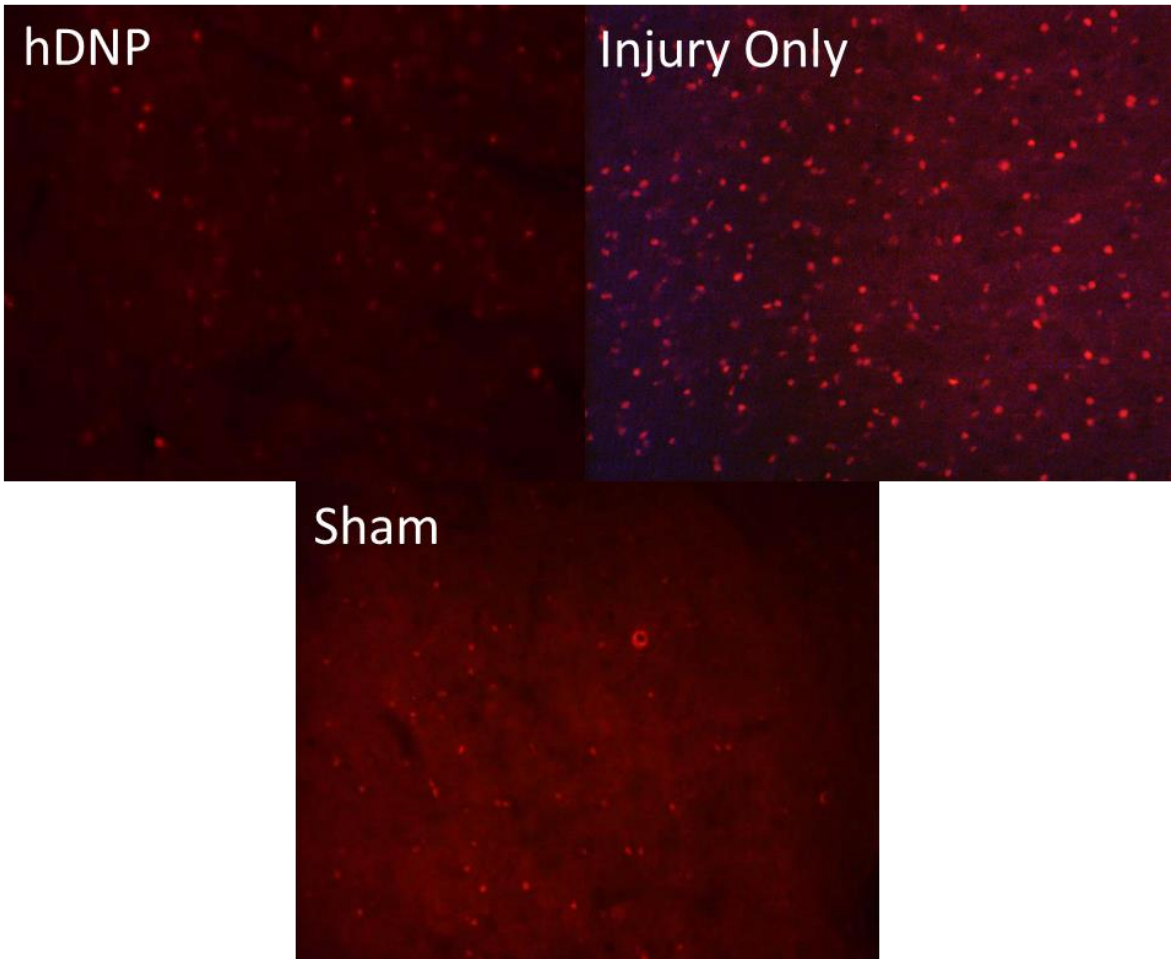

Figure 51. Representative images from the amygdala for cleaved caspase-3 (shown as red) from hDNP, IO and Sham animals.

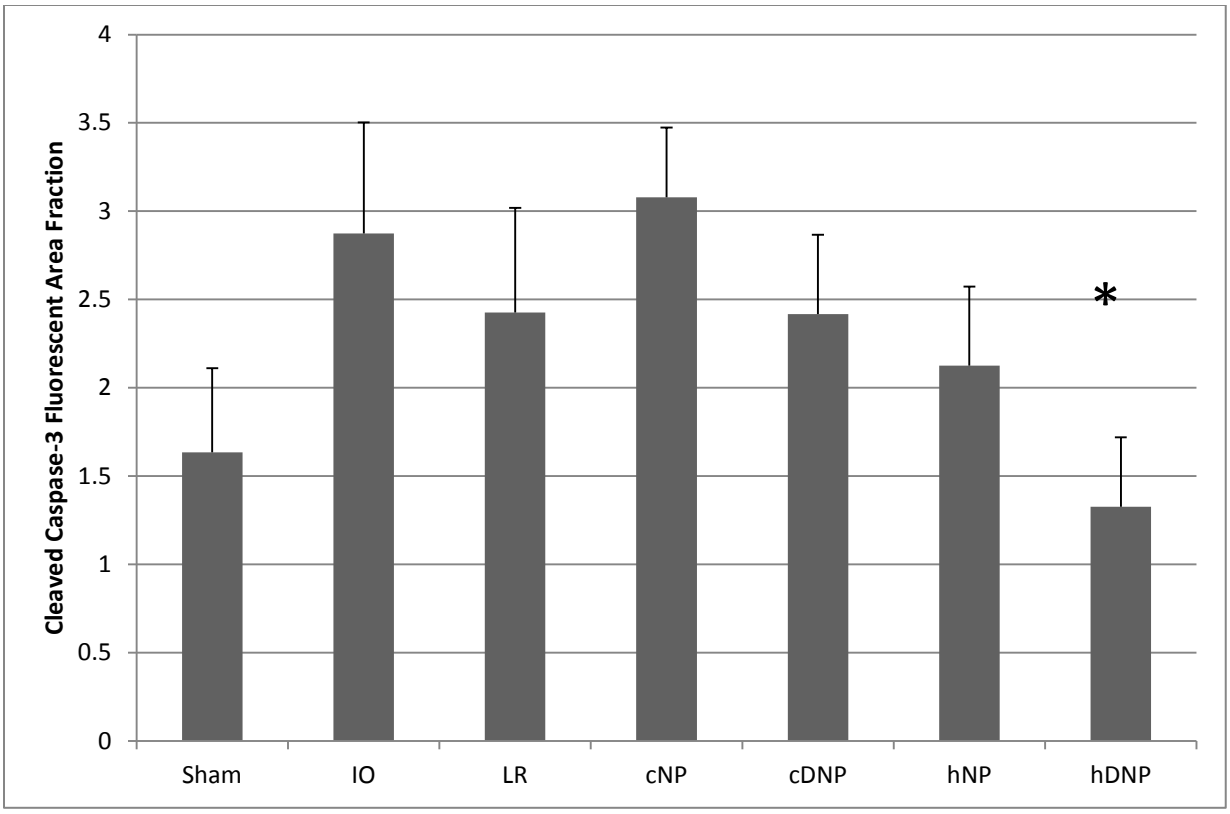

Figure 52. Fluorescent area for cleaved caspase-3, an apoptotic marker. At seven days post-blast, the hDNP group is significantly different from IO and cNP groups (*p<0.05)

6.4.5 Microglia Activation

IBA-1, marking microglia, within the amygdala was significantly decreased with IO treatment as compared to the hDNP group ($p<0.05$) (Figure 54). Representative images of IBA-1 in the amygdala depict process retraction occurring in the IO group (Figure 53) compared to hDNP, showing a possible morphology shift due to blast that is avoided with hDNP treatment.

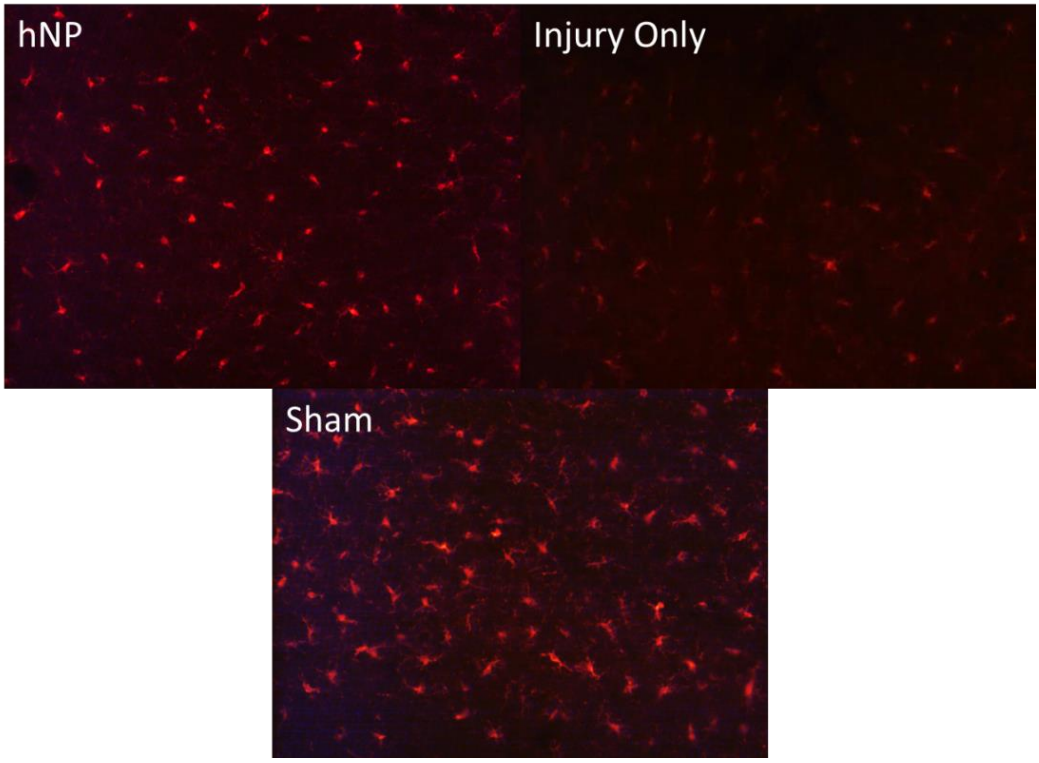

Figure 53. Representative images of the amygdala for IBA-1 from hNP, IO, and Sham animals.

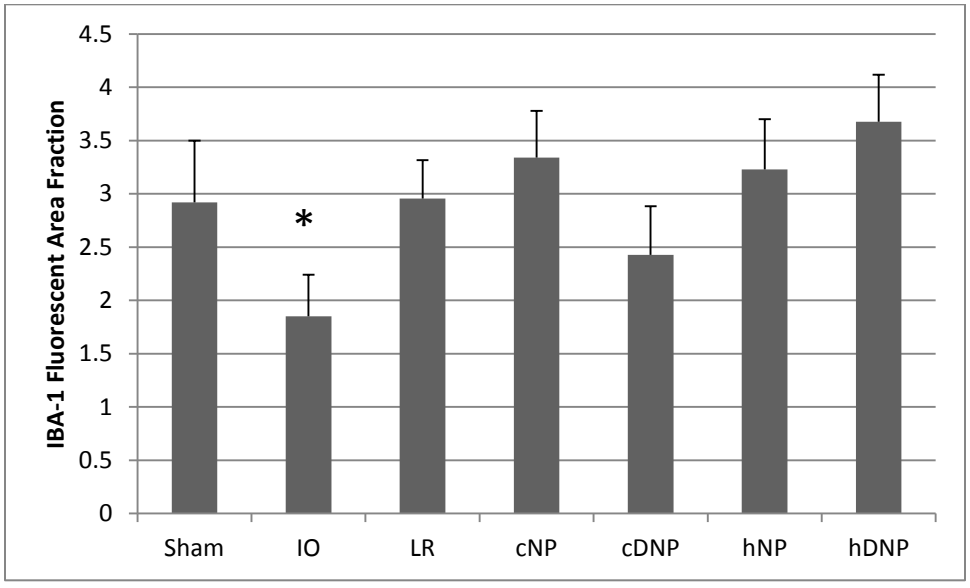

Figure 54. Fluorescent area for IBA-1. At seven days post-blast, the hDNP group was significantly different from IO and cNP groups (*p<0.05)

6.4.6 Blood-Brain Barrier Disruption

The BBB analysis revealed that the hDNP treatment significantly improved cerebrovascular integrity as compared to the IO group ($p<0.05$) (Figure 56). Images of SMI-71, an antibody targeting endothelial barrier antigen, or EBA, of the BBB, showed higher levels of EBA+ vessels in the sham and hDNP groups compared to IO (Figure 55). Higher amount of EBA+ vessels indicates a higher number of BBB-competent vessels present in the amygdala after hDNP treatment.

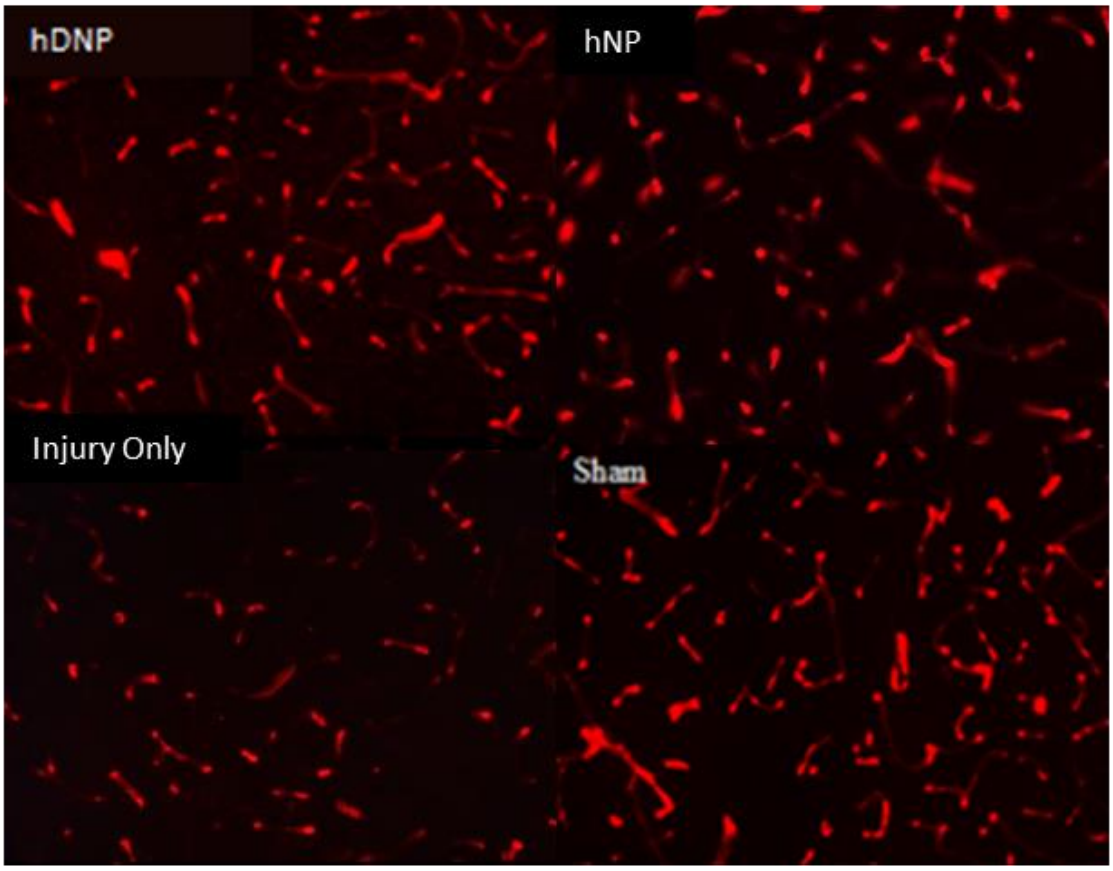

Figure 55. Representative images of the amygdala from hDNP, hNP, IO, and Sham animals. Injury Only sections contained lower number of SMI-positive vessels compared to hDNP and Sham groups.

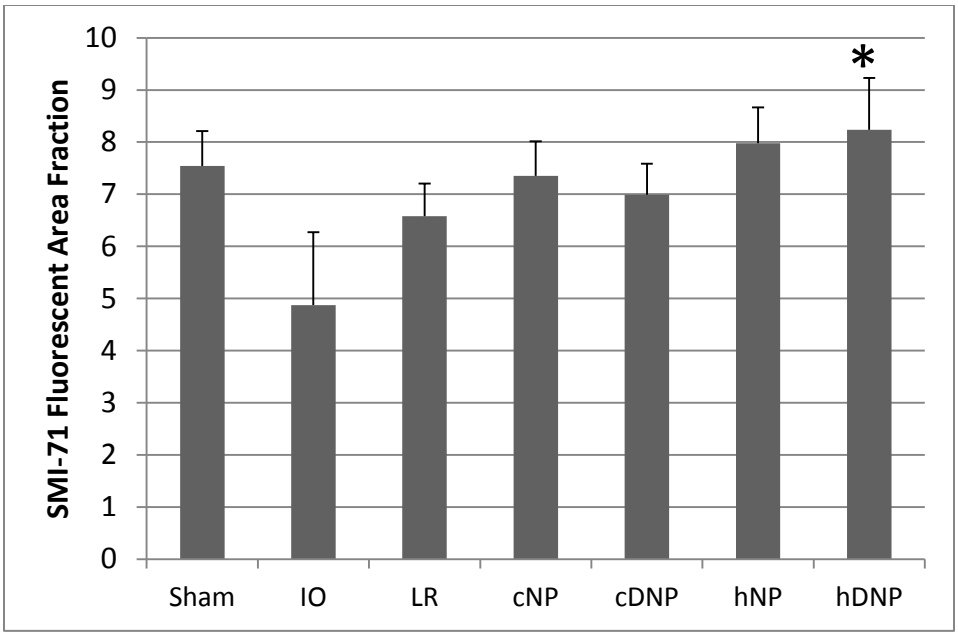

Figure 56. Fluorescent Area of SMI-71, a marker for BBB integrity. At seven days post-blast, hDNP was significantly different from the Injury Only group (*p<0.05).

6.4.7 HIF-1α Expression

HIF-1α, indictor of hypoxic conditions, within the amygdala was not significant between groups (p>0.05) (Figure 58). Representative images of HIF-1α in the amygdala depict higher levels in the cDNP group (Figure 57) compared to hDNP and sham.

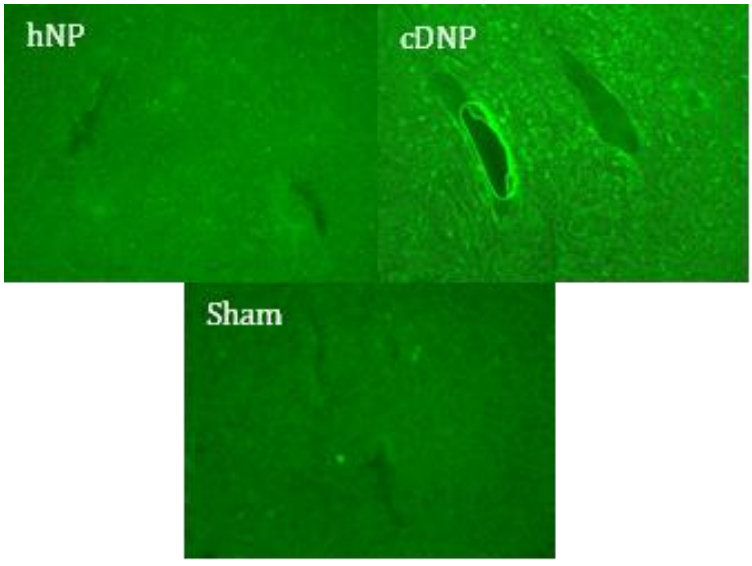

Figure 57. Representative images of HIF-1α in the amygdala for hNP, cDNP, and Sham animals.

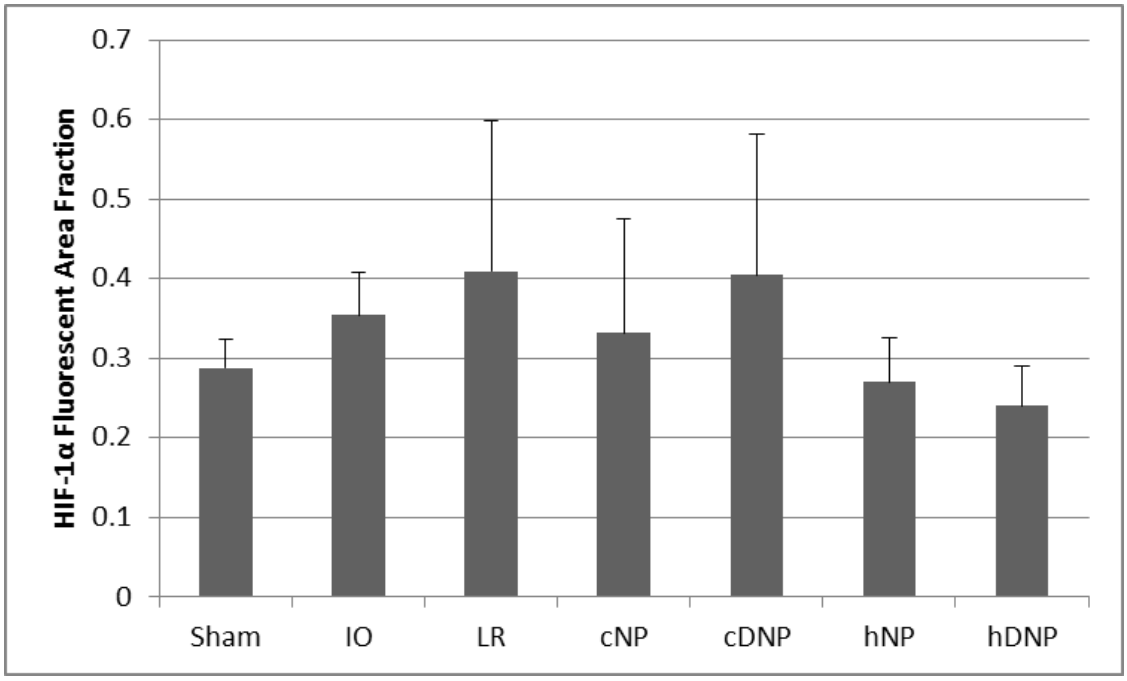

Figure 58. HIF-1α expression in the amygdala. Lower levels of HIF-1α were detected after hNP and hDNP treatment but no significance was determined.

6.4.8 VEGF Expression

VEGF expression within the amygdala was significantly increased ($p<0.05$) with IO treatment as compared to the sham and cDNP groups (Figure 60). Representative images of VEGF in the amygdala depict cells expressing high levels of VEGF in the IO group (Figure 59) compared to cDNP.

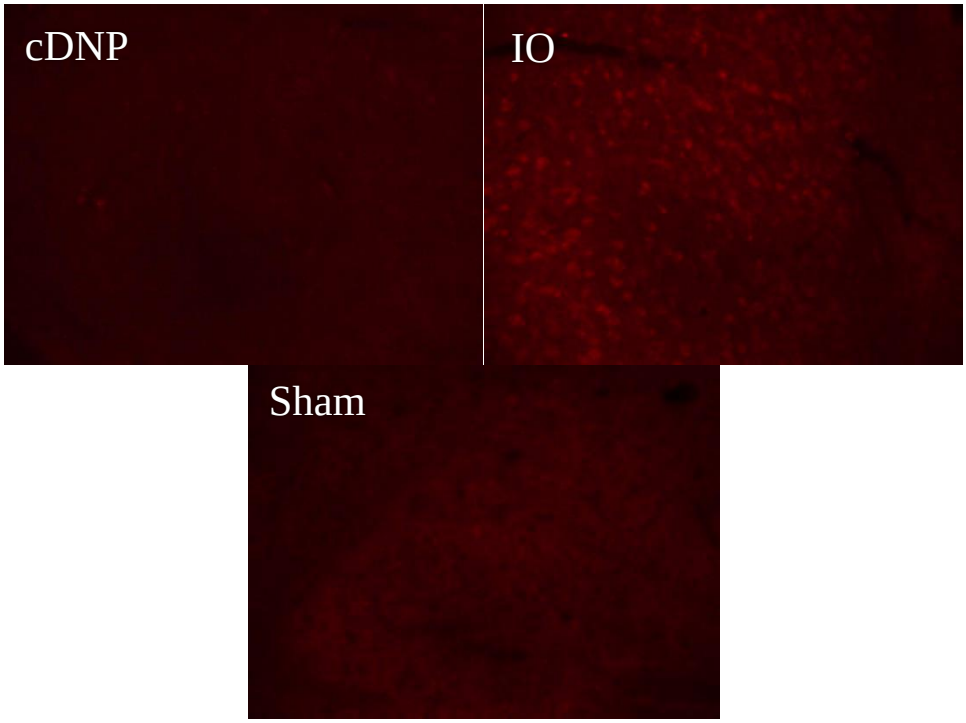

Figure 59. Representative images of VEGF in the amygdala for cDNP, IO, and Sham animals.

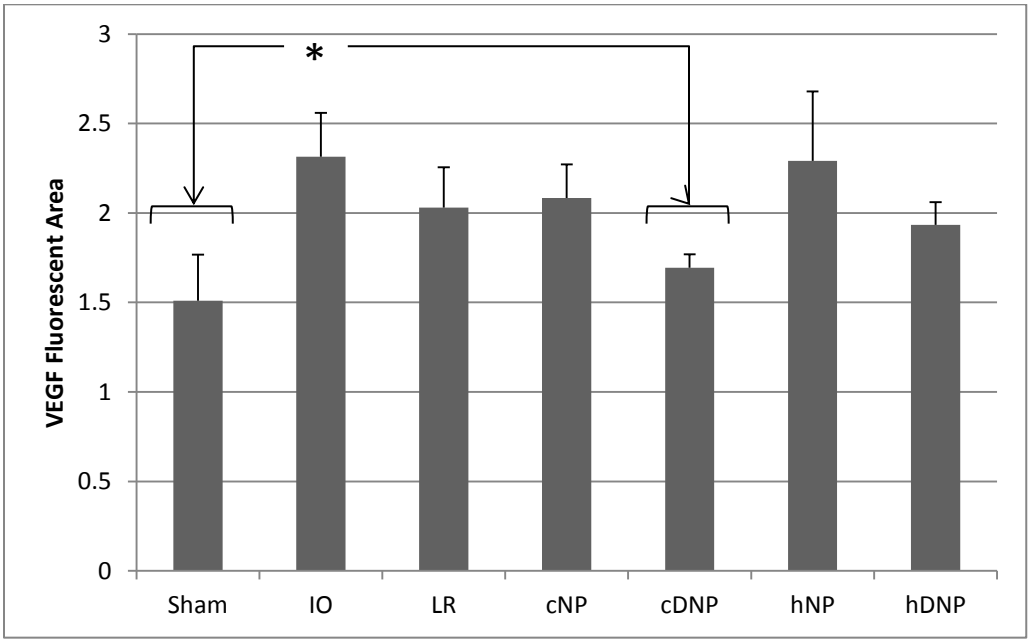

Figure 60. VEGF expression in the amygdala. IO was significantly higher than the sham and cDNP groups ($p<0.05$).

6.4.9 FJC+ Staining

FJC+ neurons, marker of neurodegeneration, within the amygdala was not significant ($p>0.05$) among treatment groups (Figure 62). Representative images of FJC in the amygdala are shown in Figure 61.

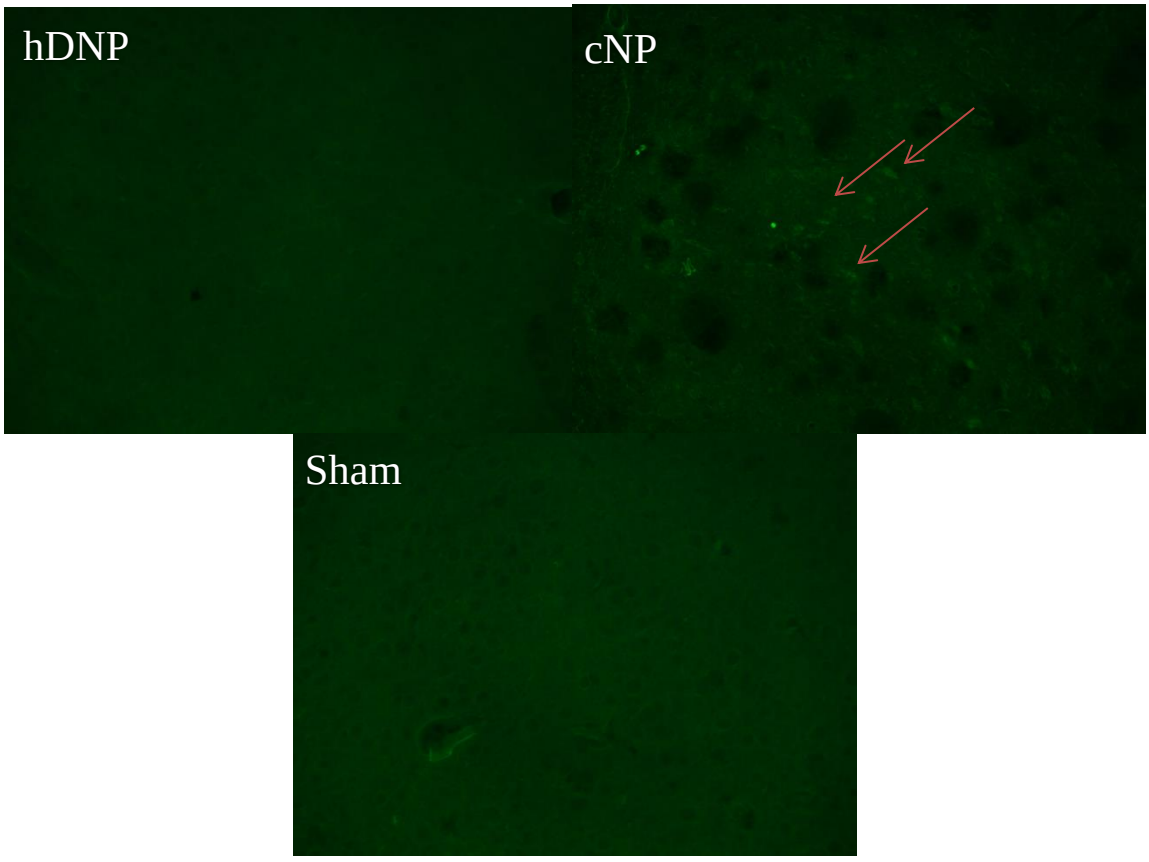

Figure 61. Representative images of FJC in the amygdala for hDNP, cNP, and Sham animals.

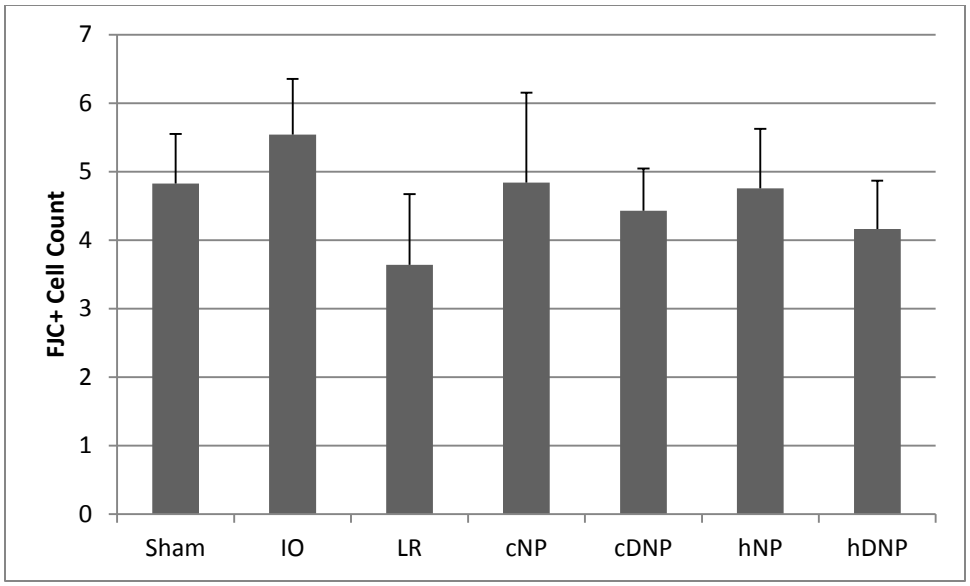

Figure 62. FJC+ neuronal count in the amygdala. Lower levels of FJC+ were detected after hDNP treatment compared to IO but no significance was determined.

6.5 Discussion

This is the first study to provide evidence that subacute outcomes of blast injury improve following hDNP or hNP administration. The amygdala has been investigated following blast-induced TBI and has been linked to the presentation of anxiety-like behavior both clinical and pre-clinical studies (Kamnaksh et al. 2011, Elder et al. 2012, Matthews et al. 2012, Sajja et al. 2015, Huang et al. 2016). Neuronal reduction and glia activation/damage have been frequently reported in the amygdala after blast exposure (Kovesdi et al. 2012, Heldt et al. 2014, Perez-Polo et al. 2015, Sajja et al. 2015, Sajja et al. 2015). Hemostatic nanoparticle treatment reduced cleaved caspase-3 and GFAP at seven days after injury in this model, demonstrating improvements in neuropathology. The role of microglia after blast injury is still up for assessment but they have a distinct role in bTBI pathology (Xu et al. 2016). Vascular dysfunction after blast has been reported with activated microglia morphologies, including ameboid cells with retracted processes (Huber et al. 2016). This activated morphology with retracted processes and lower IBA-1 expression is speculated to occur in the amygdala in this BPT model, explaining lower fluorescent intensity after blast only. Another possibility is that microglia at this time point after injury were providing a necessary recovery response to the

injury. Recent findings suggest that microglia can be activated into two opposing phenotypes, M1 and M2 (Tang and Le 2016). The ratio of these phenotypes can guide the recovery process after injury and the repair process of M2 activation can elicit necessary neuro-recovery. Given this dual role (beneficial/detrimental) that microglia display after injury, it is possible that microglia are providing a necessary response to BPT, which is lacking in after IO (Loane and Byrnes 2010, Kumar et al. 2013, Cherry et al. 2014, Turtzo et al. 2014).

Hypoxia is the principal regulator of VEGF expression (Liu et al. 1995, Krock et al. 2011). VEGF, as a downstream marker, has caused BBB dysfunction in models of TBI (Okada et al. 1998, Skold et al. 2005). Levels of HIF-1α and VEGF in plasma were elevated at 42 days post-blast in a repeated mild model of TBI demonstrating long lasting effects of hypoxia and chronic regulation of vascular permeability by VEGF (Ahmed et al. 2013). In a blast TBI model, HIF-1α was elevated in serum at three days and one week post-blast, as well as after low intensity blast exposure in the serum at two hours, one day, one week, and one month post-blast, showing constant upregulation (Ahmed et al. 2015, Liu et al. 2015). Lower levels of HIF-1α as compared to controls were seen after BPT and hDNP treatment in this study although not significant. It is possible that HIF-1α levels peak before seven days, as downstream VEGF was elevated at this time point. VEGF, a factor in BBB disruption, levels were lower in treatment groups with dexamethasone, highlighting one potential avenue of BBB restoration.

Neurodegeneration has been examined after blast-induced neurotrauma (de Lanerolle et al. 2011, Li et al. 2013, Sajja et al. 2015). While FJB+ neurons were not reported at three days and two weeks post-blast by de Lanerolle, et al. (de Lanerolle et al. 2011), others have reported positive staining at various time points (Li et al. 2013, Sajja et al. 2015). Neurodegeneration by FJB+ assessment was reported after repeated blast as well (Wang et al. 2011). In our model, FJC+ was not significant in this assessment at seven day post-blast between treatment groups, which was expected given that no differences occur between sham and IO. More time points should be assessed to garner if neurodegeneration is present in the amygdala after BPT.

Along with secondary mechanisms of neuroinflammation and apoptosis, BBB disruption has been examined in blast-induced TBI studies (Readnower et al. 2010, Abdul-Muneer et al. 2013, Hue et al. 2016). BBB impairment was reported in the hippocampus six hours after injury; however recovery of the BBB damage was noted by 30 days after blast (Perez-Polo et al. 2015).

It has been shown that there can be BBB disruption and increased permeability due to hypoxia (Kaur and Ling 2008), which occurred acutely in this full-body polytrauma model (Hubbard et al. 2015). Astrocytes play a large role in BBB health, as end-feet coverage is crucial for proper function and regulation. Clinically, compromise of astrocytic endfeet coverage of blood vessels in the brain has been reported in depressive disorders (Rajkowska et al. 2013). Disruption of brain microvasculature also impairs the ability for neuroglia to migrate, affecting the angiocrine signaling process (Dejana and Betsholtz 2016). The threshold of injury to the BBB has yet to be determined but reporting levels of blast exposure indicate BBB compromise, subsequently leading to debilitating neurological consequence (Abdul-Muneer et al. 2013, Yeoh et al. 2013). SMI-71, as a marker for BBB disruption, has been correlated with FITC-albumin infiltration (Pelz et al. 2013). Lower number of EBA+ vessels and stained vessel area were associated with regions of BBB dysfunction. Reduction of BBB disruption in the animals treated with hDNP suggests a mitigation of on-going pathology and quickly recovery of BBB function at seven days. This highlights the ability of hDNP to address initial primary injury to the BBB and persistent secondary opening of the BBB through dexamethasone release.

The added benefit of alleviating anxiety-like behavior following blast was a significant finding and may have many translational opportunities. Many studies of blast-induced neurotrauma have shown that anxiety-like behavior is displayed in rodents after injury (Kamnaksh et al. 2011, Sajja et al. 2015, Heldt et al. 2014, Park et al. 2013, Elder et al. 2012). Anxiety-like behavior, exemplified by a higher ratio of time spent in dark, enclosed spaces, has been reported seven days, as well as at one and three months, after blast exposure (Sajja et al. 2015, Sajja, et al. 2015). Other studies have shown that administration of treatment (minocycline) can reduce anxiety-like behavior seen in injured animals at eight days post-injury (Kovesdi et al. 2012). In our study, the reduction in elevated thigmotaxia, representative of anxiety, at multiple time points after injury in the animals treated with hDNP is a promising result for the therapeutic to have an impact on neurological recovery.

There have been several clinical studies reporting that Veterans suffering from major depressive disorder following blast exposure, as well as individuals with PTSD, displayed amygdalar hyperactivity (Matthews et al. 2012, Huang et al. 2016). Veterans with history of TBI have been shown to display an increase in clinician-rated PTSD symptoms (Davis et al. 2013).

Blast-related TBI has been associated with anxiety disorders and symptom crossover with combat-associated PTSD (Trudeau et al. 1998, Vanderploeg et al. 2012). Neurological symptoms, especially those with emotional impairment, are a major concern for quality of life in returning soldiers and Veterans. Directing therapeutics towards reduction in anxiety is needed for military personnel and civilians after a traumatic event.

Short-term memory loss has been widely documented in blast-induced neurotrauma studies (Cernak et al. 2001, Ahlers et al. 2012, VandeVord et al. 2012, Cho et al. 2013, Sajja et al. 2014, Sajja et al. 2014, Shetty et al. 2014, Perez-Polo et al. 2015). Repeated low blast exposure (36 kPa) in a lateral orientation blast model demonstrated no learning deficit on the Morris water maze task, though lower retention of conditioned fear was reported in a 117 kPa lateral exposure (Ahlers et al. 2012). Rats with entorhinal cortex lesions show poor discrimination of the novel objects (Aggleton et al. 2010), thus this test can reflect damage to the entorhinal cortex, which has anatomical proximity to the amygdala. NOR results in this study demonstrated hNP, cNP, and LR groups choosing to explore the familiar object during T2, marked by a significant lower exploration of the novel object compared to sham. Values were less than 0.5, which is an unbiased result. After TBI, novelty aversion has been reported in animals at seven days post-injury (Darwish et al. 2014). This seems to be occurring in this model since many groups underperformed compared to the 0.5 benchmark. Novelty aversion, relating to anxiety-like behavior, seems to mask any effects of blast exposure on memory impairment with the NOR test.

The therapeutic effect of dexamethasone has been previously investigated in other injury models (Araz et al. 2013, Hubbard et al. 2015, Lee et al. 2015). In an Alzheimer's Disease model, dexamethasone has been shown to reduce inflammation due to amyloid beta in the cerebrovasculature (Previti et al. 2006). A review by Obermeier et al. deemed glucocorticosteroids (GC) as the only applicable BBB therapeutic (Obermeier et al. 2013). Dexamethasone, an anti-inflammatory GC, inhibits matrix metalloproteinase (MMP) and consequently improves vessel wall integrity by preserving BBB components (Forster et al. 2007). In an *in vitro* model of primary blast injury, BBB restoration occurred *via* GC receptor signaling by dexamethasone (Hue et al. 2015). Dexamethasone also attenuated astrocytosis around neural prosthetic devices after peripheral injection and local delivery through polymers

(Shain et al. 2003). Hemostatic nanoparticles have been used in treatment of acute hemorrhaging in injury models (Bertram et al. 2009, Shoffstall et al. 2012, Lashof-Sullivan et al. 2014). This research is the first to examine dexamethasone's effect in a rodent model of blast trauma. In the current study, hDNP provided benefits over hNP in terms of reducing BBB dysfunction and apoptosis. Dexamethasone has promising therapeutic benefit in restoring BBB after trauma and likely played a role in BBB recovery in this model (Hue et al. 2015, Lee et al. 2015). In addition to providing enhanced coagulation, hDNP also release dexamethasone at the injury site, pinpointing areas that need anti-inflammatory therapy that can repair BBB damage.

While hNP have a role in reduction of lung injury, there is also potential that its direct therapeutic action benefits recovery in the brain. The model in this study consists of a higher blast exposure in a lateral orientation, which is understudied in terms of the effect on specific brain regions. Overpressure dependence also is known to play a role in neurologic impairment, elevated glial activity and neurodegeneration following blast (VandeVord et al. 2012, Sajja et al. 2015, Mishra et al. 2016). In a model of primary blast-induced neurotrauma, lateral blast exposure, similar to the model examined in this study, to the rodent head resulted in lesions in both hemispheres of the brain (Yeoh et al. 2013). This finding was dependent on peak blast overpressure but independent of time point, demonstrating on-going BBB disruption in the amygdala (Yeoh et al. 2013). Primary interaction of hemostatic nanoparticles in the amygdala is proposed to reduce microhemorrhaging, or capillary rupture of BBB, in order to promote BBB recovery at seven days and mitigate neuroinflammation measured by astrogliosis.

Since animals treated with cDNP had higher levels of astrogliosis and BBB disruption compared to the hDNP-treated animals, the targeting ability of the nanoparticles is a key event for successful management of the complex injury. One mechanism of indirect therapeutic benefit is the restoration of oxygen saturation by administration of hNP acutely after blast exposure (Hubbard et al. 2015). This could potentially reduce secondary mechanisms, such as upregulation of HIF-1α, in the brain after injury. Although there is no significance in HIF-1α levels at seven days post-blast, we hypothesize that these levels differ in hNP compared to controls in the acute stage after injury.

6.6 Conclusion

In addition to the benefits shown in this polytrauma model, another advantage of hNPs is that they are translatable to larger animal models in order to optimize for clinical use. If hNPs were used clinically, they would become the first therapeutic option for treating internal hemorrhaging. While this study highlights the advantages of hNPs in treating blast injuries, this novel formulation could prove useful in treating a very broad spectrum of traumatic injuries (Bertram et al. 2009, Lashof-Sullivan et al. 2014).

In conclusion, the vascular injury observed in the brain implies that blast-induced neurotrauma has a unique pathology that requires different therapeutics compared to impact-related TBI (Yeoh et al. 2013). Hemostatic nanoparticles are effective in increasing survival in a rodent model of blast trauma. In addition to immediate effects, hDNPs improve neurological recovery in the amygdala and mitigate injury pathology likely through indirect and direct interaction. While more studies are needed to assess benefits of hemostatic nanoparticles after injury, the results are promising in route to identifying a life-saving and quality of life enhancing treatment for traumatic injury.

6.7 Future Directions

Given that anxiety-like behavior was seen in the open field assessments, additional behavioral assays, such as the light-and-dark box test, should be performed to validate and determine the extent of anxiety-like behavior. Also, the NOR assessment was deemed unfruitful in determining whether memory loss was displayed after injury and whether the nanoparticle treatment improved any impairment. A multi-assay behavioral approach should be conducted to assess memory levels to provide more information. Specifically, using a battery of spatial memory/learning assessment, such as the t maze or radial arm maze, and recognition memory tests would provide a detailed evaluation of memory function (Vorhees and Williams 2014).

Since our assessment of the therapeutic effect was only evaluated at one week after injury, further studies are vital for determining the dynamic recovery phase with hDNP administration. While examining secondary neuropathology proved to be an important aspect of this study, looking at acute biomarkers to ascertain specific mechanisms of therapeutic benefit after polytrauma is needed. Hypoxia has been shown to extend until at least three hours post-blast after PBLI (Irwin et al. 1997, Knoferl et al. 2003). Examining the first emergence of HIF-

1α after injury (four hours post-blast) and the daily progression will demonstrate if this pathway is crucial to injury progression and a therapeutic target. In order to garner the full therapeutic benefit, more time points will be assessed after injury and therapeutic intervention. Proposed time points would be four, 24, and 48 hour after injury. Determining the extent of BBB disruption and whether its presentation is continuous, biphasic, or even tri-phasic is valuable information for tailoring treatment for BPT (Baskaya et al. 1997). Assessing multiple time points would give insight into whether hDNP have a direct, indirect, or combined therapeutic mechanism. BBB disruption can be a primary or secondary pathology after blast (Shetty et al. 2014). Acute evaluation of hNP, at four hours and 24 hours after injury, and the effect on BBB can determine the extent of direct interaction in the brain.

Another limitation to this study is that the nanoparticles were given immediately after injury as a proof of concept. Since immediate injection if not always feasible after traumatic injuries occur, injection should be delayed to simulate real-world applications. Additional studies to assess maximum time allowable before injection are needed to determine the therapeutic window after injury is sustained. Current protocols for management of bleeding after major trauma call for intervention as soon as possible (Spahn et al. 2013). While there are certain crucial stages of traumatic mortality, treatment of bleeding is crucial during the first hour after injury (ATLS). In this research, injection was given within five minutes of injury. Injection of the nanoparticles at short time frame (15, 30, 45, and 60 minutes) as well as delayed time frame (12 and 24 hours) after injury in a future study would demonstrate how long of a therapeutic window there is after injury.

Chapter 7: Summary

Collectively, the results presented provide evidence that hemostatic nanoparticles have the ability to reduce hemorrhage and increase survival in a rodent model of blast polytrauma. While hDNP mitigated hemorrhage that could have led to mortality, the benefits of hDNP are multi-faceted. Through BBB restoration (increased SMI-71), hDNP were shown to mitigate cellular injury and improve cognitive outcomes. Dexamethasone has also been implicated in BBB repair (Obermeier et al. 2013). Neuroprotective drugs capable of halting or mitigating secondary changes following blast, such as BBB disruption, may ease the development of subsequent neurological and neuropsychiatric impairments such as cognitive problems, non-specific mental and emotional symptoms, and PTSD (Shetty et al. 2014). hDNP are a potential therapeutic for administration in a clinical or combat setting after traumatic injury. hDNP could also serve as an agent to prevent subacute and chronic inflammatory pathways and subsequently improve neurological function.

The Defense Health Agency reported that from 2001-2011 over 80% of potentially survivable deaths from service members killed inaction were due to hemorrhage (Office 2013). There is an unmet need for technologies to control bleeding in the pre-hospital environment. Translation would provide a viable option for mitigation of internal bleeding, which contributes to alleviation of on-going injury mechanisms. While these nanoparticles have been tested in mouse and rat models of injury and polytrauma, more testing is needed in the rodent model to fully characterize the injury and therapeutic benefits. Eventually, larger animal models would be utilized when relevant evaluation is completed in the rodent model of blast polytrauma. A newly developed Göttingen minipig injury model would be a logical next step as it has similar neuroanatomy to a human, such as a pronounced falx cerebri, a gyrencephalic (containing gyri and sulci) brain, and a brainstem that exits at an angle, so conditions for blast loading to the brain would more closely resemble the human condition (Fievisohn et al. 2014). Physiology and the cardiovascular system in pigs are comparable to humans and swine models are commonly utilized in models of uncontrolled bleeding (Alam et al. 2011, Frink et al. 2011). In addition, pigs are often used as models for blood coagulation and fibrinolysis research for human comparison (Olsen et al. 1999, Munster et al. 2002, Sondeen et al. 2013). One disadvantage for using in a swine model is that pigs are sensitive to complement activation related pseudoallergy after

polymeric nanoparticle infusion (Fairbairn et al. 2011). Complement activation related pseudoallergy can be catastrophic and the mechanisms of its development and mitigation of this pseudoallergy after nanoparticle administration is needed before clinical translation (Lashof-Sullivan et al. 2013). In addition to this immune response, blood circulation time and stability of nanoparticles need optimization before clinical translation (Lashof-Sullivan et al. 2013). After these limitations are addressed, dosing requirements for larger animals and humans will need to be optimized based on efficacy and safety. After these conditions are met, Phase II and III trials are conducted to explore efficacy and safety and if the trials succeed an application is submitted for FDA approval (Ciociola et al. 2014).

7.1 Clinical Relevance

Clinical management of polytrauma has developed and changed throughout the years. The Advanced Trauma Life Support, or ATLS, protocol is currently used in many European countries and emphasizes a structured approach to treating polytrauma (Stahel et al. 2005). The ATLS protocol is focused on providing a standard procedure algorithm for the assessment and management of patients with polytrauma and puts emphasis on diagnostic and therapeutic protocols during the first minutes to hours after injury (ATLS 2004). The three stages of trauma-associated mortality are sudden death, early mortality, and delayed mortality. Sudden death mortality, such as aortic rupture, is almost always not preventable. Delayed mortality occurs weeks after initial trauma and is usually due to sepsis or organ failure. Early mortality occurs in the first hours after trauma and prehospital management is crucial. In general for trauma, the risk of mortality is highest immediately after injury and decreases with time (Spahn et al. 2007).Out of the three main time points of traumatic mortality, hNP treatment could have the largest impact on early mortality during the “golden hour” (ATLS). Intrathoracic bleeding that induces hemorrhagic shock is difficult to treat and most emphasis in the ATLS protocol is focused on fluid resuscitation and oxygen support which is commonly used because there is a lack of hemostatic therapies to prevent bleeding (ATLS 2004). Most protocols in trauma management focus on replacing blood and blood components that are lost through hemorrhage (Katsu et al. 2010). If hemostatic nanoparticles are translated for human use, it could completely change trauma management and allow for more focus on other concerns.

hNPs have the potential to revolutionize treatment of injuries in the battlefield. Primary blast injury hallmarks, such as internal barotrauma in the absence of external wounds, as caused by multiple biophysical processes, such as inertia, spalling, and implosion. These invisible injuries are hard to diagnose immediately after injury. The specific application for internal injuries can save many lives, as well as improve quality of life for those wounded. hNPs are effective even when stored at high temperatures and are stable for several weeks in dry form (Lashof-Sullivan et al. 2016). This is important when considering treatment in battlefield conditions.

7.2 Innovation of the Study

Incidence of blast polytrauma has increased due to acts of terrorism and will continue with unrest in the world. Moreover, it is possible that primary blast polytrauma is under-diagnosed due to other external injuries that are higher on the list of traumatic care. Since polytrauma occurs in high level blast exposure, it is likely that secondary and tertiary blast injuries occur as well.

While some studies have examined polytrauma from blast using pre-clinical models (Skotak et al. 2013, Mishra et al. 2016), there is a lack of studies that examine polytraumatic-specific mechanisms of neuropathology. Blood-brain barrier disruption was found in both models but its injury mechanism is not understood. Studies of blast-induced neurotrauma have identified hypoxia as a factor in BBB dysfunction (Ahmed et al. 2013, Kovacs et al. 2014) but this had yet to be examined after BPT. A more thorough understanding of this injury pathology is vital for military and civilian populations to direct treatments.

A therapy to address multiple symptoms would be highly valuable for BPT and possibly other polytraumatic injuries. Mitigation of hemorrhage after PBLI is needed to increase survival in addition to reduced secondary neuropathology. Hemostatic dexamethasone-loaded nanoparticles have the ability to fill both needs through enhanced coagulation at the injury site and release of dexamethasone over several days. Dexamethasone has been shown to promote BBB restoration in an *in vitro* model of blast neurotrauma (Hue et al. 2015). The dynamic ability of the nanoparticles to have multiples mechanisms of therapy makes them a suitable option for polytraumatic treatment. As coagulation enhancers, hemostatic nanoparticles have the opportunity to revolutionize pre-hospital management for blast-induced polytraumatic injuries.

7.3 Contributions to the Field

Publications from this dissertation are summarized in Table 4.

Table 4. Hubbard Publications

Chapter	Title	Journal
2	Examining Lethality Risk for Rodent Studies of Primary Blast Lung Injury	Biomed Sci. Instrumentation 2014; 50:92-99
3	Neuropathology of Blast-Induced Polytrauma	Journal of Neurotrauma – Estimated Submission November 2016
5	Steroid-Loaded Hemostatic Nanoparticles Combat Lung Injury after Blast Trauma	ACS Macro Letters 2015; 4(4):387-391
6	Injury-targeting Hemostatic Nanoparticles Increase Survival and Alleviate Anxiety in a Rodent Blast Trauma Model	Science Translational Medicine – In Preparation

References

(1941). "Lung injuries in air raids: a discussion on pathology and diagnosis." *British Medical Journal* 2: 239-242.

Abdul-Muneer, P. M., H. Schuetz, F. Wang, M. Skotak, J. Jones, S. Gorantla, M. C. Zimmerman, N. Chandra and J. Haorah (2013). "Induction of oxidative and nitrosative damage leads to cerebrovascular inflammation in an animal model of mild traumatic brain injury induced by primary blast." *Free Radic Biol Med* 60: 282-291.

Aggleton, J. P., S. M. O'Mara, S. D. Vann, N. F. Wright, M. Tsanov and J. T. Erichsen (2010). "Hippocampal-anterior thalamic pathways for memory: uncovering a network of direct and indirect actions." *Eur J Neurosci* 31(12): 2292-2307.

Ahlers, S. T., E. Vasserman-Stokes, M. C. Shaughness, A. A. Hall, D. A. Shear, M. Chavko, R. M. McCarron and J. R. Stone (2012). "Assessment of the effects of acute and repeated exposure to blast overpressure in rodents: toward a greater understanding of blast and the potential ramifications for injury in humans exposed to blast." *Front Neurol* 3: 32.

Ahmed, F., S. Plantman, I. Cernak and D. V. Agoston (2015). "The Temporal Pattern of Changes in Serum Biomarker Levels Reveals Complex and Dynamically Changing Pathologies after Exposure to a Single Low-Intensity Blast in Mice." *Front Neurol* 6: 114.

Ahmed, F. A., A. Kamnaksh, E. Kovesdi, J. B. Long and D. V. Agoston (2013). "Long-term consequences of single and multiple mild blast exposure on select physiological parameters and blood-based biomarkers." *Electrophoresis* 34(15): 2229-2233.

Alam, H. B., K. B. Hamwi, M. Duggan, K. Fikry, J. Lu, E. Y. Fukudome, W. Chong, A. Bramos, K. Kim and G. Velmahos (2011). "Hemostatic and pharmacologic resuscitation: results of a long-term survival study in a swine polytrauma model." *J Trauma* 70(3): 636-645.

Alford, P. W., B. E. Dabiri, J. A. Goss, M. A. Hemphill, M. D. Brigham and K. K. Parker (2011). "Blast-induced phenotypic switching in cerebral vasospasm." *Proc Natl Acad Sci U S A* 108(31): 12705-12710.

Amaral, D. G., M. D. Bauman, J. P. Capitanio, P. Lavenex, W. A. Mason, M. L. Mauldin-Jourdain and S. P. Mendoza (2003). "The amygdala: is it an essential component of the neural network for social cognition?" *Neuropsychologia* 41(4): 517-522.

Araz, O., E. Demirci, E. Yilmazel Ucar, M. Calik, D. Pulur, A. Karaman, M. Yayla, E. Altun, Z. Halici and M. Akgun (2013). "Comparison of reducing effect on lung injury of dexamethasone and bosentan in acute lung injury: an experimental study." *Multidiscip Respir Med* 8(1): 74.

Armed Forces Health Surveillance, C. (2013). "Anxiety disorders, active component, U.S. Armed Forces, 2000-2012." *MSMR* 20(10): 2-6; discussion 4-6.

Arnold, J. L., P. Halpern, M. C. Tsai and H. Smithline (2004). "Mass casualty terrorist bombings: a comparison of outcomes by bombing type." *Ann Emerg Med* 43(2): 263-273.

Aroniadou-Anderjaska, V., F. Qashu and M. F. Braga (2007). "Mechanisms regulating GABAergic inhibitory transmission in the basolateral amygdala: implications for epilepsy and anxiety disorders." *Amino Acids* 32(3): 305-315.

Aschkenasy-Steuer, G., M. Shamir, A. Rivkind, R. Mosheiff, Y. Shushan, G. Rosenthal, Y. Mintz, C. Weissman, C. L. Sprung and Y. G. Weiss (2005). "Clinical review: the Israeli experience: conventional terrorism and critical care." *Crit Care* 9(5): 490-499.

ATLS (2004). "Advanced Trauma Life Support (ATLS) for Doctors, 7th ed." *American College of Surgeons Committee on Trauma*.

Axelsson, H., H. Hjelmqvist, A. Medin, J. K. Persson and A. Suneson (2000). "Physiological changes in pigs exposed to a blast wave from a detonating high-explosive charge." *Mil Med* 165(2): 119-126.

Badami, C. D., D. H. Livingston, Z. C. Sifri, F. J. Caputo, L. Bonilla, A. M. Mohr and E. A. Deitch (2007). "Hematopoietic progenitor cells mobilize to the site of injury after trauma and hemorrhagic shock in rats." *J Trauma* 63(3): 596-600; discussion 600-592.

Bailey, K. R. and J. N. Crawley (2009). "Anxiety-Related Behaviors in Mice." *Methods of Behavior Analysis in Neuroscience, Second Edition*: 77-101.

Bala, M., N. Shussman, A. I. Rivkind, U. Izhar and G. Almogy (2010). "The pattern of thoracic trauma after suicide terrorist bombing attacks." *J Trauma* 69(5): 1022-1028; discussion 1028-1029.

Barnett, N. and L. B. Ware (2011). "Biomarkers in acute lung injury--marking forward progress." *Crit Care Clin* 27(3): 661-683.

Barr, J. S., R. H. Draeger and W. W. Sager (1946). "Solid blast personnel injury; a clinical study." *Mil Surg* 98: 1-12.

Baskaya, M. K., A. M. Rao, A. Dogan, D. Donaldson and R. J. Dempsey (1997). "The biphasic opening of the blood-brain barrier in the cortex and hippocampus after traumatic brain injury in rats." *Neurosci Lett* 226(1): 33-36.

Bass, C. R., K. A. Rafaels and R. S. Salzar (2008). "Pulmonary injury risk assessment for short-duration blasts." *J Trauma* 65(3): 604-615.

Bauman, R. A., N. Elsayed, J. M. Petras and J. Widholm (1997). "Exposure to sublethal blast overpressure reduces the food intake and exercise performance of rats." *Toxicology* 121(1): 65-79.

Bauman, R. A., G. Ling, L. Tong, A. Januszkiewicz, D. Agoston, N. Delanerolle, Y. Kim, D. Ritzel, R. Bell, J. Ecklund, R. Armonda, F. Bandak and S. Parks (2009). "An introductory characterization of a combat-casualty-care relevant swine model of closed head injury resulting from exposure to explosive blast." *J Neurotrauma* 26(6): 841-860.

Bertram, J. P., C. A. Williams, R. Robinson, S. S. Segal, N. T. Flynn and E. B. Lavik (2009). "Intravenous hemostat: nanotechnology to halt bleeding." *Sci Transl Med* 1(11): 11ra22.

Besheer, J. and R. A. Bevins (2000). "The role of environmental familiarization in novel-object preference." *Behav Processes* 50(1): 19-29.

Bevins, R. A. and J. Besheer (2006). "Object recognition in rats and mice: a one-trial non-matching-to-sample learning task to study 'recognition memory'." *Nat Protoc* 1(3): 1306-1311.

Blane, G. (1785). "Observations on the diseases incident to seamn." *London, UK: Joseph Cooper* 1st edn.

Bolander, R., B. Mathie, C. Bir, D. Ritzel and P. VandeVord (2011). "Skull flexure as a contributing factor in the mechanism of injury in the rat when exposed to a shock wave." *Ann Biomed Eng* 39(10): 2550-2559.

Bourdeaux, C., Manara, A. (2008). "Burns and smoke inhalation." *Anaesthesia & Intensive Care Medicine* 9(9): 404-408.

Bowen, I. G., E. R. Fletcher, D. R. Richmond, F. G. Hirsch and C. S. White (1968). "Biophysical mechanisms and scaling procedures applicable in assessing responses of the thorax

energized by air-blast overpressures or by nonpenetrating missiles." *Ann N Y Acad Sci* 152(1): 122-146.

Bowen, I. G., Fletcher, E.R, Richmond, D.R. (1968). "Estimate of man's tolerance to the direct effects of air blast." *Defense Atomic Support Agency* #2113(AD693105).

Brismar, B. and L. Bergenwald (1982). "The terrorist bomb explosion in Bologna, Italy, 1980: an analysis of the effects and injuries sustained." *J Trauma* 22(3): 216-220.

Brown, R. F., G. J. Cooper and R. L. Maynard (1993). "The ultrastructure of rat lung following acute primary blast injury." *Int J Exp Pathol* 74(2): 151-162.

Carola, V., F. D'Olimpio, E. Brunamonti, F. Mangia and P. Renzi (2002). "Evaluation of the elevated plus-maze and open-field tests for the assessment of anxiety-related behaviour in inbred mice." *Behavioural Brain Research* 134(1-2): 49-57.

CDC (2006). "Bombings: injury patterns and care. Blast curriculum: one-hour module."

Celander, H., C. J. Clemedson, U. A. Ericsson and H. I. Hultman (1955). "The use of a compressed air operated shock tube for physiological blast research." *Acta Physiol Scand* 33(1): 6-13.

Cernak, I., Z. Wang, J. Jiang, X. Bian and J. Savic (2001). "Cognitive deficits following blast injury-induced neurotrauma: possible involvement of nitric oxide." *Brain Inj* 15(7): 593-612.

Cernak, I., Z. Wang, J. Jiang, X. Bian and J. Savic (2001). "Ultrastructural and functional characteristics of blast injury-induced neurotrauma." *J Trauma* 50(4): 695-706.

Chai, J. K., J. H. Cai, H. P. Deng, X. F. Zou, W. Liu, Q. G. Hu, C. A. Shen, H. N. Yin, X. B. Zhang, Y. F. Chi, L. Ma and R. Feng (2013). "Role of neutrophil elastase in lung injury induced by burn-blast combined injury in rats." *Burns* 39(4): 745-753.

Chai, J. K., W. Liu, H. P. Deng, J. H. Cai, Q. G. Hu, X. F. Zou, C. A. Shen, H. N. Yin, Y. F. Han, X. B. Zhang, Y. F. Chi, L. Ma, T. J. Sun, R. Feng and Y. T. Lan (2013). "A novel model of burn-blast combined injury and its phasic changes of blood coagulation in rats." *Shock* 40(4): 297-302.

Champion, H. R., R. F. Bellamy, C. P. Roberts and A. Leppaniemi (2003). "A profile of combat injury." *J Trauma* 54(5 Suppl): S13-19.

Chavko, M., S. Adeeb, S. T. Ahlers and R. M. McCarron (2009). "Attenuation of pulmonary inflammation after exposure to blast overpressure by N-acetylcysteine amide." *Shock* 32(3): 325-331.

Chavko, M., W. K. Prusaczyk and R. M. McCarron (2006). "Lung injury and recovery after exposure to blast overpressure." *J Trauma* 61(4): 933-942.

Chavko, M., W. K. Prusaczyk and R. M. McCarron (2008). "Protection against blast-induced mortality in rats by hemin." *J Trauma* 65(5): 1140-1145; discussion 1145.

Chen, C., Q. Hu, J. Yan, X. Yang, X. Shi, J. Lei, L. Chen, H. Huang, J. Han, J. H. Zhang and C. Zhou (2009). "Early inhibition of HIF-1alpha with small interfering RNA reduces ischemic-reperfused brain injury in rats." *Neurobiol Dis* 33(3): 509-517.

Cheng, J., B. A. Teply, I. Sherifi, J. Sung, G. Luther, F. X. Gu, E. Levy-Nissenbaum, A. F. Radovic-Moreno, R. Langer and O. C. Farokhzad (2007). "Formulation of functionalized PLGA-PEG nanoparticles for in vivo targeted drug delivery." *Biomaterials* 28(5): 869-876.

Cherry, J. D., J. A. Olschowka and M. K. O'Banion (2014). "Neuroinflammation and M2 microglia: the good, the bad, and the inflamed." *J Neuroinflammation* 11: 98.

Cho, H. J., V. S. Sajja, P. J. VandeVord and Y. W. Lee (2013). "Blast induces oxidative stress, inflammation, neuronal loss and subsequent short-term memory impairment in rats." *Neuroscience* 253: 9-20.

Chodobski, A., B. J. Zink and J. Szmydynger-Chodobska (2011). "Blood-brain barrier pathophysiology in traumatic brain injury." *Transl Stroke Res* 2(4): 492-516.

Ciociola, A. A., L. B. Cohen, P. Kulkarni and F. D.-R. M. C. o. t. A. C. o. Gastroenterology (2014). "How drugs are developed and approved by the FDA: current process and future directions." *Am J Gastroenterol* 109(5): 620-623.

Clemedson, C. J. (1949). "An experimental study on air blast." *Acta Physiol Scand* 18(Suppl LXI): 7-200.

Clemedson, C. J. (1956). "Blast injury." *Physiol Rev* 36(3): 336-354.

Clemedson, C. J., Granstom, S.A. (1950). "Studies on the genesis of "rib markings" in lung blast injury." *Acta Physiol Scand.* 21: 131-144.

Clemedson, C. J., Nelson A. (1957). "The effects of a high explosive blast in mice with radiation injury." *Acta Radiology* 47(1): 79-85.

Clifford, C. C. (2004). "Treating traumatic bleeding in a combat setting." *Mil Med* 169(12 Suppl): 8-10, 14.

Cockerham, G. C., G. L. Goodrich, E. D. Weichel, J. C. Orcutt, J. F. Rizzo, K. S. Bower and R. A. Schuchard (2009). "Eye and visual function in traumatic brain injury." *J Rehabil Res Dev* 46(6): 811-818.

Coll Ferrer, M. C., V. V. Shuvaev, B. J. Zern, R. J. Composto, V. R. Muzykantov and D. M. Eckmann (2014). "Icam-1 targeted nanogels loaded with dexamethasone alleviate pulmonary inflammation." *PLoS One* 9(7): e102329.

Cooper, G. J., R. L. Maynard, N. L. Cross and J. F. Hill (1983). "Casualties from terrorist bombings." *J Trauma* 23(11): 955-967.

Cooper, G. J., D. J. Townend, S. R. Cater and B. P. Pearce (1991). "The role of stress waves in thoracic visceral injury from blast loading: modification of stress transmission by foams and high-density materials." *J Biomech* 24(5): 273-285.

Coppel, D. L. (1976). "Blast injuries of the lungs." *Br J Surg* 63(10): 735-737.

Covey, D. C. (2002). "Blast and fragment injuries of the musculoskeletal system." *J Bone Joint Surg Am* 84-A(7): 1221-1234.

D'Addio, S. M., C. Kafka, M. Akbulut, P. Beattie, W. Saad, M. Herrera, M. T. Kennedy and R. K. Prud'homme (2010). "Novel method for concentrating and drying polymeric nanoparticles: hydrogen bonding coacervate precipitation." *Mol Pharm* 7(2): 557-564.

Dal Cengio Leonardi, A., N. J. Keane, C. A. Bir, A. G. Ryan, L. Xu and P. J. VandeVord (2012). "Head orientation affects the intracranial pressure response resulting from shock wave loading in the rat." *J Biomech* 45(15): 2595-2602.

Darwish, H., A. Mahmood, T. Schallert, M. Chopp and B. Therrien (2014). "Simvastatin and environmental enrichment effect on recognition and temporal order memory after mild-to-moderate traumatic brain injury." *Brain Inj* 28(2): 211-226.

Davis, J. J., K. H. Walter, K. M. Chard, R. B. Parkinson and W. S. Houston (2013). "Treatment adherence in cognitive processing therapy for combat-related PTSD with history of mild TBI." *Rehabil Psychol* 58(1): 36-42.

Davis, M., D. L. Walker and K. M. Myers (2003). "Role of the amygdala in fear extinction measured with potentiated startle." *Ann N Y Acad Sci* 985: 218-232.

Davis, S., S. Renaudineau, R. Poirier, B. Poucet, E. Save and S. Laroche (2010). "The formation and stability of recognition memory: what happens upon recall?" *Front Behav Neurosci* 4: 177.

de Lanerolle, N. C., F. Bandak, D. Kang, A. Y. Li, F. Du, P. Swauger, S. Parks, G. Ling and J. H. Kim (2011). "Characteristics of an explosive blast-induced brain injury in an experimental model." *J Neuropathol Exp Neurol* 70(11): 1046-1057.

Dejana, E. and C. Betsholtz (2016). "NEURODEVELOPMENT. Oligodendrocytes follow blood vessel trails in the brain." *Science* 351(6271): 341-342.

Dell, R. B., S. Holleran and R. Ramakrishnan (2002). "Sample size determination." *ILAR J* 43(4): 207-213.

DeWitt, D. S. and D. S. Prough (2009). "Blast-induced brain injury and posttraumatic hypotension and hypoxemia." *J Neurotrauma* 26(6): 877-887.

DoD, B. I. R. P. C. O., U.S. Army Medical Research & Materiel Command (2014). "Prevention, Mitigation, and Treatment of Blast Injuries." *FY14 Report to the Executive Agent*.

Elder, G. A. (2015). "Update on TBI and Cognitive Impairment in Military Veterans." *Curr Neurol Neurosci Rep* 15(10): 68.

Elder, G. A., N. P. Dorr, R. De Gasperi, M. A. Gama Sosa, M. C. Shaughness, E. Maudlin-Jeronimo, A. A. Hall, R. M. McCarron and S. T. Ahlers (2012). "Blast exposure induces post-traumatic stress disorder-related traits in a rat model of mild traumatic brain injury." *J Neurotrauma* 29(16): 2564-2575.

Elsayed, N. M. (1997). "Toxicology of blast overpressure." *Toxicology* 121(1): 1-15.

Elsayed, N. M., K. L. Armstrong, M. T. William and M. F. Cooper (2000). "Antioxidant loading reduces oxidative stress induced by high-energy impulse noise (blast) exposure." *Toxicology* 155(1-3): 91-99.

Elsayed, N. M. and N. V. Gorbunov (2003). "Interplay between high energy impulse noise (blast) and antioxidants in the lung." *Toxicology* 189(1-2): 63-74.

Elsayed, N. M. and N. V. Gorbunov (2007). "Pulmonary biochemical and histological alterations after repeated low-level blast overpressure exposures." *Toxicol Sci* 95(1): 289-296.

Elsayed, N. M., N. V. Gorbunov and V. E. Kagan (1997). "A proposed biochemical mechanism involving hemoglobin for blast overpressure-induced injury." *Toxicology* 121(1): 81-90.

Engelhardt, S., A. J. Al-Ahmad, M. Gassmann and O. O. Ogunshola (2014). "Hypoxia selectively disrupts brain microvascular endothelial tight junction complexes through a hypoxia-inducible factor-1 (HIF-1) dependent mechanism." *J Cell Physiol* 229(8): 1096-1105.

Engelhardt, S., S. Patkar and O. O. Ogunshola (2014). "Cell-specific blood-brain barrier regulation in health and disease: a focus on hypoxia." *Br J Pharmacol* 171(5): 1210-1230.

Fairbairn, L., R. Kapetanovic, D. P. Sester and D. A. Hume (2011). "The mononuclear phagocyte system of the pig as a model for understanding human innate immunity and disease." *J Leukoc Biol* 89(6): 855-871.

Fandrey, J. and M. Gassmann (2009). "Oxygen sensing and the activation of the hypoxia inducible factor 1 (HIF-1)--invited article." *Adv Exp Med Biol* 648: 197-206.

Fievisohn, E. M., V. S. Sajja, P. J. VandeVord and W. N. Hardy (2014). "Evaluation of impact-induced traumatic brain injury in the Gottingen Minipig using two input modes." *Traffic Inj Prev* 15 Suppl 1: S81-87.

Fitzgerald, G. J. (2008). "Chemical warfare and medical response during World War I." *Am J Public Health* 98(4): 611-625.

Fitzpatrick, G. M., R. Cliff and N. Tandon (2013). "Thrombosomes: a platelet-derived hemostatic agent for control of noncompressible hemorrhage." *Transfusion* 53 Suppl 1: 100S-106S.

Flierl, M. A., M. Perl, D. Rittirsch, C. Bartl, H. Schreiber, V. Fleig, G. Schlaf, U. Liener, U. B. Brueckner, F. Gebhard and M. S. Huber-Lang (2008). "The role of C5a in the innate immune response after experimental blunt chest trauma." *Shock* 29(1): 25-31.

Forbes, P. (1812). "Observations on death from the wind of a ball." *Edinburgh Med Surg* 8: 310-312.

Forster, C., T. Kahles, S. Kietz and D. Drenckhahn (2007). "Dexamethasone induces the expression of metalloproteinase inhibitor TIMP-1 in the murine cerebral vascular endothelial cell line cEND." *J Physiol* 580(Pt.3): 937-949.

Friedlander, F. G. (1955). "Propagation of a Pulse in an Inhomogeneous Medium." *Ulan Press*.

Frink, M., H. Andruszkow, C. Zeckey, C. Krettek and F. Hildebrand (2011). "Experimental trauma models: an update." *J Biomed Biotechnol* 2011: 797383.

Frykberg, E. R. and J. J. Tepas, 3rd (1988). "Terrorist bombings. Lessons learned from Belfast to Beirut." *Ann Surg* 208(5): 569-576.

Fung, Y. C., R. T. Yen, Z. L. Tao and S. Q. Liu (1988). "A hypothesis on the mechanism of trauma of lung tissue subjected to impact load." *J Biomech Eng* 110(1): 50-56.

Fung, Y. C., Yen, M.R. (1984). "Experimental Investigation of Lung Injury Mechanisms." *San Diego, Calif: Jaycor, Inc.*

Fung, Y. C., Yen, M.R. (1985). "Characterization and modeling of thoraco-abdominal response to blast waves." *Final Report - U.S. Army*.

Garman, R. H., L. W. Jenkins, R. C. Switzer, 3rd, R. A. Bauman, L. C. Tong, P. V. Swauger, S. A. Parks, D. V. Ritzel, C. E. Dixon, R. S. Clark, H. Bayir, V. Kagan, E. K. Jackson and P. M. Kochanek (2011). "Blast exposure in rats with body shielding is characterized primarily by diffuse axonal injury." *J Neurotrauma* 28(6): 947-959.

Gawande, A. (2004). "Casualties of war--military care for the wounded from Iraq and Afghanistan." *N Engl J Med* 351(24): 2471-2475.

Gean, A. D. (2014). "Brain injury: applications from war and terrorism." *Wolters Kluwer*.

Gegel, B. T., P. N. Austin and A. D. Johnson (2013). "An evidence-based review of the use of a combat gauze (QuikClot) for hemorrhage control." *AANA J* 81(6): 453-458.

Goldstein, L. E., A. M. Rasmusson, B. S. Bunney and R. H. Roth (1996). "Role of the amygdala in the coordination of behavioral, neuroendocrine, and prefrontal cortical monoamine responses to psychological stress in the rat." *J Neurosci* 16(15): 4787-4798.

Gorbunov, N. V., L. V. Asher, V. Ayyagari and J. L. Atkins (2006). "Inflammatory leukocytes and iron turnover in experimental hemorrhagic lung trauma." *Exp Mol Pathol* 80(1): 11-25.

Gorbunov, N. V., N. M. Elsayed, E. R. Kisin, A. V. Kozlov and V. E. Kagan (1997). "Air blast-induced pulmonary oxidative stress: interplay among hemoglobin, antioxidants, and lipid peroxidation." *Am J Physiol* 272(2 Pt 1): L320-334.

Gorbunov, N. V., S. J. McFaul, S. Van Albert, C. Morrissette, G. M. Zaucha and J. Nath (2004). "Assessment of inflammatory response and sequestration of blood iron transferrin complexes in a rat model of lung injury resulting from exposure to low-frequency shock waves." *Crit Care Med* 32(4): 1028-1034.

Gorbunov, N. V., J. Nath, J. M. Parker and G. M. Zaucha (2003). "Electron paramagnetic resonance analysis of transferrin-bound iron in animal models of blunt trauma." *J Trauma* 54(3): 574-583.

Grommes, J. and O. Soehnlein (2011). "Contribution of neutrophils to acute lung injury." *Mol Med* 17(3-4): 293-307.

Gullotti, D. M., M. Beamer, M. B. Panzer, Y. C. Chen, T. P. Patel, A. Yu, N. Jaumard, B. Winkelstein, C. R. Bass, B. Morrison and D. F. Meaney (2014). "Significant head accelerations can influence immediate neurological impairments in a murine model of blast-induced traumatic brain injury." *J Biomech Eng* 136(9): 091004.

Hadden, W. A., W. H. Rutherford and J. D. Merrett (1978). "The injuries of terrorist bombing: a study of 1532 consecutive patients." *Br J Surg* 65(8): 525-531.

Hampton, C. E. and P. J. VandeVord (2012). "Vibrational frequency response to impact loading of skull models." *Biomed Sci Instrum* 48: 157-164.

Heldt, S. A., A. J. Elberger, Y. Deng, N. H. Guley, N. Del Mar, J. Rogers, G. W. Choi, J. Ferrell, T. S. Rex, M. G. Honig and A. Reiner (2014). "A novel closed-head model of mild traumatic brain injury caused by primary overpressure blast to the cranium produces sustained emotional deficits in mice." *Front Neurol* 5: 2.

Hermanson, G. (1996). "Bioconjugate Techniques." *Academic Press, San Diego*: pp xxv, 785.

Hicks, R. R., S. J. Fertig, R. E. Desrocher, W. J. Koroshetz and J. J. Pancrazio (2010). "Neurological effects of blast injury." *J Trauma* 68(5): 1257-1263.

Higashida, T., C. W. Kreipke, J. A. Rafols, C. Peng, S. Schafer, P. Schafer, J. Y. Ding, D. Dornbos, 3rd, X. Li, M. Guthikonda, N. F. Rossi and Y. Ding (2011). "The role of hypoxia-inducible factor-1alpha, aquaporin-4, and matrix metalloproteinase-9 in blood-brain barrier disruption and brain edema after traumatic brain injury." *J Neurosurg* 114(1): 92-101.

Hirsch, M. and J. Bazini (1969). "Blast injury of the chest." *Clin Radiol* 20(4): 362-370.

Hockey, K. S., W. B. Hubbard, V. S. Sajja, C. A. Sholar, C. Thorpe, P. J. VandeVord and B. A. Rzigalinski (2013). "A new model for mild blast injury utilizing Drosophila melanogaster - biomed 2013." *Biomed Sci Instrum* 49: 134-140.

Hooker, D. (1924). "Physiological effects of air concussion." *American Journal of Physiology - Legacy Content* 67(2): 219.

Huang, E., M. Ngo, S. Yee, L. Held, K. Norman, A. M. Scremin and O. Scremin (2013). "Repeated blast exposure alters open field behavior recorded under low illumination." *Brain Res* 1529: 125-133.

Huang, M., M. Risling and D. G. Baker (2016). "The role of biomarkers and MEG-based imaging markers in the diagnosis of post-traumatic stress disorder and blast-induced mild traumatic brain injury." *Psychoneuroendocrinology* 63: 398-409.

Huang, M. X., K. A. Yurgil, A. Robb, A. Angeles, M. Diwakar, V. B. Risbrough, S. L. Nichols, R. McLay, R. J. Theilmann, T. Song, C. W. Huang, R. R. Lee and D. G. Baker (2014). "Voxel-wise resting-state MEG source magnitude imaging study reveals neurocircuitry abnormality in active-duty service members and veterans with PTSD." *Neuroimage Clin* 5: 408-419.

Hubbard, W. B., Bailey, Z., VandeVord P.J. (2016). "Cellular Mechanisms and Behavioral Outcomes in Blast-induced Neurotrauma: Comparing Experimental Set-ups." *Methods in Molecular Biology* "In Press".

Hubbard, W. B., C. Hall, V. Siva Sai Suijith Sajja, E. Lavik and P. VandeVord (2014). "Examining lethality risk for rodent studies of primary blast lung injury." *Biomed Sci Instrum* 50: 92-99.

Hubbard, W. B., M. M. Lashof-Sullivan, E. B. Lavik and P. J. VandeVord (2015). "Steroid-Loaded Hemostatic Nanoparticles Combat Lung Injury after Blast Trauma." *ACS Macro Letters* 4(4): 387-391.

Huber, B. R., J. S. Meabon, Z. S. Hoffer, J. Zhang, J. G. Hoekstra, K. F. Pagulayan, P. J. McMillan, C. L. Mayer, W. A. Banks, B. C. Kraemer, M. A. Raskind, D. B. McGavern, E. R. Peskind and D. G. Cook (2016). "Blast exposure causes dynamic microglial/macrophage responses and microdomains of brain microvessel dysfunction." *Neuroscience* 319: 206-220.

Hue, C. D., F. S. Cho, S. Cao, C. R. Dale Bass, D. F. Meaney and B. Morrison, 3rd (2015). "Dexamethasone potentiates in vitro blood-brain barrier recovery after primary blast injury by glucocorticoid receptor-mediated upregulation of ZO-1 tight junction protein." *J Cereb Blood Flow Metab* 35(7): 1191-1198.

Hue, C. D., F. S. Cho, S. Cao, R. E. Nicholls, E. W. Vogel Iii, C. Sibindi, O. Arancio, C. R. Dale Bass, D. F. Meaney and B. Morrison Iii (2016). "Time Course and Size of Blood-Brain

Barrier Opening in a Mouse Model of Blast-Induced Traumatic Brain Injury." *J Neurotrauma* 33(13): 1202-1211.

Huller, T. and Y. Bazini (1970). "Blast injuries of the chest and abdomen." *Arch Surg* 100(1): 24-30.

Hunt, B. J. (2015). "The current place of tranexamic acid in the management of bleeding." *Anaesthesia* 70 Suppl 1: 50-53, e18.

Iremonger, M. (1997). "Physics of Detonations and Blast-waves." *Scientific Foundation of Trauma; Oxford: Butterworth-Heinemann* 1: 189-199.

Irvin, C. G. and J. H. Bates (2003). "Measuring the lung function in the mouse: the challenge of size." *Respir Res* 4: 4.

Irwin, R. J., M. R. Lerner, J. F. Bealer, D. J. Brackett and D. W. Tuggle (1997). "Cardiopulmonary physiology of primary blast injury." *J Trauma* 43(4): 650-655.

Irwin, R. J., M. R. Lerner, J. F. Bealer, S. A. Lightfoot, D. J. Brackett and D. W. Tuggle (1998). "Global primary blast injury: a rat model." *J Okla State Med Assoc* 91(7): 387-392.

Irwin, R. J., M. R. Lerner, J. F. Bealer, P. C. Mantor, D. J. Brackett and D. W. Tuggle (1999). "Shock after blast wave injury is caused by a vagally mediated reflex." *J Trauma* 47(1): 105-110.

Jaffin, J. H., L. McKinney, R. C. Kinney, J. A. Cunningham, D. M. Moritz, J. M. Kraimer, G. M. Graeber, J. B. Moe, J. M. Salander and J. W. Harmon (1987). "A laboratory model for studying blast overpressure injury." *J Trauma* 27(4): 349-356.

Johansen, J. P., C. K. Cain, L. E. Ostroff and J. E. LeDoux (2011). "Molecular mechanisms of fear learning and memory." *Cell* 147(3): 509-524.

Jones, E., N. T. Fear and S. Wessely (2007). "Shell shock and mild traumatic brain injury: a historical review." *Am J Psychiatry* 164(11): 1641-1645.

Kamnaksh, A., E. Kovesdi, S. K. Kwon, D. Wingo, F. Ahmed, N. E. Grunberg, J. Long and D. V. Agoston (2011). "Factors affecting blast traumatic brain injury." *J Neurotrauma* 28(10): 2145-2153.

Kamnaksh, A., S. K. Kwon, E. Kovesdi, F. Ahmed, E. S. Barry, N. E. Grunberg, J. Long and D. Agoston (2012). "Neurobehavioral, cellular, and molecular consequences of single and multiple mild blast exposure." *Electrophoresis* 33(24): 3680-3692.

Katsu, M., K. Niizuma, H. Yoshioka, N. Okami, H. Sakata and P. H. Chan (2010). "Hemoglobin-induced oxidative stress contributes to matrix metalloproteinase activation and blood-brain barrier dysfunction in vivo." *J Cereb Blood Flow Metab* 30(12): 1939-1950.

Katz, E., B. Ofek, J. Adler, H. B. Abramowitz and M. M. Krausz (1989). "Primary blast injury after a bomb explosion in a civilian bus." *Ann Surg* 209(4): 484-488.

Kaur, C. and E. A. Ling (2008). "Blood brain barrier in hypoxic-ischemic conditions." *Curr Neurovasc Res* 5(1): 71-81.

Kaur, C., J. Singh, M. K. Lim, B. L. Ng, E. P. Yap and E. A. Ling (1995). "The response of neurons and microglia to blast injury in the rat brain." *Neuropathol Appl Neurobiol* 21(5): 369-377.

Kirkman, E. and S. Watts (2011). "Characterization of the response to primary blast injury." *Philos Trans R Soc Lond B Biol Sci* 366(1562): 286-290.

Kirsch, D. L., L. R. Price, F. Nichols, J. A. Marksberry and K. T. Platoni (2014). "Military service member and veteran self reports of efficacy of cranial electrotherapy stimulation for anxiety, posttraumatic stress disorder, insomnia, and depression." *US Army Med Dep J*: 46-54.

Knoferl, M. W., U. C. Liener, D. H. Seitz, M. Perl, U. B. Bruckner, L. Kinzl and F. Gebhard (2003). "Cardiopulmonary, histological, and inflammatory alterations after lung contusion in a novel mouse model of blunt chest trauma." *Shock* 19(6): 519-525.

Knutson, K. M., S. T. Rakowsky, J. Solomon, F. Krueger, V. Raymont, M. C. Tierney, E. M. Wassermann and J. Grafman (2013). "Injured brain regions associated with anxiety in Vietnam veterans." *Neuropsychologia* 51(4): 686-694.

Kovacs, S. K., F. Leonessa and G. S. Ling (2014). "Blast TBI Models, Neuropathology, and Implications for Seizure Risk." *Front Neurol* 5: 47.

Kovesdi, E., A. Kamnaksh, D. Wingo, F. Ahmed, N. E. Grunberg, J. B. Long, C. E. Kasper and D. V. Agoston (2012). "Acute minocycline treatment mitigates the symptoms of mild blast-induced traumatic brain injury." *Front Neurol* 3: 111.

Krock, B. L., N. Skuli and M. C. Simon (2011). "Hypoxia-induced angiogenesis: good and evil." *Genes Cancer* 2(12): 1117-1133.

Kuehn, R., P. F. Simard, I. Driscoll, K. Keledjian, S. Ivanova, C. Tosun, A. Williams, G. Bochicchio, V. Gerzanich and J. M. Simard (2011). "Rodent model of direct cranial blast injury." *J Neurotrauma* 28(10): 2155-2169.

Kumar, A., B. A. Stoica, B. Sabirzhanov, M. P. Burns, A. I. Faden and D. J. Loane (2013). "Traumatic brain injury in aged animals increases lesion size and chronically alters microglial/macrophage classical and alternative activation states." *Neurobiol Aging* 34(5): 1397-1411.

Lashof-Sullivan, M., M. Holland, R. Groynom, D. Campbell, A. Shoffstall and E. Lavik (2016). "Hemostatic Nanoparticles Improve Survival Following Blunt Trauma Even after 1 Week Incubation at 50 degrees C." *Acs Biomaterials-Science & Engineering* 2(3): 385-392.

Lashof-Sullivan, M., A. Shoffstall and E. Lavik (2013). "Intravenous hemostats: challenges in translation to patients." *Nanoscale* 5(22): 10719-10728.

Lashof-Sullivan, M. M., E. Shoffstall, K. T. Atkins, N. Keane, C. Bir, P. VandeVord and E. B. Lavik (2014). "Intravenously administered nanoparticles increase survival following blast trauma." *Proc Natl Acad Sci U S A* 111(28): 10293-10298.

Lee, I. N., W. C. Cheng, C. Y. Chung, M. H. Lee, M. H. Lin, C. H. Kuo, H. H. Weng and J. T. Yang (2014). "Dexamethasone reduces brain cell apoptosis and inhibits inflammatory response in rats with intracerebral hemorrhage." *J Neurosci Res*.

Lee, I. N., W. C. Cheng, C. Y. Chung, M. H. Lee, M. H. Lin, C. H. Kuo, H. H. Weng and J. T. Yang (2015). "Dexamethasone reduces brain cell apoptosis and inhibits inflammatory response in rats with intracerebral hemorrhage." *J Neurosci Res* 93(1): 178-188.

Lee, J. H., M. Hanaoka, Y. Kitaguchi, D. Kraskauskas, L. Shapiro, N. F. Voelkel and L. Taraseviciene-Stewart (2012). "Imbalance of apoptosis and cell proliferation contributes to the development and persistence of emphysema." *Lung* 190(1): 69-82.

Leonardi, A. D., C. A. Bir, D. V. Ritzel and P. J. VandeVord (2011). "Intracranial pressure increases during exposure to a shock wave." *J Neurotrauma* 28(1): 85-94.

Li, A., X. Sun, Y. Ni, X. Chen and A. Guo (2013). "HIF-1alpha involves in neuronal apoptosis after traumatic brain injury in adult rats." *J Mol Neurosci* 51(3): 1052-1062.

Li, Y., M. Chavko, J. L. Slack, B. Liu, R. M. McCarron, J. D. Ross and J. J. Dalle Lucca (2013). "Protective effects of decay-accelerating factor on blast-induced neurotrauma in rats." *Acta Neuropathol Commun* 1: 52.

Liao, F., Q. Q. Dan, R. F. Du, J. T. Li and Y. H. Zhang (2012). "[Expression of TNF-alpha in lung tissue of rats with lung injury induced by brain ischemia]." *Sichuan Da Xue Xue Bao Yi Xue Ban* 43(6): 914-917.

Liener, U. C., M. W. Knoferl, J. Strater, T. F. Barth, E. M. Pauser, A. K. Nussler, L. Kinzl, U. B. Bruckner and F. Gebhard (2003). "Induction of apoptosis following blunt chest trauma." *Shock* 20(6): 511-516.

Lin, B. and M. D. Ginsberg (2000). "Quantitative assessment of the normal cerebral microvasculature by endothelial barrier antigen (EBA) immunohistochemistry: application to focal cerebral ischemia." *Brain Res* 865(2): 237-244.

Liu, M., C. Zhang, W. Liu, P. Luo, L. Zhang, Y. Wang, Z. Wang and Z. Fei (2015). "A novel rat model of blast-induced traumatic brain injury simulating different damage degree: implications for morphological, neurological, and biomarker changes." *Front Cell Neurosci* 9: 168.

Liu, Y., S. R. Cox, T. Morita and S. Kourembanas (1995). "Hypoxia regulates vascular endothelial growth factor gene expression in endothelial cells. Identification of a 5' enhancer." *Circ Res* 77(3): 638-643.

Lo, C. T., P. R. Van Tassel and W. M. Saltzman (2010). "Poly(lactide-co-glycolide) nanoparticle assembly for highly efficient delivery of potent therapeutic agents from medical devices." *Biomaterials* 31(13): 3631-3642.

Loane, D. J. and K. R. Byrnes (2010). "Role of microglia in neurotrauma." *Neurotherapeutics* 7(4): 366-377.

Lovering, M. E., S. P. Proctor and K. J. Heaton (2013). "A retrospective study of anxiety disorder diagnoses in the military from 2000 to 2009." *J Anxiety Disord* 27(1): 25-32.

Lundberg, A. H., K. Fukatsu, L. Gaber, S. Callicutt, M. Kotb, H. Wilcox, K. Kudsk and A. O. Gaber (2001). "Blocking pulmonary ICAM-1 expression ameliorates lung injury in established diet-induced pancreatitis." *Ann Surg* 233(2): 213-220.

Mackenzie, I. M. and B. Tunnicliffe (2011). "Blast injuries to the lung: epidemiology and management." *Philos Trans R Soc Lond B Biol Sci* 366(1562): 295-299.

Mahan, A. L. and K. J. Ressler (2012). "Fear conditioning, synaptic plasticity and the amygdala: implications for posttraumatic stress disorder." *Trends Neurosci* 35(1): 24-35.

Marti, M., M. Parron, F. Baudraxler, A. Royo, N. Gomez Leon and R. Alvarez-Sala (2006). "Blast injuries from Madrid terrorist bombing attacks on March 11, 2004." *Emerg Radiol* 13(3): 113-122.

Matthews, S. C., A. D. Spadoni, J. B. Lohr, I. A. Strigo and A. N. Simmons (2012). "Diffusion tensor imaging evidence of white matter disruption associated with loss versus alteration of consciousness in warfighters exposed to combat in Operations Enduring and Iraqi Freedom." *Psychiatry Res* 204(2-3): 149-154.

Mayorga, M. A. (1997). "The pathology of primary blast overpressure injury." *Toxicology* 121(1): 17-28.

Michiels, C. (2004). "Physiological and pathological responses to hypoxia." *Am J Pathol* 164(6): 1875-1882.

Mishra, V., M. Skotak, H. Schuetz, A. Heller, J. Haorah and N. Chandra (2016). "Primary blast causes mild, moderate, severe and lethal TBI with increasing blast overpressures: Experimental rat injury model." *Sci Rep* 6: 26992.

Morey, R. A., A. L. Gold, K. S. LaBar, S. K. Beall, V. M. Brown, C. C. Haswell, J. D. Nasser, H. R. Wagner, G. McCarthy and M. W. Mid-Atlantic (2012). "Amygdala volume changes in posttraumatic stress disorder in a large case-controlled veterans group." *Arch Gen Psychiatry* 69(11): 1169-1178.

Moss, W. C., M. J. King and E. G. Blackman (2009). "Skull flexure from blast waves: a mechanism for brain injury with implications for helmet design." *Phys Rev Lett* 103(10): 108702.

Mott, F. W. (1916). "The effects of high explsives upon the central nervous system." *Lancet.* 48: 331-338.

Munster, A. M., A. K. Olsen and E. M. Bladbjerg (2002). "Usefulness of human coagulation and fibrinolysis assays in domestic pigs." *Comp Med* 52(1): 39-43.

Murphy, C. M., Q. Deeley, E. M. Daly, C. Ecker, F. M. O'Brien, B. Hallahan, E. Loth, F. Toal, S. Reed, S. Hales, D. M. Robertson, M. C. Craig, D. Mullins, G. J. Barker, T. Lavender, P. Johnston, K. C. Murphy and D. G. Murphy (2012). "Anatomy and aging of the amygdala and hippocampus in autism spectrum disorder: an in vivo magnetic resonance imaging study of Asperger syndrome." *Autism Res* 5(1): 3-12.

Musselman, M. M. and E. L. Berry (1951). "The management of patients burned by atomic explosion." *J Mich State Med Soc* 50(3): 275-277; passim.

Nakagawa, A., G. T. Manley, A. D. Gean, K. Ohtani, R. Armonda, A. Tsukamoto, H. Yamamoto, K. Takayama and T. Tominaga (2011). "Mechanisms of primary blast-induced traumatic brain injury: insights from shock-wave research." *J Neurotrauma* 28(6): 1101-1119.

Neigh, G. N., M. J. Owens, W. R. Taylor and C. B. Nemeroff (2010). "Changes in the vascular area fraction of the hippocampus and amygdala are induced by prenatal dexamethasone and/or adult stress." *J Cereb Blood Flow Metab* 30(6): 1100-1104.

Nibbeling, N., R. R. Oudejans, E. M. Ubink and H. A. Daanen (2014). "The effects of anxiety and exercise-induced fatigue on shooting accuracy and cognitive performance in infantry soldiers." *Ergonomics* 57(9): 1366-1379.

Obermeier, B., R. Daneman and R. M. Ransohoff (2013). "Development, maintenance and disruption of the blood-brain barrier." *Nat Med* 19(12): 1584-1596.

Office, U. S. G. A. (2013). "Defense Health: Actions needed to help ensure combat casualty care research achieves goals." *Report to Congressional Committees*.

Ogunshola, O. O. and A. Al-Ahmad (2012). "HIF-1 at the blood-brain barrier: a mediator of permeability?" *High Alt Med Biol* 13(3): 153-161.

Okada, S., R. Okeda, S. Matsushita and A. Kawano (1998). "Histopathological and morphometric study of the late effects of heavy-ion irradiation on the spinal cord of the rat." *Radiat Res* 150(3): 304-315.

Olsen, A. K., A. K. Hansen, J. Jespersen, P. Marckmann and E. M. Bladbjerg (1999). "The pig as a model in blood coagulation and fibrinolysis research." *Scandinavian Journal of Laboratory Animal Science* 26(4): 214-224.

Park, E., R. Eisen, A. Kinio and A. J. Baker (2013). "Electrophysiological white matter dysfunction and association with neurobehavioral deficits following low-level primary blast trauma." *Neurobiol Dis* 52: 150-159.

Paxinos, G. a. W., C. (2006). "The rat brain in stereotaxic coordinates." *Elsevier* 6th edition.

Peitzman AB, R. M., Schwab CW, Yealy DM, Fabian TC (2007). "The Trauma Manual: Trauma and Acute Care Surgery (Spiral Manual Series). Third Edition." *Hagerstown, MD: Lippincott Williams & Wilkins*: 223.

Pelz, J., W. Hartig, C. Weise, C. Hobohm, D. Schneider, M. Krueger, J. Kacza and D. Michalski (2013). "Endothelial barrier antigen-immunoreactivity is conversely associated with blood-brain barrier dysfunction after embolic stroke in rats." *Eur J Histochem* 57(4): e38.

Perez-Polo, J. R., H. C. Rea, K. M. Johnson, M. A. Parsley, G. C. Unabia, G. Y. Xu, D. Prough, D. S. DeWitt, H. Spratt and C. E. Hulsebosch (2015). "A rodent model of mild traumatic brain blast injury." *J Neurosci Res* 93(4): 549-561.

Phillips, Y. Y. (1986). "Primary blast injuries." *Ann Emerg Med* 15(12): 1446-1450.

Pittet, J. F., R. C. Mackersie, T. R. Martin and M. A. Matthay (1997). "Biological markers of acute lung injury: prognostic and pathogenetic significance." *Am J Respir Crit Care Med* 155(4): 1187-1205.

Pizov, R., A. Oppenheim-Eden, I. Matot, Y. G. Weiss, L. A. Eidelman, A. I. Rivkind and C. L. Sprung (1999). "Blast lung injury from an explosion on a civilian bus." *Chest* 115(1): 165-172.

Previti, M. L., W. Zhang and W. E. Van Nostrand (2006). "Dexamethasone diminishes the pro-inflammatory and cytotoxic effects of amyloid beta-protein in cerebrovascular smooth muscle cells." *J Neuroinflammation* 3: 18.

Pun, P. B., E. M. Kan, A. Salim, Z. Li, K. C. Ng, S. M. Moochhala, E. A. Ling, M. H. Tan and J. Lu (2011). "Low level primary blast injury in rodent brain." *Front Neurol* 2: 19.

Rabinovici, R., G. Feuerstein, F. Abdullah, M. Whiteford, P. Borboroglu, E. Sheikh, D. R. Phillip, P. Ovadia, L. Bobroski, O. Bagasra and L. F. Neville (1996). "Locally produced tumor necrosis factor-alpha mediates interleukin-2-induced lung injury." *Circ Res* 78(2): 329-336.

Rabinowitz, P. M. and M. D. Siegel (2002). "Acute inhalation injury." *Clin Chest Med* 23(4): 707-715.

Rafaels, K. A., C. R. Bass, M. B. Panzer, R. S. Salzar, W. A. Woods, S. H. Feldman, T. Walilko, R. W. Kent, B. P. Capehart, J. B. Foster, B. Derkunt and A. Toman (2012). "Brain injury risk from primary blast." *J Trauma Acute Care Surg* 73(4): 895-901.

Rajkowska, G., J. Hughes, C. A. Stockmeier, J. Javier Miguel-Hidalgo and D. Maciag (2013). "Coverage of blood vessels by astrocytic endfeet is reduced in major depressive disorder." *Biol Psychiatry* 73(7): 613-621.

Ramasamy, A., S. E. Harrisson, J. C. Clasper and M. P. Stewart (2008). "Injuries from roadside improvised explosive devices." *J Trauma* 65(4): 910-914.

Rath, P. C. and B. B. Aggarwal (1999). "TNF-induced signaling in apoptosis." *J Clin Immunol* 19(6): 350-364.

Readnower, R. D., M. Chavko, S. Adeeb, M. D. Conroy, J. R. Pauly, R. M. McCarron and P. G. Sullivan (2010). "Increase in blood-brain barrier permeability, oxidative stress, and activated microglia in a rat model of blast-induced traumatic brain injury." *J Neurosci Res* 88(16): 3530-3539.

Ritenour, A. E. and T. W. Baskin (2008). "Primary blast injury: update on diagnosis and treatment." *Crit Care Med* 36(7 Suppl): S311-317.

Rodoplu, U., J. L. Arnold, R. Tokyay, G. Ersoy, S. Cetiner and T. Yucel (2004). "Mass-casualty terrorist bombings in Istanbul, Turkey, November 2003: report of the events and the prehospital emergency response." *Prehosp Disaster Med* 19(2): 133-145.

Rosenfeld, J. V. (2006). "A neurosurgeon in Iraq: a personal perspective." *J Clin Neurosci* 13(10): 986-990.

Rube, C. E., F. Wilfert, D. Uthe, K. W. Schmid, R. Knoop, N. Willich, A. Schuck and C. Rube (2002). "Modulation of radiation-induced tumour necrosis factor alpha (TNF-alpha) expression in the lung tissue by pentoxifylline." *Radiother Oncol* 64(2): 177-187.

Rubovitch, V., M. Ten-Bosch, O. Zohar, C. R. Harrison, C. Tempel-Brami, E. Stein, B. J. Hoffer, C. D. Balaban, S. Schreiber, W. T. Chiu and C. G. Pick (2011). "A mouse model of blast-induced mild traumatic brain injury." *Exp Neurol* 232(2): 280-289.

Ruiz Junior, R. L., L. R. de Carvalho and A. J. Cataneo (2005). "Compensatory lung growth: protein, DNA and RNA lung contents in undernourished trilobectomized rats." *Acta Cir Bras* 20(3): 219-224.

Sah, P., E. S. Faber, M. Lopez De Armentia and J. Power (2003). "The amygdaloid complex: anatomy and physiology." *Physiol Rev* 83(3): 803-834.

Sajja, V. S., E. S. Ereifej and P. J. VandeVord (2014). "Hippocampal vulnerability and subacute response following varied blast magnitudes." *Neurosci Lett* 570: 33-37.

Sajja, V. S., W. B. Hubbard, C. S. Hall, F. Ghoddoussi, M. P. Galloway and P. J. VandeVord (2015). "Enduring deficits in memory and neuronal pathology after blast-induced traumatic brain injury." *Sci Rep* 5: 15075.

Sajja, V. S., W. B. Hubbard and P. J. VandeVord (2015). "Subacute Oxidative Stress and Glial Reactivity in the Amygdala are Associated with Increased Anxiety Following Blast Neurotrauma." *Shock* 44 Suppl 1: 71-78.

Sajja, V. S., S. A. Perrine, F. Ghoddoussi, C. S. Hall, M. P. Galloway and P. J. VandeVord (2014). "Blast neurotrauma impairs working memory and disrupts prefrontal myo-inositol levels in rats." *Mol Cell Neurosci* 59: 119-126.

Saljo, A., F. Bao, K. G. Haglid and H. A. Hansson (2000). "Blast exposure causes redistribution of phosphorylated neurofilament subunits in neurons of the adult rat brain." *J Neurotrauma* 17(8): 719-726.

Sasser, S. M., R. W. Sattin, R. C. Hunt and J. Krohmer (2006). "Blast lung injury." *Prehosp Emerg Care* 10(2): 165-172.

Seitz, D. H., M. Perl, S. Mangold, A. Neddermann, S. T. Braumuller, S. Zhou, M. G. Bachem, M. S. Huber-Lang and M. W. Knoferl (2008). "Pulmonary contusion induces alveolar type 2 epithelial cell apoptosis: role of alveolar macrophages and neutrophils." *Shock* 30(5): 537-544.

Shain, W., L. Spataro, J. Dilgen, K. Haverstick, S. Retterer, M. Isaacson, M. Saltzman and J. N. Turner (2003). "Controlling cellular reactive responses around neural prosthetic devices using peripheral and local intervention strategies." *IEEE Trans Neural Syst Rehabil Eng* 11(2): 186-188.

Shetty, A. K., V. Mishra, M. Kodali and B. Hattiangady (2014). "Blood brain barrier dysfunction and delayed neurological deficits in mild traumatic brain injury induced by blast shock waves." *Front Cell Neurosci* 8: 232.

Shoffstall, A. J., K. T. Atkins, R. E. Groynom, M. E. Varley, L. M. Everhart, M. M. Lashof-Sullivan, B. Martyn-Dow, R. S. Butler, J. S. Ustin and E. B. Lavik (2012). "Intravenous hemostatic nanoparticles increase survival following blunt trauma injury." *Biomacromolecules* 13(11): 3850-3857.

Shoffstall, A. J., L. M. Everhart, M. E. Varley, E. S. Soehnlen, A. M. Shick, J. S. Ustin and E. B. Lavik (2013). "Tuning ligand density on intravenous hemostatic nanoparticles dramatically increases survival following blunt trauma." *Biomacromolecules* 14(8): 2790-2797.

Simard, J. M., A. Pampori, K. Keledjian, C. Tosun, G. Schwartzbauer, S. Ivanova and V. Gerzanich (2014). "Exposure of the thorax to a sublethal blast wave causes a hydrodynamic pulse that leads to perivenular inflammation in the brain." *J Neurotrauma* 31(14): 1292-1304.

Singleton, J. A., I. E. Gibb, A. M. Bull, P. F. Mahoney and J. C. Clasper (2013). "Primary blast lung injury prevalence and fatal injuries from explosions: insights from postmortem computed tomographic analysis of 121 improvised explosive device fatalities." *J Trauma Acute Care Surg* 75(2 Suppl 2): S269-274.

Skold, M. K., C. von Gertten, A. C. Sandberg-Nordqvist, T. Mathiesen and S. Holmin (2005). "VEGF and VEGF receptor expression after experimental brain contusion in rat." *J Neurotrauma* 22(3): 353-367.

Skotak, M., F. Wang, A. Alai, A. Holmberg, S. Harris, R. C. Switzer and N. Chandra (2013). "Rat injury model under controlled field-relevant primary blast conditions: acute response to a wide range of peak overpressures." *J Neurotrauma* 30(13): 1147-1160.

Smith, J. E. (2011). "The epidemiology of blast lung injury during recent military conflicts: a retrospective database review of cases presenting to deployed military hospitals, 2003-2009." *Philos Trans R Soc Lond B Biol Sci* 366(1562): 291-294.

Snell, F. I. and M. J. Halter (2010). "A signature wound of war: mild traumatic brain injury." *J Psychosoc Nurs Ment Health Serv* 48(2): 22-28.

Sondeen, J. L., R. de Guzman, I. A. Polykratis, M. D. Prince, O. Hernandez, A. P. Cap and M. A. Dubick (2013). "Comparison between human and porcine thromboelastograph parameters in response to ex-vivo changes to platelets, plasma, and red blood cells." *Blood Coagulation & Fibrinolysis* 24(8): 818-829.

Spahn, D. R., B. Bouillon, V. Cerny, T. J. Coats, J. Duranteau, E. Fernandez-Mondejar, D. Filipescu, B. J. Hunt, R. Komadina, G. Nardi, E. Neugebauer, Y. Ozier, L. Riddez, A. Schultz, J. L. Vincent and R. Rossaint (2013). "Management of bleeding and coagulopathy following major trauma: an updated European guideline." *Crit Care* 17(2): R76.

Spahn, D. R., V. Cerny, T. J. Coats, J. Duranteau, E. Fernandez-Mondejar, G. Gordini, P. F. Stahel, B. J. Hunt, R. Komadina, E. Neugebauer, Y. Ozier, L. Riddez, A. Schultz, J. L. Vincent, R. Rossaint and T. Task Force for Advanced Bleeding Care in (2007).

"Management of bleeding following major trauma: a European guideline." *Crit Care* 11(1): R17.

Stahel, P. F., C. E. Heyde, W. Wyrwich and W. Ertel (2005). "[Current concepts of polytrauma management: from ATLS to "damage control"]." *Orthopade* 34(9): 823-836.

Stewart, C. (2006). "Blast Injuries: Preparing for the Inevitable." *Emergency Medicine Practice* 8(4).

Sullivan, W. H. (1951). "Some public health aspects of an atomic explosion." *Ind Med Surg* 20(1): 1-6.

Svetlov, S. I., V. Prima, D. R. Kirk, H. Gutierrez, K. C. Curley, R. L. Hayes and K. K. Wang (2010). "Morphologic and biochemical characterization of brain injury in a model of controlled blast overpressure exposure." *J Trauma* 69(4): 795-804.

Tang, Y. and W. Le (2016). "Differential Roles of M1 and M2 Microglia in Neurodegenerative Diseases." *Mol Neurobiol* 53(2): 1181-1194.

Tenney, S. M. and J. E. Remmers (1963). "Comparative quantitative morphology of the mammalian lung: diffusing area." *Nature* 197: 54-56.

Trudeau, D. L., J. Anderson, L. M. Hansen, D. N. Shagalov, J. Schmoller, S. Nugent and S. Barton (1998). "Findings of mild traumatic brain injury in combat veterans with PTSD and a history of blast concussion." *J Neuropsychiatry Clin Neurosci* 10(3): 308-313.

Turegano-Fuentes, F., P. Caba-Doussoux, J. M. Jover-Navalon, E. Martin-Perez, D. Fernandez-Luengas, L. Diez-Valladares, D. Perez-Diaz, P. Yuste-Garcia, H. Guadalajara Labajo, R. Rios-Blanco, F. Hernando-Trancho, F. Garcia-Moreno Nisa, M. Sanz-Sanchez, C. Garcia-Fuentes, A. Martinez-Virto, J. L. Leon-Baltasar and J. Vazquez-Estevez (2008). "Injury patterns from major urban terrorist bombings in trains: the Madrid experience." *World J Surg* 32(6): 1168-1175.

Turtzo, L. C., J. Lescher, L. Janes, D. D. Dean, M. D. Budde and J. A. Frank (2014). "Macrophagic and microglial responses after focal traumatic brain injury in the female rat." *J Neuroinflammation* 11: 82.

Valerius, K. P. (1996). "Size-dependent morphology of the conductive bronchial tree in four species of myomorph rodents." *J Morphol* 230(3): 291-297.

Vanderploeg, R. D., H. G. Belanger, R. D. Horner, A. M. Spehar, G. Powell-Cope, S. L. Luther and S. G. Scott (2012). "Health outcomes associated with military deployment: mild

traumatic brain injury, blast, trauma, and combat associations in the Florida National Guard." *Arch Phys Med Rehabil* 93(11): 1887-1895.

VandeVord, P. J., R. Bolander, V. S. Sajja, K. Hay and C. A. Bir (2012). "Mild neurotrauma indicates a range-specific pressure response to low level shock wave exposure." *Ann Biomed Eng* 40(1): 227-236.

VandeVord, P. J., Leonardi, A., Ritzel, D. (2016). "Bridging the gap of standardized animal models for blast neurotrauma: methodology for appropriate experimental testing." *Methods in Molecular Biology* In Press.

Vorhees, C. V. and M. T. Williams (2014). "Assessing spatial learning and memory in rodents." *ILAR J* 55(2): 310-332.

Walker, W. C., L. M. Franke, S. D. McDonald, A. P. Sima and L. Keyser-Marcus (2015). "Prevalence of mental health conditions after military blast exposure, their co-occurrence, and their relation to mild traumatic brain injury." *Brain Inj* 29(13-14): 1581-1588.

Wang, Y., Y. Wei, S. Oguntayo, W. Wilkins, P. Arun, M. Valiyaveettil, J. Song, J. B. Long and M. P. Nambiar (2011). "Tightly coupled repetitive blast-induced traumatic brain injury: development and characterization in mice." *J Neurotrauma* 28(10): 2171-2183.

Westin, J. E., H. S. Lindgren, J. Gardi, J. R. Nyengaard, P. Brundin, P. Mohapel and M. A. Cenci (2006). "Endothelial proliferation and increased blood-brain barrier permeability in the basal ganglia in a rat model of 3,4-dihydroxyphenyl-L-alanine-induced dyskinesia." *J Neurosci* 26(37): 9448-9461.

Wightman, J. M. and S. L. Gladish (2001). "Explosions and blast injuries." *Ann Emerg Med* 37(6): 664-678.

Wilde, E. A., E. D. Bigler, J. V. Hunter, M. A. Fearing, R. S. Scheibel, M. R. Newsome, J. L. Johnson, J. Bachevalier, X. Li and H. S. Levin (2007). "Hippocampus, amygdala, and basal ganglia morphometrics in children after moderate-to-severe traumatic brain injury." *Dev Med Child Neurol* 49(4): 294-299.

Wolf, S. J., V. S. Bebarta, C. J. Bonnett, P. T. Pons and S. V. Cantrill (2009). "Blast injuries." *Lancet* 374(9687): 405-415.

Xu, L., M. L. Schaefer, R. M. Linville, A. Aggarwal, W. Mbuguiro, B. A. Wester and V. E. Koliatsos (2016). "Neuroinflammation in primary blast neurotrauma: Time course and prevention by torso shielding." *Exp Neurol* 277: 268-274.

Yeh, D. D. and W. P. Schecter (2012). "Primary blast injuries--an updated concise review." *World J Surg* 36(5): 966-972.

Yeh, W. L., D. Y. Lu, C. J. Lin, H. C. Liou and W. M. Fu (2007). "Inhibition of hypoxia-induced increase of blood-brain barrier permeability by YC-1 through the antagonism of HIF-1alpha accumulation and VEGF expression." *Mol Pharmacol* 72(2): 440-449.

Yeoh, S., E. D. Bell and K. L. Monson (2013). "Distribution of blood-brain barrier disruption in primary blast injury." *Ann Biomed Eng* 41(10): 2206-2214.

Zhang, J., Z. Wang, H. Leng and Z. Yang (1996). "Studies on lung injuries caused by blast underpressure." *J Trauma* 40(3 Suppl): S77-80.

Appendix A: Details of Blast Model

For blast exposure of 195 kPa peak static overpressure at the location of the animal, a combined membrane thickness of 0.070 inches was used. This consisted of three sheets of 0.02 inch acetate membrane with one sheet of 0.01 inch acetate membrane. Passive rupture of the acetate membrane resulted in complete fracture seen in Figure 63.

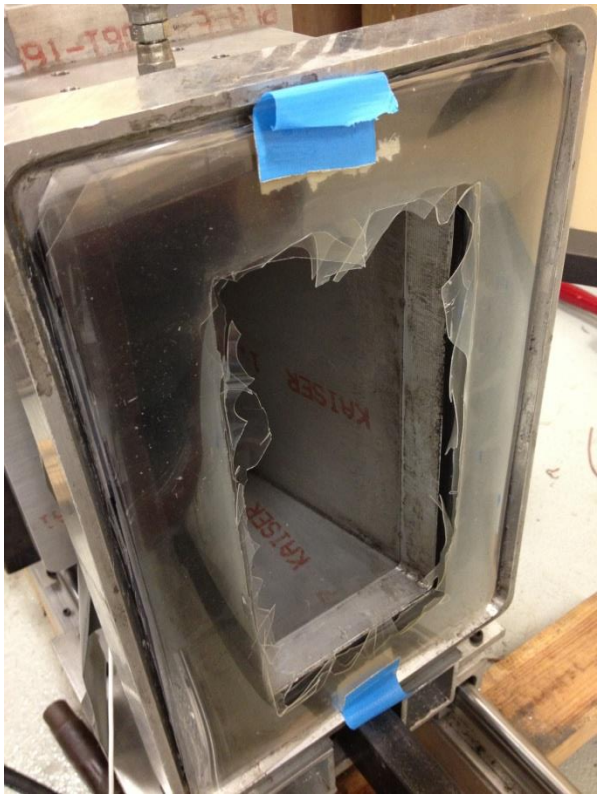

Figure 63. Acetate membrane rupture after blast.

A mesh sling was used to hold the anesthetized animal during blast exposure. This harness was tethered to three fixed points outside of the tube to restrict motion but provide give so the animal is not experiencing tertiary blast exposure of blunt impact against rigid structure. An image of the sling without an animal is seen in Figure 64.

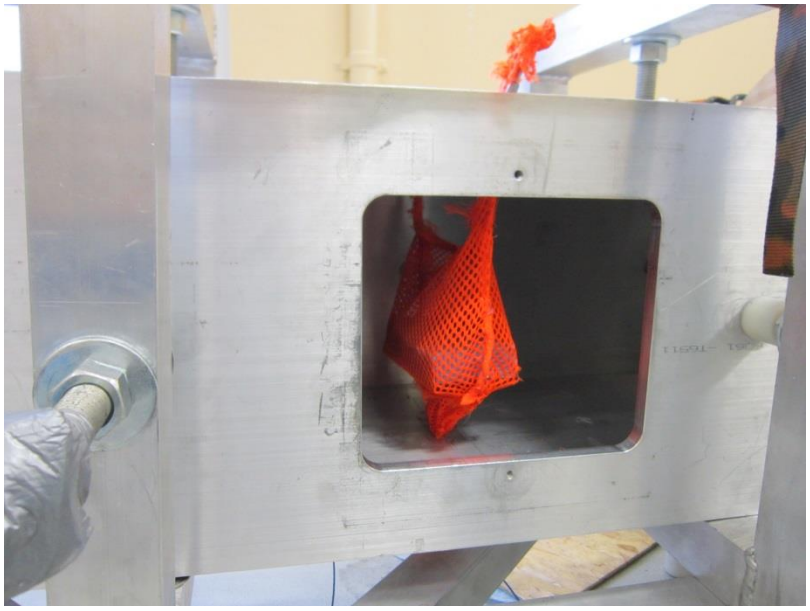

Figure 64. Animal harness in blast tube test section.

A darker colored sling was used during motion analysis to contrast the bright marker of sling/rodent position. Phantom Miro Ex2 camera with Pentax C60812 (1/2 inch, 8 ~ 48 mm focal length, Manual Iris, C mount, 1.0 F-stop) lens was used to capture videos of animal motion during lateral blast exposure. Details include: sample rate = 1000 fps; resolution = 640 x 480; exposure = 990 µs. A manual capture trigger was used at time of blast.

The blast overpressure and blast wind create lateral motion of the sling. In order to confirm that the animal does not impact any surface of the tube, this motion was quantified. For the blast exposure in Figure 65, the lateral motion with respect to the initial position towards the back of the tube was 3.78 inches. The lateral motion occurring upon descent back towards the front of the tube was 2.58 inches with respect to the initial position. Total range of motion was 6.36 inches after blast. Since motion in the y-axis had a range of only 0.48 inches, it was determined that there was no potential for impact against the tube wall. The average range of lateral motion was 5.49 ± 0.71 inches. Average motion in the y-axis was 0.53 ± 0.48 inches.

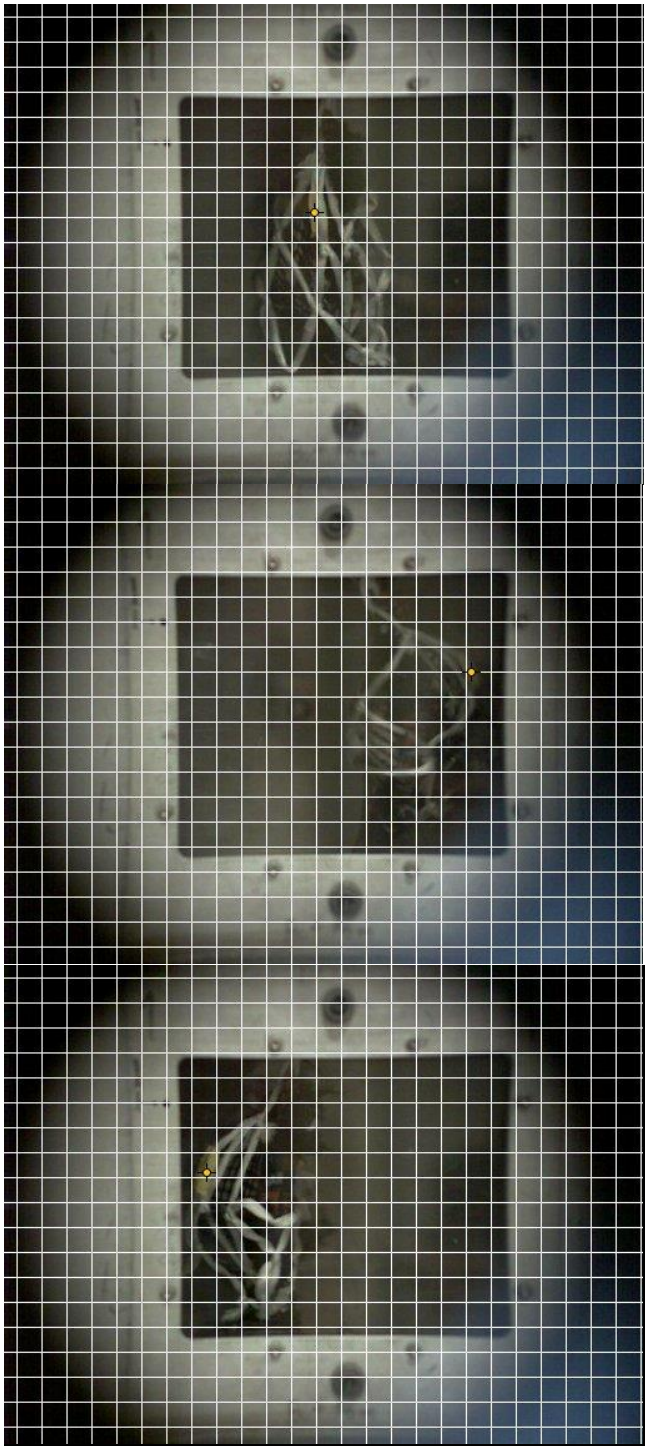

Figure 65. Marker of lateral motion of animal harness.

Appendix B: Gross Brain Injury in Blast Polytrauma

Out of 240 blast exposures conducted, only four animals were reported to have intracranial hematomas (Table 5). High speed video was used to ensure only primary injury was sustained during blast exposure.

Table 5. List of Animals with Intracranial Hematomas

Animal Number	Injection	Membrane Combination Used	Static Overpressure from Wave Speed Calculation (kPa)	Wave Speed (m/s)	Survival Time	Intracranial Hematoma Sustained
213	cNP	20-20-20	189.12	554.5455	Death (12 min)	Subdural
316	hDNP	20+20+20+15	232.91	595.7031	Death (10 min)	Subarachnoid
373	LR	20+20+20+15	207.95	575.4717	Death (10 min)	Subarachnoid
537	cDNP	20+20+20	203.26	569.0299	Alive (7 days)	Subdural

In a lateral blast exposure model with 117 kPa exposure, 30% of rats tested had evidence of subdural hemorrhage and cortical contusions (Ahlers et al. 2012). The brain, without perfusion, sustained subdural hematoma (Figure 66). Cross-section showed blood underneath the dura. Evans blue dye binds to albumin after entering the bloodstream and afterwards was not permeable across blood vessels in normal conditions. In Figure 66, a perfused brain showed Evans blue dye still present, confirming that a hematoma had occurred.

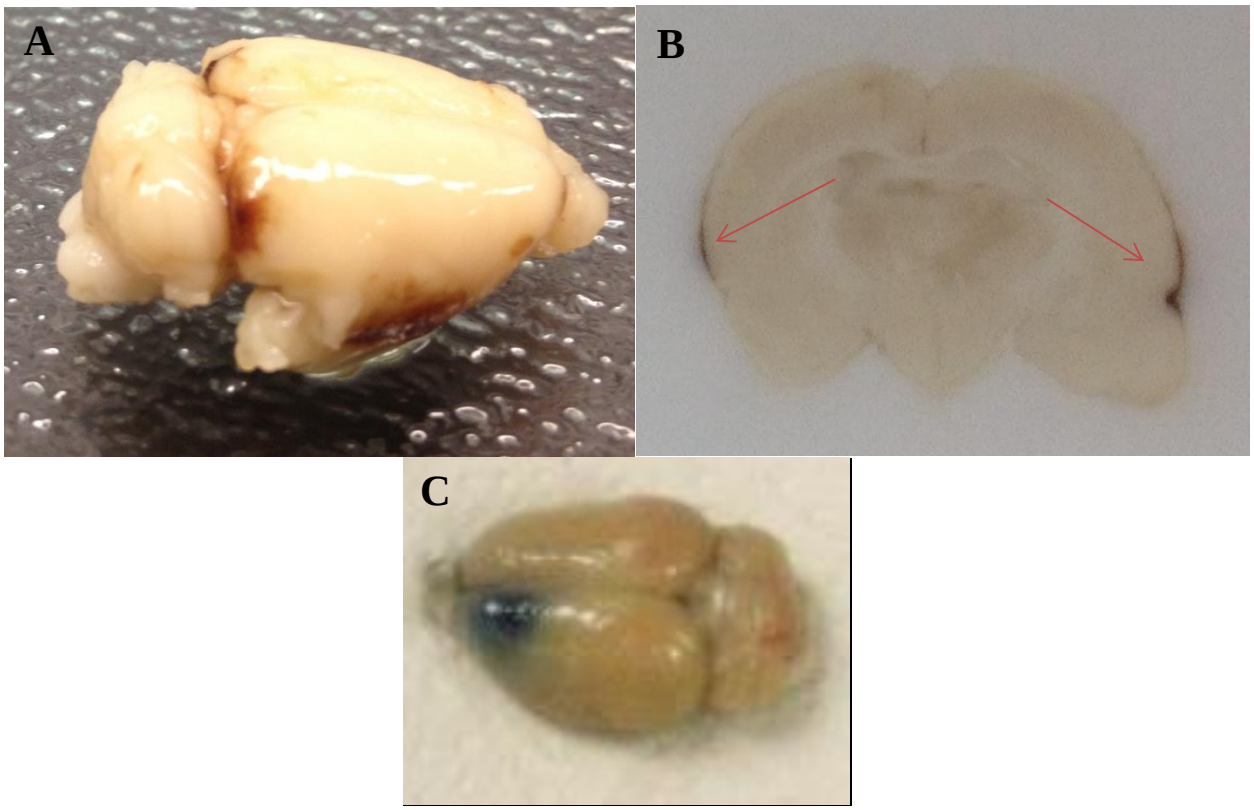

Figure 66. (A, B) Rodent exposed to 189 kPa static overpressure blast and injected with cNP. (C) Rodent exposed to 203 kPa and injected with cDNP.

Two animals presented with subarachnoid hematoma seen with blood in subarachnoid space. The animal in Figure 67A was exposed to 233 kPa static overpressure blast while the rodent in Figure 67B was exposed to 208 kPa static overpressure blast. Figure 67C was a sham brain (0 kPa exposure). One model of primary blast in ferrets determined that hematomas were present in the brain at high level blast exposure (Rafaels et al. 2012). In a model of direct cranial blast injury, exposure at 400 kPa created subarachnoid hemorrhage in the brain (Kuehn et al. 2011). Since this is the first study of high level lateral full-body blast exposure, there were no findings in the literature similar to these.

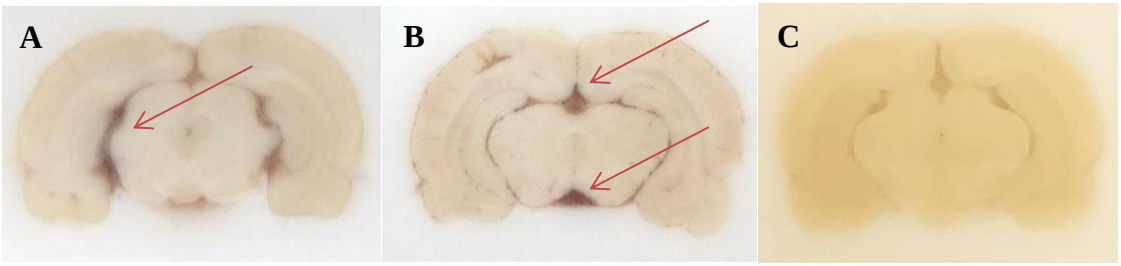

Figure 67. Brain cross-sections with arrows pointing to areas of hemorrhage. (A) Rodent exposed to 233 kPa static overpressure blast and inject with hDNP. (B) Rodent exposed to 208 kPa static overpressure blast and injected with LR. (C) Sham rodent brain.

Appendix C: Primary Antibody List

Table 6. List of Primary Antibodies

Description	Antibody	Secondary Antibody	Dilution	Company Name	Catalog Number
Systemic Inflammation	Anti-TNF-α	Alexa Fluor 488	1:500	Abnova	H00007124-M03
BBB Disruption	Anti-SMI-71	Alexa Fluor 594	1:250	Covance	836801 (previously SMI-71R)
Astrocyte Activation	Anti-GFAP	FITC	1:500	Invitrogen	130300
Microglial Activation	Anti-IBA-1	Alexa Fluor 555	1:500	Biocare Medical	CP290A
Programmed Cellular Death	Anti-Caspase-3	Alexa Fluor 555	1:500	Cell Signaling Technology	9661L
Hypoxia	Anti-HIF-1α	Alexa Fluor 488	1:250	Novus Biologicals	NB100-131
Angiogenesis	Anti-VEGF	Alexa Fluor 594	1:250	Santa Cruz	Sc-507
Astrocytic End-feet	Anti-AQP-4	FITC	1:250	Santa Cruz	Sc-20812

Appendix D: Matlab Code

Logistic Regression

```
clc; clear
%input static overpressure values in psi
k = [19.64, 19.15, 22.69, 20.34, 23.84, 19.89, 20.64, 19.44, 19.44, 20.9,
19.64, 19.39, 23.52, 25, 25, 23.84, 22.59, 21.1, 26.18, 26.5, 23.42, 25.59,
27.26, 27.753, 24.8385, 25.7665]';
%convert values to kPa
x=6.89475.*k;
%establish x-axis range for the graph
r=[50:300];
%literature pressure values
litpress=[61,130,190,230,250,290,165,120,118,118,86,112,76,76,73,62,62,136,12
9,83,62];
%lethality risk corresponding to pressure values
litrisk=[0,0,.3,0,.24,1,.35,.1,.08,.25,0,0,.1,.1,.05,0,0,0,.5,0,0];
%lethality outcome from static overpressure values
y = [0, 0, 0, 0, 1, 0, 0, 0, 0, 0, 0, 0, 0, 0, 1, 1, 0, 0, 1, 1, 0, 0, 1, 1,
1, 1]';
%logistic regression function
[b, dev, stats] = glmfit(x,y,'binomial','link','logit');
%lethality risk values for each overpressure
yfit = glmval(b, x,'logit');
%plot categorical experimental values
plot(x, y,'o')
%sort through values
a=sort(x);
d=sort(yfit);
hold on
%plot sorted values
plot(a, d,'c-')
hold on
%plot logistic regression
P=1-(1./(1+exp(b(1)+(b(2).*r))));
plot(r,P,'r')
```

```
%plot literature values
plot(litpress,litrisk,'o')
```

Receiver Operating Characteristic Curve

```
clc; clear
%load static overpressure values
k = [19.64, 19.15, 22.69, 20.34, 23.84, 19.89, 20.64, 19.44, 19.44, 20.9,
19.64, 19.39, 23.52, 25, 25, 23.84, 22.59, 21.1, 26.18, 26.5, 23.42, 25.59,
27.26, 27.753, 24.8385, 25.7665]';
x=6.89475.*k;
% load literature values
litpress=[61,130,190,230,250,290,165,120,118,118,86,112,76,76,73,62,62,136,12
9,83,62]';
litrisk=[0,0,.3,0,.24,1,.35,.1,.08,.25,0,0,.1,.1,.05,0,0,0,.5,0,0]';

%input lethality outcomes
y = [0, 0, 0, 0, 1, 0, 0, 0, 0, 0, 0, 0, 0, 0, 1, 1, 0, 0, 1, 1, 0, 0, 1, 1,
1, 1]';
% glmfit
b = glmfit(x,y,'binomial');
% logistic regression
p = glmval(b,x,'logit');
% fit probabilities for ROC
[X,Y,T,AUC] = perfcurve(y,p,1);
% plot ROC
plot(X,Y)
xlabel('False positive rate'); ylabel('True positive rate')
title('ROC for classification by logistic regression')

hold off
b = glmfit(litpress,litrisk,'binomial','link','probit');
% logistic regression for literature values
p = glmval(b,litpress,'probit');
% fit probabilities for ROC
[X,Y,T,AUC] = perfcurve(litrisk,p,1);
% plot ROC
```

```
plot(X,Y,'r-.')
xlabel('Specificity'); ylabel('1-Sensitivity')
title('ROC for classification by logistic regression')
```

Appendix E: Citations of Copyrighted Works

Figure 1. [public domain]
Stuhmiller, J.H., Phillips, Y.Y., Richmond, D.R. “The physics and mechanisms of primary blast injury” in Conventional Warfare: Ballistic, Blast, And Burn Injuries. P. 244 https://ke.army.mil/bordeninstitute/published_volumes/conventional_warfare/ch07.pdf (accessed June 28, 2016)
Works by the U.S. government are not eligible for U.S. copyright protection.

Figure 2. [public domain]
Stuhmiller, J.H., Phillips, Y.Y., Richmond, D.R. “The physics and mechanisms of primary blast injury” in Conventional Warfare: Ballistic, Blast, And Burn Injuries. P. 250m https://ke.army.mil/bordeninstitute/published_volumes/conventional_warfare/ch07.pdf (accessed June 28, 2016)
Works by the U.S. government are not eligible for U.S. copyright protection.

Figure 3. [public domain]
Number Of Diagnosed TBIs In Military Service Members From 2000-2015. Source: Defense And Veteran Brain Injury Center. http://dvbic.dcoe.mil/dod-worldwide-numbers-tbi (accessed June 28, 2016)
Works by the U.S. government are not eligible for U.S. copyright protection.

Figure 4. [fair use]
Wolf, S. J., V. S. Bebarta, C. J. Bonnett, P. T. Pons And S. V. Cantrill (2009). "Blast Injuries." Lancet 374(9687): 405-415. http://www.thelancet.com/pdfs/journals/lancet/PIIS0140-6736(09)60257-9.pdf (accessed June 28, 2016) Fair use determination attached.

Figure 5. [fair use]
Stewart, C. (2006). "Blast Injuries: Preparing For The Inevitable." Emergency Medicine Practice 8(4). https://www.ebmedicine.net/topics.php?paction=dLoadTopic&topic_id=18 (accessed June 28, 2016) Fair use determination attached.

Figure 7. [fair use]
Ruiz Junior, R. L., L. R. De Carvalho And A. J. Cataneo (2005). "Compensatory Lung Growth: Protein, Dna And Rna Lung Contents In Undernourished Trilobectomized Rats." Acta Cir Bras 20(3): 219-224. http://www.scielo.br/scielo.php?script=sci_arttext&pid=S0102-86502005000300005 (accessed June 28, 2016) Fair use determination attached.

Figure 8. [fair use]
Kuehn, R., P. F. Simard, I. Driscoll, K. Keledjian, S. Ivanova, C. Tosun, A. Williams, G. Bochicchio, V. Gerzanich And J. M. Simard (2011). "Rodent Model Of Direct Cranial Blast

Injury." J Neurotrauma 28(10): 2155-2169. http://online.liebertpub.com/doi/abs/10.1089/neu.2010.1532 (accessed June 28, 2016) Fair use determination attached.

Figure 16. [fair use]
Engelhardt, S., S. Patkar And O. O. Ogunshola (2014). "Cell-Specific Blood-Brain Barrier Regulation In Health And Disease: A Focus On Hypoxia." Br J Pharmacol 171(5): 1210-1230. http://www.ncbi.nlm.nih.gov/pmc/articles/PMC3952799/ (accessed June 28, 2016) Fair use determination attached.

Figure 18. [fair use]
Paxinos, G. A. W., C. (2006). "The Rat Brain In Stereotaxic Coordinates." Elsevier 6th Edition. http://store.elsevier.com/The-Rat-Brain-in-Stereotaxic-Coordinates/George-Paxinos/isbn-9780125476126/ (accessed June 28, 2016) Fair use determination attached.

Figure 44. [fair use]
Sah, P., E. S. Faber, M. Lopez De Armentia And J. Power (2003). "The Amygdaloid Complex: Anatomy And Physiology." Physiol Rev 83(3): 803-834. http://physrev.physiology.org/content/83/3/803.long (accessed June 28, 2016) Fair use determination attached.